THESIS - TM185400

NUMERICAL SIMULATIONS ON HYBRID SAVONIUS - DARRIEUS WIND TURBINE WITH VARYING AIRFOIL SHAPE AND SOLIDITY RATIO

SAVRY CHHIN

02111850087003

SUPERVISORS

VIVIEN SUPHANDANI DJANALI, S. T, M.E., Ph.D.

MASTER PROGRAM

MECHANICAL ENGINEERING

DEPARTMENT OF MECHANICAL ENGINEERING

FACULTY OF INDUSTRIAL TECHNOLOGY

INSTITUT TEKNOLOGI SEPULUH NOPEMBER

SURABAYA

2020

This page is blank

THESIS TM185400

NUMERICAL SIMULATIONS ON HYBRID SAVONIUS - DARRIEUS WIND TURBINE WITH VARYING AIRFOIL SHAPE AND SOLIDITY RATIO

SAVRY CHHIN
02111850087003

SUPERVISORS

VIVIEN SUPHANDANI DJANALI, S. T, M.E., Ph.D.

MASTER PROGRAM
MECHANICAL ENGINEERING
DEPARTMENT OF MECHANICAL ENGINEERING
FACULTY OF INDUSTRIAL TECHNOLOGY
INSTITUT TEKNOLOGI SEPULUH NOPEMBER
SURABAYA

2020

This page is blank

APPROVAL SHEET

This thesis is written to comply with one of the requirements for obtaining the
degree of **Magister Teknik (MT)**
at
Institut Teknologi Sepuluh Nopember
By:
SAVRY CHHIN
NRP: 02111850087003

Oral Defense Date: 30 July 2020
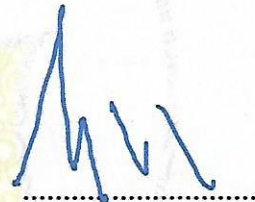Graduation Period: September 2020

Approved by:
Supervisors:

VIVIEN SUPHANDANI DJANALI, S. T, M.E., Ph.D.
NIP: 198105292003122001
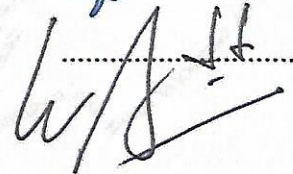
Examiners:

1. TRIYOGI YUWONO, Ir. DEA. Dr. Prof.
   NIP: 196001291987011001

2. Prof. Ir. SUTARDI, M.Eng., PhD.,
   NIP: 196412281990031002

3. WAWAN ARIES WIDODO, ST. MT. Dr.
   NIP: 197104051997021001

The head of the Mechanical Engineering department
Faculty of Industrial Technology and System Engineering

Dr.Ir.Atok Setiyawan, M.Eng, Sc
NIP. 196604021989031002

iii

This page is blank

STATEMENT OF THESIS ORIGINALITY

I hereby declare that the entire content of my Thesis entitled "**NUMERICAL SIMULATIONS ON HYBRID SAVONIUS - DARRIEUS WIND TURBINE WITH VARYING AIRFOIL SHAPE AND SOLIDITY RATIO**" is truly the attainment of independent intellectuals, completed without the use of unauthorized materials, and not the work of others that I claim as my own.

All references cited or referred have been fully written in the bibliography. If this statement is not true, I am willing to accept sanctions in accordance with applicable regulations.

Surabaya, 30 July 2020

Savry Chhin
ID. 02111850087003

NUMERICAL SIMULATIONS ON HYBRID SAVONIUS - DARRIEUS WIND TURBINE WITH VARYING AIRFOIL SHAPE AND SOLIDITY RATIO

Student Name : Savry Chhin
Student ID : 02111850087003
Supervisor : Vivien Suphandani Djanali, S. T, M.E., Ph.D

ABSTRACT

The demand for green and clean energy is increasing all over the world. Vertical Axial Wind Turbine (VAWT) is utilized to convert mechanical energy into electrical energy, which is commonly used in urban areas. In addition, at low wind speed is located at a low range of height, so it is significant to implement the small wind turbine in the residential area. The combined of H-Darrieus and Savonius rotors is called a hybrid wind turbine. It has the Darrieus blades form as the airfoils, and the Savonius blades in the middle. H-Darrieus rotor has high power efficiency, but it is difficult to start-rotating, as the inverse of the Savonius rotor, which is better self-starting capability, low efficiency. Moreover, H-Darrieus and Savonius rotors are commonly popular, simple construction features, and less cost of manufacturing and installation.

The aims of this study will evaluate numerically the power performance of the hybrid turbine, where compares the coefficient of power (C_P) between the two types of hybrid turbine that is a different form of NACA-airfoils as symmetric and asymmetric standard. Also, there is an attempt to state a suitable configuration by varying solidities ratios. The model will implement by varying some parameters such as tip speed ratio, TSR= (0.5-4) free stream velocity of 4 m/sec, and solidity ratio, σ =(0.2-0.8). Two-dimensional (2-D) computational fluid dynamic (CFD) unsteady (transient) model will use for simulating the whole model. A moving mesh is applied for the rotating part. The simulation will be carried out by using a shear stress transport (SST) $k\text{-}\omega$ turbulent model.

Definitely, the results are generated by respecting the performance of the wind turbine such as coefficients of power (C_P), coefficient of the moment (C_M) over the range of the tip speed ratio (TSR), and aerodynamic performance of the fluid flow interaction to the wind turbine. The entire model had completed; therefore, the turbine contours and graphic performance are generated. Firstly, the C_M of the combined rotor of the two configurations in different of symmetric and asymmetric of the NACA standard airfoil is presented about 0.12 and 0.13 respectively at a TSR of 2.75 with an inlet velocity of 4 m/sec. Also, the achievement of the C_P value is determined by NACA-0018 was 35.14% and NACA-2415 was 36.62%. Secondly, a low solidity ratio (σ=0.2) has generated a high coefficient of power at a large range of TSRs. But high solidity ratio (σ=0.8) is conducted high performance along with the low range of the TSR. Meanwhile, a medium solidity ratio (σ=0.4) operated at the same range of TSRs. It has appeared at the peak of the turbine performance which is compared to conventional analysis. Based on the evidence of the graphic performance is that the solidity of 0.4 illustrated the higher C_P of 36.41% at a TSR of 2.5. Moreover, the low TSR of the combined rotor has generated the capabilities of self-starting which is compared to a single H-Darrieus rotor.

PREFACE

The renewable energy is the most significant to alive. However, this thesis is made as a completion of the master research in fluid mechanic that is applied numerical simulation on a small wind turbine. Significantly, the energy source can be extract from the nature such as wind energy, wave energy, and solar energy etc. The consumption of the huge among of the electrical energy is increased annually. Hence, how can we provide any facility to produce the product of the renewable energy.

In truth, I could not have achieved my current level of success without a strong of the financial support. I would like to express my gratitude from the bottom of my heart toward to **KNB scholarship**, **International Office (IO)** and **Institut Teknologi Sepuluh Nopember (ITS)** for providing good education system; without this financial support and scholarship I could not have a chance to continue my master's degree in such a good institution. I would like to thank my supervisors **Vivien Suphandani Djanali, S. T, M.E., Ph.D** for her excellent guidance, strongly support, and worth advice during this process of my research. I also wish to thank all of the respondents forward all the examiners **TRIYOGI YUWONO, Ir. DEA. , Dr. Prof., SUTARDI, M.Eng., Ir., PhD., Prof.,** and **WAWAN ARIES WIDODO, ST. MT. Dr.** without their advices and revisions I would not have been able to correct this thesis research.

To my other colleagues at ITS, I would like to thank you for your wonderful cooperation as well. It was always helpful to bat ideas about my research around with you. I also received help from debating issues with my friends and family. If I ever lost interest, you kept me motivated. My parents deserve a particular note of thanks: your wise counsel and kind words have, as always, served me well.

Surabaya, 30 July 2020

Savry Chhin

viii

TABLE OF CONTENTS

LIST OF FIGURES

xiii

LIST OF TABLES

This page is blank

ABBREVIATIONS AND SYMBOLS

Nomenclature

c	Darrieus chord length (m)
C_P	Power coefficient (-)
C_M	Moment coefficient (-)
R_D	The radius of H-Darrieus rotor (m)
R_S	The radius of Savonius rotor (m)
N_s	Savonius blade number (-)
N_D	H-Darrieus blade number (-)
t	The thickness of the Savonius blade (m)
T	Aerodynamic torque (Nm)
V	Free stream velocity (m/sec)
D	Diameter of H-Darrieus rotor (m)
Δs	First layer thickness (m)
y^+	Non-dimensional distance (-)
S	Turbine swept area (m^2)
C_f	Coefficient friction (-)
U_f	Velocity friction (-)
k	Turbulent kinetic energy (m^2/sec^2)

$Pa = kg/m \cdot sec^2 \,; Pa \cdot sec = kg/m \cdot sec$

Greek Symbols

σ	Solidity ratio (-)
ω	Angular velocity (rad/sec)
τ_{wall}	Wall share stress (Pa)
α	Pitch angle (deg)
ε	Dissipation of turbulent kinetic energy (m^2/sec^3)
μ	Air viscosity ($Pa \cdot sec$)
λ	Tip speed ratio, TSR (-)
ψ	Azimuth angle (deg)
ρ	Air density (kg/m^3)
φ	Savonius bucket angle (deg)
θ	Attachment angle (deg)

Abbreviations

KD	Radius Ratio (R_S/R_D)
OR	Overlap Ratio
SST	Shear Stress Transport
CFD	Computational Fluid Dynamic
Re	Reynolds Number
AR	Aspect Ratio
NACA	National Advisory Committee for Aeronautics
VAWT	Vertical Axial Wind Turbine

CHAPTER 1
INTRODUCTION

In the last few years, it has been significantly drawing towards the requirement for finding a cost-effective and clean energy source. Principally due to the continuous reduction in fossil fuels. Renewable energy is the source of permanent or finite energy, the wind was a type of energy source that fits into these criteria which is harnessed via wind turbines [21]. There are many concepts to extract mechanical energy from wind. Also, the investigators have been struggled to develop the optimum features and cost economy for saving energy by manipulative the best performance of wind turbines. As the previous researches have been stated that wind turbine is divided into two types, namely being a Horizontal Axis Wind Turbine (HAWT) and Vertical Axis Wind Turbine (VAWT), where VAWT will be presented on this study. However, VAWT is separated into two types such as the Darrieus and the Savonius rotor. In this statement, the performance of VAWT is provided by the research's topic that is combined both Darrieus and Savonius is called a hybrid turbine.

This section will be illustrated the previous research by establishing the capacity of the small wind turbine (VAWT) that is including with the scope and the objective of the present study. Moreover, the limitation of the subsection is derived to limit on this present research.

1.1 Background

Wind energy is a clean and renewable energy source that has developed a variety of technological applications and industrial uses in recent years. Researchers have regarded wind energy as the foremost source of renewable energy that is reasonable, understood as being capable of generating electricity for business, industrial, and residential uses at rates that are comparable with conventional energy sources, with or without subsidies. The statistical has been studied on the conventional wind energy, which is evaluated the different design of HAWT, VAWT, and SWT (Small Wind Turbine), has been provided by the advance

numerical to model [22]. In 2008, the United States advanced to the top rank of global wind energy producers, but China surpassed the United States in this area in 2010. Surpassing the United States in terms of production of wind energy, China simultaneously outpaced India, which had led the Asian region until 2007 [23]. Meanwhile, China is currently generating three times more energy from wind sources than India. Based on the plans to begin production of another 200GW, China is expected to remain the world leader in wind energy production soon. With the need for sustainable energy increasing annually as a direct consequence of ongoing depletion of fossil fuels and the resulting energy crisis, wind energy has taken on as being of prime significance. Unlike fossil fuels, wind energy is both renewable and not a contributor to any environmental ill effects. Therefore, it can be identified as both a clean and renewable energy source. The classification of the wind turbine was arranged as shown in Figure 1.1 that is included efficiencies respectively. The ideal efficiency became high while the application stood as moderate low such as the Savonius and the Darrieus turbine types.

(a)   (b)
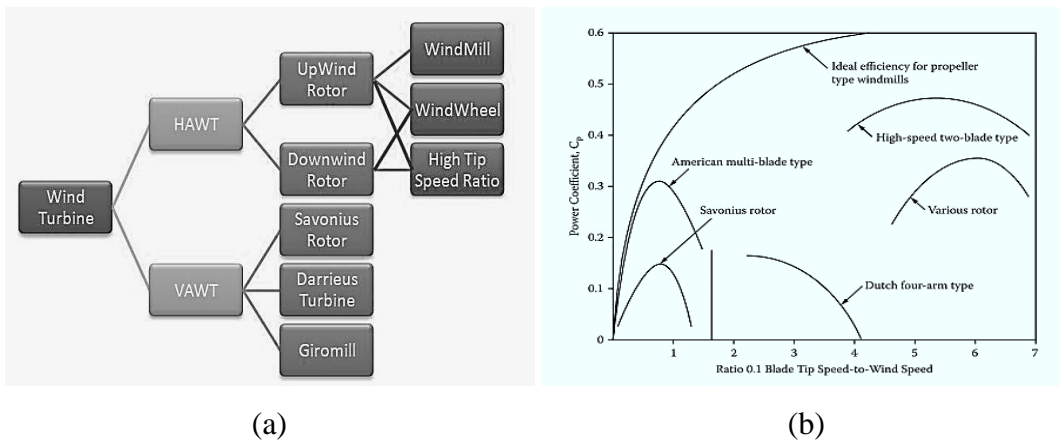
Figure 1.1. Properties of the turbine, (a) classification of the wind turbine, (b) efficiencies

Noticed that since 2000, the total capacity of installed wind power in the European Union (EU) has been 12.9GW and by 2012, as shown in Figure 1.2 has grown to 106GW. It is anticipated that by 2020, under development by the European Wind Energy Association (EWEA), growth in wind energy will reach 230GW with 40GW obtained from offshore installations. Bonn, 25 February 2019 (WWEA) the overall capacity of all wind turbines installed worldwide by the end

of 2018 reached 597 GW, according to preliminary statistics published by WWEA today. 50'100 MW were added in the year 2018, slightly less than in 2017 when 52'552 MW was installed. Since 2018, which was the second year in a row with a growing number of new installations, meanwhile at a lower rate of 9,1%, after 10,8% growth in 2017. Many wind turbines installed by the end of 2018 can cover close to 6% of the global electricity demand [24]. The demand for the consumption of the energy was increased slightly the day by day, Therefore, modern technology has developed the turbine became a high performance and to increase more electric supply. Thus data, which had shown in Figure 1.2, the amount of global electricity shown by graph static of the wind turbine that much electricity of year by year.

GLOBAL WIND INSTALLATIONS

Installed Capacity by the end of 2018 (MW)*

Country/Region1	2018	2017	2016	2015
China	216'870	195'730	168'730	148'000
United States	96'363	88'775	82'033	73'867
Germany	59'313	56'190	50'019	45'192
India**	35'017	32'879	28'279	24'759
Spain*	23'494	23'026	23'020	22'987
United Kingdom	20'743	17'852	14'512	13'614
France	15'313	13'760	12'065	10'293
Brazil**	14'490	12'763	10'800	8'715
Canada	12'816	12'239	11'898	11'205
Rest of the World*	102'138	93'173	85'582	76'653
Grand Total	596'556	546'388	486'939	435'284
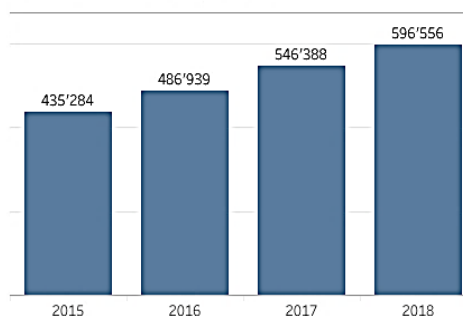
* Preliminary data
** By November 2018

Figure 1.2. World statistic of wind energy [1]

To focus out that energy is quite simply a necessity for technological and economic development, while also noting that the energy choices made by countries such as the United States and other industrialized nations have significant developments for the rest of the world. These developments are economic, environmental, and political as well as military requires too many energies to irrigate. Energy resources and specifically fossil fuels or mineral resources have

3

long formed the basis of energy consumption in both the developed and the developing world.

For example, many countries in South-East Asia (including Indonesia, Philippines, Thailand, Vietnam Malaysia, Laos, Myanmar, and other smaller markets), the rising energy demand is driven by economic growth, growth of population, and increased urbanization. The fundamentals of wind energy are suitable to play a leading part to produce energy. Governments in South-East Asian markets have set targets for wind energy deployment [1]. Among wind turbines which had already installed in South-East Asian as shown in Figure 1.3.

(a)   (b)
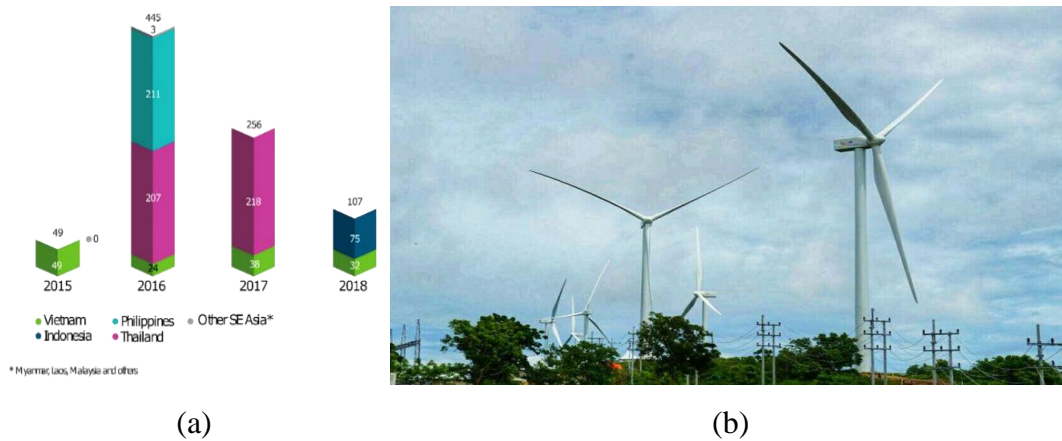
Figure 1.3. Data installation capacity in south-east Asia in (MW), (a) Chart data, (b) the turbine has been installed.

1.2 Research Scope

The main concern for the hybrid turbine is the interaction between the Savonius and the Darrieus blades. The wake shading of a particular Darrieus airfoil blade affects the flow that impinged the Savonius blade, and further the wake shading of the downstream affects the flow over the downstream Darrieus airfoil.

This study is focused on the Computational Fluid Dynamics (CFD) approach to investigate the configuration of the hybrid turbine with the Bach-profile blade as the Savonius blades, and the NACA airfoils as the H-Darrieus blades. The variations performed include the blade shape and solidity ratio variations. Each configuration is simulated at varying tip speed ratio, so that it is obtained the maximum power coefficients at the optimum tip-speed ratio. The configurations are tested with a wind speed of 4 m/sec.

4

Based on the previous studies of the hybrid turbine [14, 20, 25, 26], the peak of the power coefficient of the combined rotors was obtained at a specific configuration. This study attempts to implement varying airfoil shapes and solidity ratio, which affects the turbine performance. The hypothesis is that asymmetric airfoil will result in a higher moment because the lift resulted will be higher. Meanwhile, the solidity ratio represents the size of the H-Darrieus airfoil relative to the rotor diameter. With the various solidity ratio, the effect of H-Darrieus airfoils becomes more dominant in turbine performance. It is expected that the optimum solidity ratio will give the maximum power coefficient, with a good capability of self-starting.

1.3 Research objective

The primary aim of this study is to investigate the characteristic of the performance parameters and configuration of the hybrid turbine. The objectives of this study are to investigate:

1. The effect of the airfoil shapes of the H-Darrieus blades, particularly the difference between the symmetric and asymmetrical blade profile.
2. The effect of the solidity ratio on the performance of the blade profile.

The performance of the hybrid turbine is extracted from numerical results, such as the power coefficient and moment coefficient. Furthermore, the flow characteristics over the rotor blades are obtained by extracting the velocity contours and pressure contours.

Moreover, it is expected that this study will provide an insight into the configuration of the hybrid VAWT turbine.

1.4 Research limitation

The limitation of the simulation is provided to limit the area of research such as configuration and model procedure:

- Two-dimensional (2-D) simulation, moving mesh
- VAWT simulated with no shaft
- H-Darrieus type is selected for the simulation

5

- Unsteady, incompressible fluid flow
- Constant wind velocity
- The results were limited to compare with the previous research and conventional research.
- The coupling with the generator is negligible
- Structure vibration is negligible.
- Bach type of 135 deg of bucket blade with no shaft for Savonius turbine
- The diameter of the Savonius wind turbine fixed and constant
- Savonius turbine has two blades

CHAPTER 2
LITERATURE REVIEW

The framework will provide a detail of the available literature in the overall wind energy, including on the performance characteristic of VAWT operating in the atmospheric condition and review some of the previous researchers who are already focused on the type of VAWT field. Meanwhile, studies on characteristics of single-Darrieus and single-Savonius with some mathematical models are specified to the site on this present study.

2.1 Introduction

Energy is an important part of daily life, especially in developing countries. Every country requires to produce sustainable energy for supplying to the other sectors to develop the country. Currently, there are many people who attempted to discover how to conduct suitable renewable energy such as hydro, solar, and wind energies, etc. Recently, VAWT fails in interest for wind energy harvesting in two new potential locations, i.e., offshore and rural environments or urban regions. The extraction of the kinetic aerodynamic energy from wind and its conversion to useful types of energy is a process that has been used for the entire century [27]. Since 5000BC, ancient researchers known as American Windmills have been using wind power to pump the water and grind grains.

2.1.1 Benefits

As a general is that energy is significant for daily life. Many researchers have discovered the prototypes for experiments, numerical simulation, and reality applications. Thereby, they have stated many definitions for the benefit of the VAWT.

- Elimination of yawing mechanisms
- High efficiency at the residential wind speed
- Omnidirectional wind from any direction and low wind velocity.
- Simple design, no yaw gear, and drop cables

-   Have driven trains at ground level.
-   Low-cost operation due to reduced overturning moments and lower tower top mass.
-   Unexplored technology may offer more potential for cost reductions.
-   Used less material

2.1.2 Disadvantage

According to what the benefits stated, therefore, there are many disadvantages as well. The list below is specified down the obstacle points for the VAWT:

-   Worst starting torque
-   Operation of dynamic problem
-   Sensibility to off-design condition
-   Generally, install near the ground where wind poorer
-   Power generation Limiting
-   Require support at the top of the rotor
-   It well knew that lift-driven wind turbines have much higher performance than drag-driven types from the aerodynamic theory.
-   Longer blade length, about twice the length of HAWTs. Blades are major wind turbine cost items; low-cost blades are essential to VAWTs.

The declaration above has described the benefits of the wind turbine, Also, Table 2.2 is shown the classification configuration between VAWT and HAWT. Table 2.1 is addressed the superiority and disability of the three types of the VAWT.

Table 2.1. Classification characteristics of wind turbine

Items	VAWT	HAWT
Performance	Lift-driven and high (Darrieus Motor), drag - driven and low (Savonius rotors)	Lift-driven and high

Power/speed control	Usually, variable pitch control is not possible	Variable pitch control is possible
Yaw control	Free from yaw control	Needed
Structural arrangement	All the components except rotor are on the ground level	The nacelle is on the top of the tower

Table 2.2. The advantage and disadvantage of the H-Darrieus, Savonius, and combined rotor

Advantage		
H-Darrieus Rotor	**Savonius Rotor**	**Combined rotor**
High coefficient of power	High starting torque at low wind speed	Optimum coefficient at a TSR
Low-cost installation and manufacturing	Low-cost installation and manufacturing	Low-cost installation and manufacturing
Operate at high wind velocity	Operate at low wind velocity	Operate combined at low and high wind velocity
Omnidirectional	Omnidirectional	Omnidirectional
Have driven at the ground level	Have driven at the ground level	Have driven at the ground level
low vortices or shading on blades turbine	low vortices or shading on blades turbine	-
Disadvantage		
H-Darrieus Rotor	**Savonius Rotor**	**Combined rotor**
-	-	High vortices and shading between Savonius and H-Darrieus
Hard to start at low wind speed	Low coefficient of power	Reduced coefficient of power at optimum TSR
Construction in complex	-	Construction in complex

The prototypes were focusing on wind turbines; almost, they already performed the numerical or experimental. The context discussion above has described the benefits and weaknesses of VAWT and HAWT. Therefore, VAWT (or hybrid Savonius-Darrieus rotor) is significant for the case study and real prototype, which is operated within low wind speed and take into the simple characteristic. In general, it has many benefits such as the capability of self-starting torque and driven into high torque when it is combined into a body.

For example, an application is conducted, which called ERIGEN wind generator, had a system design used in telecommunication. Also, this application is intended in sea-leveled in Argentina. It is claimed that it has been generating high efficiency of the electrical power based on low wind speed. Consequently, it seems like the mechanical concept became in successful design by operating independently of omnidirectional wind speed [28].

The significate of the hybrid turbine as shown by the previous researches are the major for an extended study of the geometrical and aerodynamic performance of the turbine. Some parameters such as the shape of blades, solidity, number of blades, radius ratio, and the optimal TSR are elucidated.

2.2 Betz Equation and limit C_p

The theoretical wind machine has developed by Betz at Gottingen Institute in Germany (Le Gourieres Desire 1982). The Betz equation is analogous to the Carnot cycle efficiency in thermodynamics, which suggested heating the engine cannot that is extracted all the energy from a given source of energy. It rejects part of its heat input back to the environment [5]. In the actual of Betz equation, V_1 and V_2 respect to upstream and downstream, respectively. Moreover, V as the uniform of wind speed passing through the turbine rotors

$$V_2 < V_1 \qquad\qquad 2.1$$

The cross-section area of wind turbine has defined, downstream and upstream, S_1 and S_2 respectively:

$$S_2 > S_1 \qquad\qquad 2.2$$

Conservation of mass has applied to the incompressible flow of air stream.

$$m = \rho S_1 V_1 = \rho S V = \rho S_2 V_2$$

Flow diagram over wind turbine shown in Figure 2.1, the flow is expressed upstream and downstream of wind velocity.
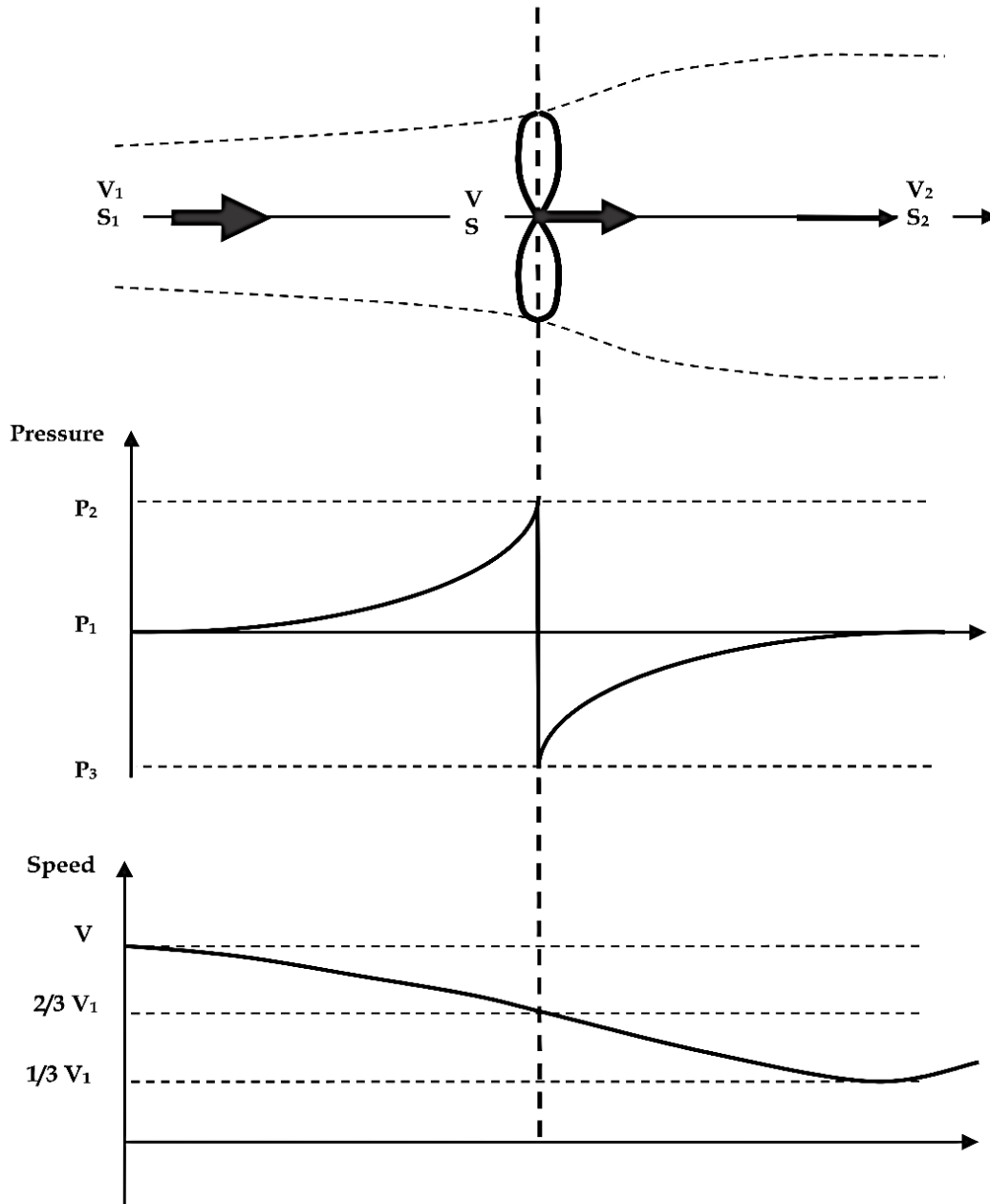
Figure 2.1. Flow model over the turbine [5]

The expression of the mass flow rate is constant along the wind stream. Euler's Theorem continues with the derivation given the force exerted by the wind on the rotor as [5], the force is given by mass (m) multiply by acceleration (a).

$$F = ma = m\frac{dV}{dt} = m\Delta V = \rho SV(V_1 - V_2) \qquad 2.3$$

Energy derivative has derived as:

$$dE = Fdx \qquad 2.4$$

$$P = \frac{dE}{dt} = F\frac{dx}{dt} = FV \qquad 2.5$$

Replacing force by

$$P = \rho V^2(V_1 - V_2) \qquad 2.6$$

On the other hand, can be derived into derivative per rate as:

$$P = \frac{dE}{\Delta t} \qquad \textbf{2.7}$$

$$P = \frac{0.5mV_1^2 - 0.5mV_2^2}{\Delta t}$$

$$P = 0.5m(V_1^2 - V_2^2)$$

Apply the continuity equation:

$$P = 0.5\rho SV(V_1^2 - V_2^2)$$

The expression of force F and the power P function of wind speed downstream and upstream by substituting the value of V:

$$F = \rho SV(V_1 - V_2) \qquad 2.8$$

$$F = 0.5\rho S(V_1^2 - V_2^2)$$

$$P = \rho SV^2(V_1 - V_2)$$

$$= 0.25\rho S(V_1 + V_2)^2(V_1 - V_2)$$

$$= 0.25\rho S(V_1^2 + V_2^2)(V_1 - V_2)$$

Where the expression of velocity term can derive as:

$$0.5(V_1^2 + V_2^2) = 0.5(V_1 - V_2)(V_1 + V_2)$$

$$= V(V_1 - V_2) \qquad \forall V, S, \rho \neq 0$$

Define b as the ration of downstream and upstream as:

$$b = \frac{V_2}{V_1} \qquad 2.9$$

Force F and power P obtained by the expression below:

$$F = 0.5\rho S V_1^2 (1-b^2) \qquad\qquad 2.10$$

$$P = 0.25\rho S \left(1-b^2\right)(1+b) \qquad\qquad 2.11$$

The flow rate of energy per area defined as:

$$P' = \frac{P}{S} = \frac{0.5\rho S V^3}{S} \qquad\qquad 2.12$$

$$P' = 0.5\rho V^3$$

The kinetic power (*W*) content of the undisturbed upstream wind stream with $V=V_1$ and cross-sectional area *S* as:

$$W = 0.5\rho S V_1^3 \qquad\qquad 2.13$$

The performance coefficient is the dimensionless ratio of the extractable power *P* to *W* available in the undisturbed stream [5]

$$C_p = \frac{P}{W} = 0.5(1-b^2)(1+b) \qquad\qquad 2.14$$

The maximum condition defined as the factor *b*, so the derivative equal to zero has applied by the chain rule:

$$\frac{d}{dx}(uv) = u\frac{dv}{dx} + v\frac{du}{dx} \qquad\qquad 2.15$$

$$\frac{dC_p}{db} = \frac{1}{2}\frac{d}{db}\left[\left(1-b^2\right)(1+b)\right]$$

$$= \frac{1}{2}(1-3b)(1+b)$$

$$= 0$$

The two conditions, as shown below:

$$\oplus \ (1-3b) = 0$$

$$\Leftrightarrow b = \frac{V_2}{V_1} = \frac{1}{3} \Rightarrow V_2 = \frac{1}{3}V_1$$

$$\oplus \ (1+b) = 0$$

$$\Leftrightarrow b = \frac{V_2}{V_1} = -1 \Rightarrow V_2 = -V_1$$

Thus, the power coefficient output state with the optimum value as the equation below:

$$C_{p,opt} = 0.5(1-b^2)(1+b) = 0.5\left(1-\left(\frac{1}{3}\right)^2\right)\left(1+\frac{1}{3}\right) = \frac{16}{27}$$

$$\textit{Betz coefficient of } \frac{16}{27} = 0.592593 = 59.26\% \qquad\qquad 2.16$$

The power coefficient available between 35 to 40 percent during wind extractable under practical condition.

2.3 Savonius rotor

The pressure drop on each side of the blades is defined as the force that is acting on the turbine blades. There is a mathematical as shown below that is applied to measure the forces on the Savonius turbine [27]. As shown in Figure 2.2, the mathematical was described.
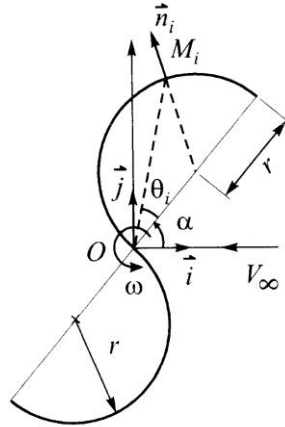
Figure 2.2. The scheme mathematical model through Savonius turbine [27]

$$Q = \sum_i (\overrightarrow{OM} \times \vec{F_i}) \cdot \vec{k} \qquad\qquad 2.17$$

where the turbine overlap ratio is $\dfrac{s}{d} = 0$

if $\vec{\omega} = \dot{\alpha}\vec{k}$ the instantaneous rotational vector

There are two components to conduct the total torque of the Savonius turbine:

$$Q = Q_M + Q_D \qquad\qquad 2.18$$

where: Q_M is a driven component and Q_D is a resistant component.

Then, the formula can be derived relate to the pressure different respectively:

$$Q = 2r^2 H \int_0^{\pi/2} (\Delta p_M - \Delta p_D) \sin(2\theta) d\theta \qquad 2.19$$

The average power P is obtained by integrating the torque from 0 to π

$$P = \omega \cdot Q = \frac{\omega}{\pi} \int_0^\pi Q d\alpha \qquad 2.20$$

The power coefficient can be set as:

$$C_p = \frac{P}{0.5 \rho V_\infty^3 A} \qquad 2.21$$

where A which is the frontal area of the Savonius rotor, in the case in the 3-D model the area is presented into length scale (L) multiply by diameter (D) of the turbine.

The Savonius Vertical Axial Wind Turbine is the type of multi of haft cycles, which is used for converting the drag force on blades of the wind and extracting the torque of the rotating shaft. It was found by the Finnish engineer Sigurdj Savonius since 1922. The turbine is operated with low TSR and performed in the minimum of the coefficient of power. The Savonius machine is useful and economical for small power requirements for example of water pumping, small electrical generator, and ventilation providing [3]. Figure 2.3 is the streamline flow over the turbine and an application that has been designing for pumping.

(a)   (b)
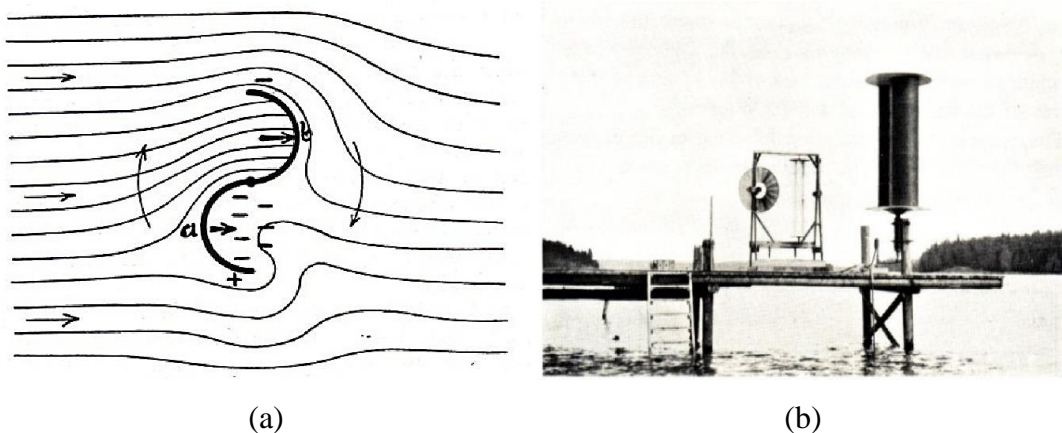
Figure 2.3. The implementation of the Savonius turbine, (a) streamflow through the blade turbine, (b) pumping Wingrotor [3]

The number of blades of the Savonius turbine is also an effective factor for the efficiency of the wind turbine. According to what the previous study is stated on the number of the Savonius blades, it is sough that two blades are efficient while the start-up wind speed operation in the smallest values; moreover, it has a high-pressure gradient and drags force. The power coefficient is shown in Figure 2.4 that is arranged in the order different by the number of blades [4].

| (a) | (b) |
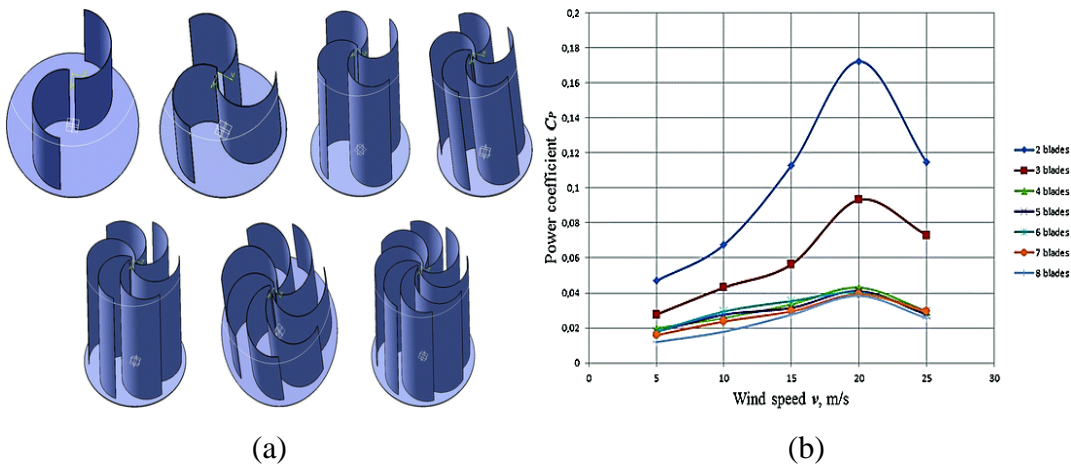
Figure 2.4. The feature of Savonius turbine, (a) range of the Savonius's blades, (b) the power coefficient [4]

As, there are many characteristics of the Savonius turbines, which is the auditor attempted to vary the shapes to define the best performance while it was operating. The four different shapes of the Savonius turbines are presented in Figure 2.5. The coefficient of power is arranged by semicircular, Benesh, modified Bach, and elliptical profile are 0.272, 0.294, 0.304, and 0.34 respectively. Moreover, those wind turbines were testing to demonstrate the maximum moment of the coefficient of 0.158, 0.159, 0.162, and 0.19 respectively [7].
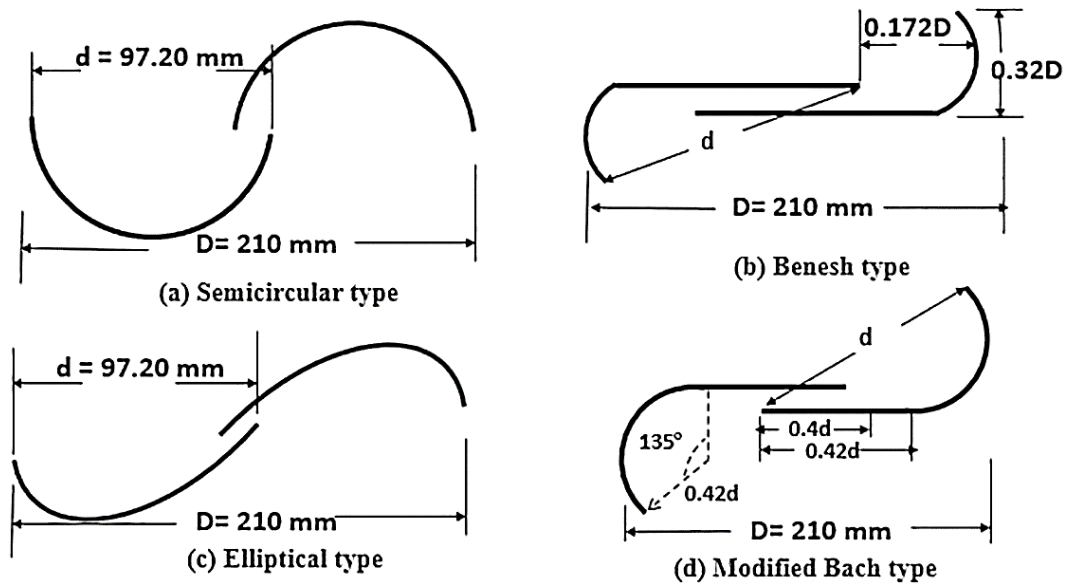
Figure 2.5. Dimension profile of Savonius turbine is investigated by [7]

Another auditor has been tested by simulating in three different shapes configurations of the Savonius turbine such as standard shape, Bach shape of arc angle 124^0, and Bach shape of arc angle 135^0; the simulation had implemented without rotating shaft moreover, the turbulence model of k-kl-ω transition is used for this model; based on this work the progressing is applied in different of the constant wind speed (4m/sec and 7m/sec); the result has been found that Bach type profile 135° had reached on the average static torque efficiency 0.45 and 0.451 at wind speed 4m/sec and 7 m/sec respectively compared to the standard Savonius and Bach type profile 124°[11]. Figure 2.6 is modified the power coefficient of the Savonius turbines that are described by different profiles and stream velocity. In addition, it has detailed the parameters and static coefficient for the simulation.

(a)

(b)

Parameter	Variations
Blade type	Standard (half semicircular cylinder with overlap), Bach-profile with arc angle $\alpha = 124^0$ (no overlap), Bach-profile with arc angle $\alpha = 135^0$
Rotor angle	0^0, 30^0, 60^0, 90^0, 120^0, and 150^0
Freestream speed	4 m/s and 7 m/s ($Re_{blade} \approx 43,500$ to 93,000)

(c)

(d)
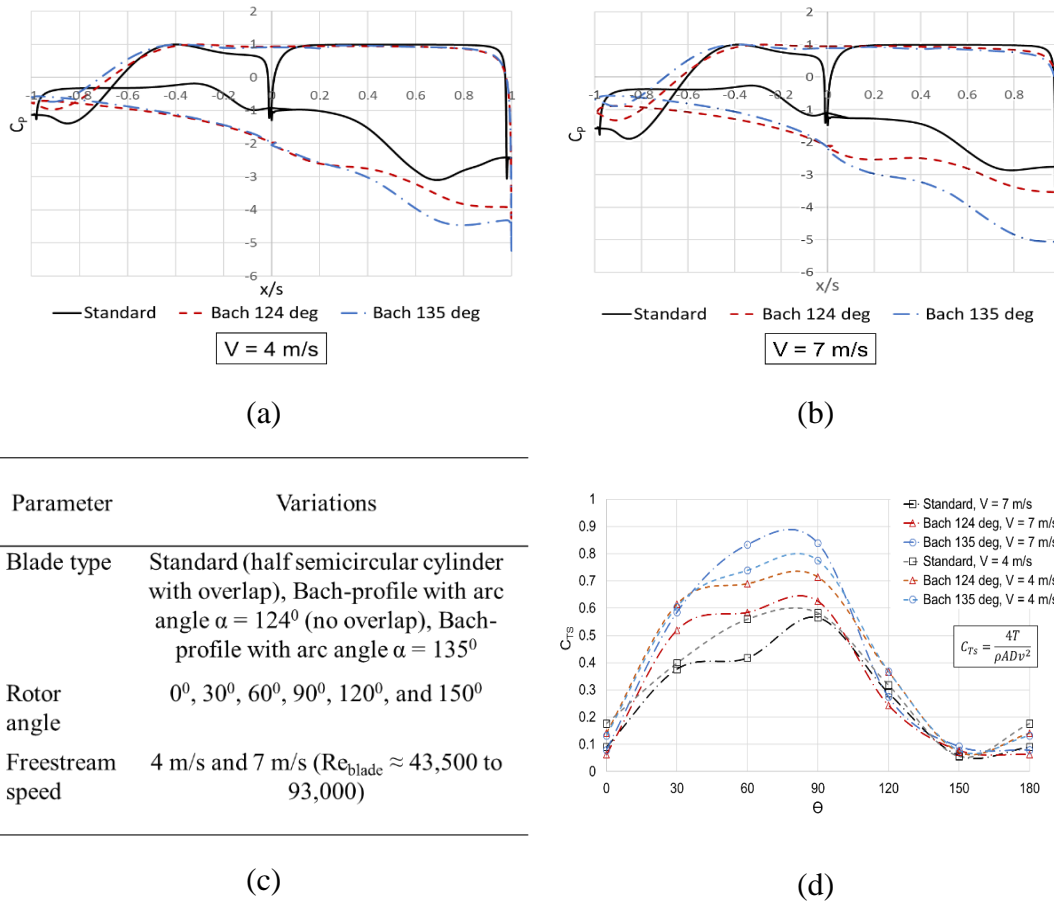
Figure 2.6. The characteristics of the Savonius turbine, (a) pressure coeff. of V=4 m/sec, pressure coeff. of V=7 m/sec, (c) parameter for the model, (d) torque coeff. [11].

2.4 Darrieus rotor

Darrieus wind turbine is a type of VAWT where generates electricity from wind energy. Also, high rotational speed and high efficiency can simplify. It was innovated and designed by Geores Jean Marie Darrieus, a French aeronautical engineer filing for the patent was October 01, 1926 [29]. The rotor application has been using the feature of the airfoil to construct and tested within numerical or experimental. However, Horatio F. Phillips, 1884, has patented and developed airfoil shapes. He was an Englishman who invented out the first serious wind-tunnel experiments on airfoils, moreover, in 1902, the Wright brothers conducted their airfoil tests in a wind tunnel, developing relatively efficient shapes [30].

The discussion such as the double multiple stream tube, vortex, and cascade models have been carried out extensively by many research activities. Also, They have been defining the strength and weaknesses of several aerodynamic performances and computational models [12]. The configuration of the Darrieus wind turbine is divided into two types as shown in Figure 2.7.
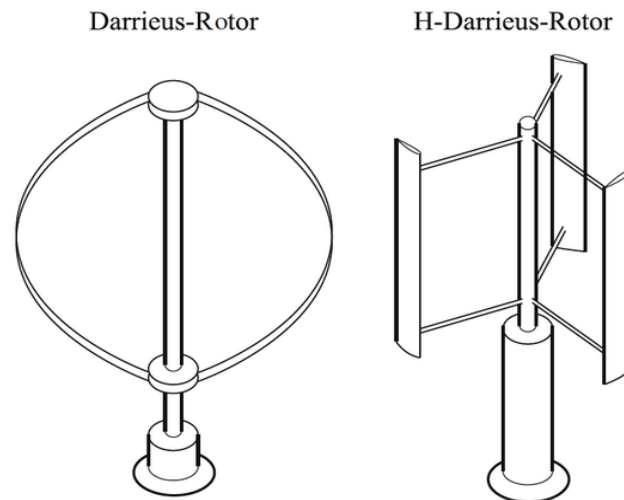
Figure 2.7. Feature of airfoils motion in space.

2.4.1 Airfoil shapes

The immersion solid body into the fluid surrounding it, where is relative motion, the body will implement the net force. The magnitude of the force depends on many factors such as fluid properties, relative velocity, and certainly the shape and size of the body. As it can be attempted to derive the net force by integrating these over the body surface. Based on [], the pressure distribution is computed depends on the shape of the immerge body. Then integrate the pressure over the body surface to obtain the contribution of the pressure force to the net force.

Airfoil is a significant shape of a cross-sectional blade that is for fluid occurs an aerodynamic force. The component of the force perpendicular to the direction of motion is called lift whereas parallel is call drag. The characteristic of the airfoil as shown in Figure 2.8.
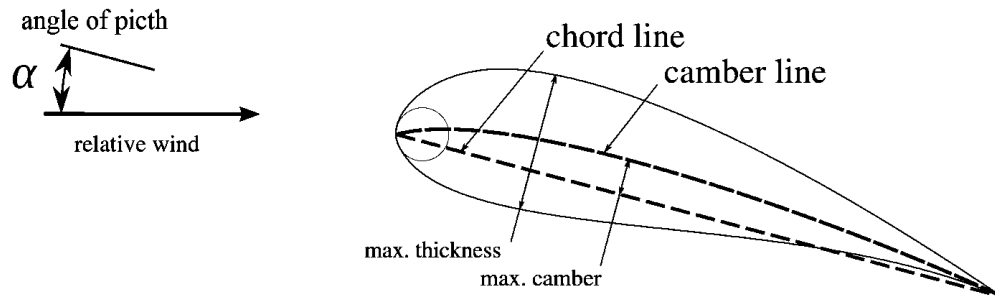
Figure 2.8. Airfoil feature.

It is assigned the name position of the airfoil. The analysis on a series of 4-digit NACA airfoil shape characteristic and its aeroacoustics performance is performed by unsteady CFD flow simulation, the procedure is identified the optimum symmetric and asymmetric airfoils, which the model has been performed with Mach number of 0.2, the turbulent intensity of 1%, Re_c of 1.4 million, the length of a chord of 0.3, and attachment angle of 20 deg, As the result is shown the better optimum combined aerodynamic performance of NACA 0018 and 0024 for symmetric airfoil [6].

| (a) | (b) |
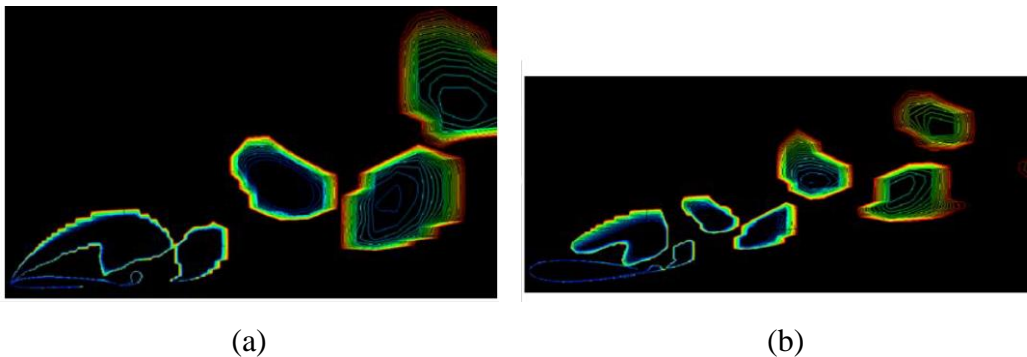
Figure 2.9. Vortex structure through airfoil, (a) NACA 2419 (b) NACA 0018 [6]

Another auditor has been implemented on airfoils by various several configurations for obtaining high torque and best power coefficient; however, the two types of airfoils are defined and compared to which one is the higher value of the power coefficient. The result has reported the effects of surface condition on the lifts and drags configuration [31].

The aerodynamic force is applied on the NACA-2415 camber by varying attack angles, Also, the results between CFD and experimental data were validated. At the final, the average torque is established by the model has been defining that

the cambered airfoil of NACA-2415 is self-starting. Also, the power coefficient of the simulation shown a reduction in peak efficiencies [10]. At a TSR, NACA-2415 has sought a peak of the power coefficient as shown in Figure 2.10.

<div align="center">(a)   (b)</div>
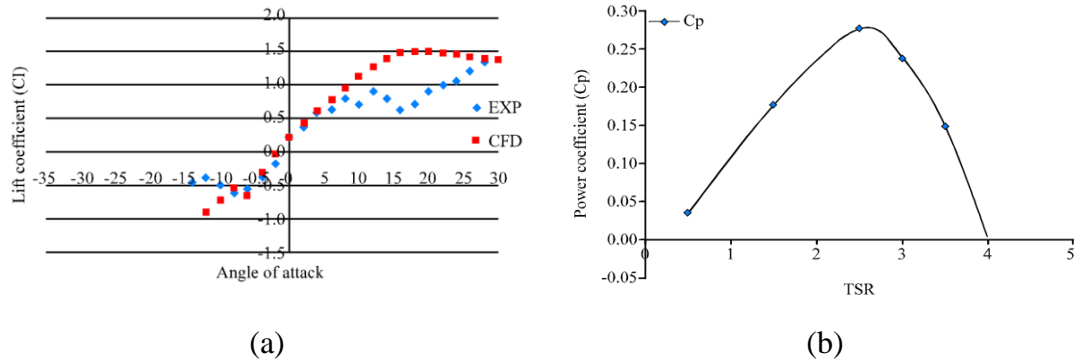
Figure 2.10. The experiment data compare with the simulation of NACA-2415 [10].

2.4.2 Power coefficient C_P

The power coefficient is a factor for modifying wind turbine efficiency. C_p is the ratio of actual electric power (available) conduct by wind turbine divide by the total wind power which is flowed through the turbine blade at the specific wind speed.

The key components to derive a mathematical concept for H-Darrieus rotor:

- Calculations of local relative velocities and angle of attacks at different tip speed ratios and azimuthal (orbital) positions
- Calculation of ratio of induced to freestream velocity ($V_a =V$) considering the blade/blade-wake interaction
- Mathematical expressions based on different approaches to calculate normal and tangential forces
- 'Pre-Stall airfoil characteristics' (C_l, C_d, and C_M) for the attached regime at different Reynolds numbers/stream velocities
- 'Flow Curvature Model' to consider the circular blade motion.

The aerodynamic performance for the H-Darrieus rotor is based on the feature of the wing blade. The significant parameters are that the airfoil shape, the

reduction frequency, mean angle, Mach number, Reynolds numbers, types of motion, three-dimensional effect, and turbulent level effect. This statement will explain the mathematical theory and literature review of the Darrieus wind turbine.

The velocity of the upstream and downstream side are differences of the Darrieus-type and still variable depend on the wind speed velocity. The following expression of the velocity components presents to include the collinear velocity of the chord line and normal velocity below [12].

$$W = \sqrt{V_c^2 + V_n^2} \qquad 2.22$$
$$V_c = R\omega + V_a \cos\theta \qquad 2.23$$
$$V_n = V_a \sin\theta \qquad 2.24$$
$$V_a = V(1-\alpha) \qquad 2.25$$

where: V_a: is the axial velocity through the rotor, V_n: the normal velocity

$$\alpha = \tan^{-1}\left(\frac{V_n}{V_c}\right) = \tan^{-1}\left(\frac{(1-a)\sin\theta}{(1-a)\cos\theta + \lambda}\right) \qquad 2.26$$

where λ is the tip speed ratio of the turbine.

(a)   (b)
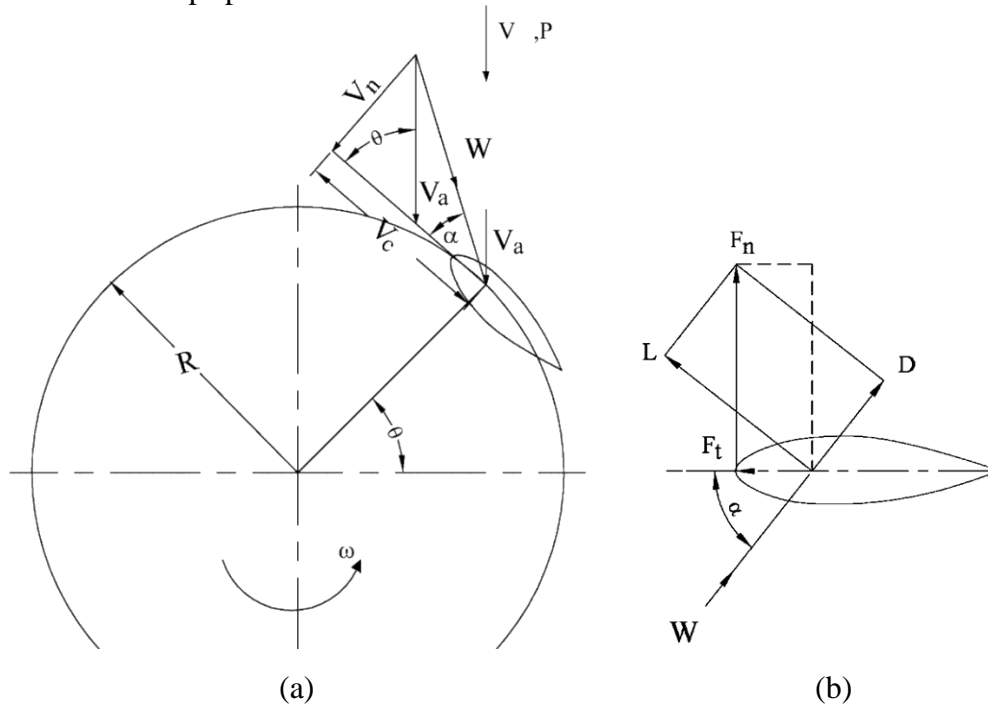
Figure 2.11. Free body diagram of H-Darrieus wind turbine [12].

The normal tangential coefficients (C_t) defined as:

$$C_n = C_L \cos\alpha + C_D \sin\alpha \qquad\qquad 2.27$$

$$C_t = C_L \sin\alpha - C_D \cos\alpha \qquad\qquad 2.28$$

The net tangential and normal forces can be defined as

$$F_t(\theta) = \frac{1}{2}\rho C_t chW^2 \qquad\qquad 2.29$$

$$F_n(\theta) = \frac{1}{2}\rho C_n chW^2 \qquad\qquad 2.30$$

The n blades were produced the average torque form tangential force acting form the blades:

$$T(\theta) = \frac{n}{2\pi}\int_0^{2\pi} F_t(\theta)Rd\theta \qquad\qquad 2.31$$

The instantaneous thrust force (T_i) on a single airfoil at a certain azimuth angle θ

$$T_i = \frac{1}{2}\rho V_R^2 hc(C_t \cos\theta - C_n \sin\theta) \qquad\qquad 2.32$$

The instantaneous torque (Q_i) defined on an airfoil at azimuth angle, as:

$$Q_i = \frac{1}{2}\rho V_R^2 hcC_t R \qquad\qquad 2.33$$

The equations below which are defined as the power generated by kinetic energy or power of wind stream:

$$P_{turbine} = Q\omega = \frac{2\pi NQ}{60} \qquad\qquad 2.34$$

$$P_{avaialable} = 0.5\rho AV^3 \qquad\qquad 2.35$$

First, the moment coefficient is presented based on the characteristic of the turbine:

$$C_M = \frac{Q}{Q_{available}} = \frac{Q}{0.5\rho ARV^2} \qquad\qquad 2.36$$

As shown in the expression below, it generally defined as the ratio of the electrical power produced by the wind turbine. In terms of the power coefficient commonly used to designate the efficiency of the entire turbine power system.

$$C_p = \frac{P_{Turbine}}{P_{available}} = \frac{Q\omega}{0.5\rho A V^3} = \frac{Q}{0.5\rho A V^2 R} \cdot \frac{R\omega}{V}$$

$$C_P = C_M TSR \qquad\qquad 2.37$$

Thus, the numerical simulation will be extracted the value of C_M then, C_P is found by the equation (2.26).

2.3.1 Tip Speed Ratio (TSR, λ)

The tip-speed ratio, which is an important parameter related to the power efficiency that consisted of the optimum radius of the wind turbine and wind velocity. TSR is definitely of the ratio between the tangential speed of the tip of a blade and the actual stream velocity V.

$$\lambda = \frac{R\omega}{V} \qquad\qquad 2.38$$

2.3.2 Solidity

The solidity is a ratio which is the most important that can be affected by the aerodynamic performance of the wind turbine. The solidity has been described as the ratio that modifies the relationship of the total area of the turbine blades to the swept area of the turbine. In case, this equation applied forward to the H-rotor. The optimal value of the solidity would be identified for the best performance of the turbine.

The equation as shown below is definitely look forward to the solidity formulation:

$$\sigma = \frac{Nc}{D} \qquad\qquad 2.39$$

The optimum value of the solidities and number of blades had optimized, these values were the impact of the performance of the turbine. Also, this working area has been performed by numerical simulation [8]. Figure 2.12 as shown below are diffident of the number of blades turbines in the range of solidities ratios within a graph of the coefficient of power via tip speed ratio.

(a)   (b)
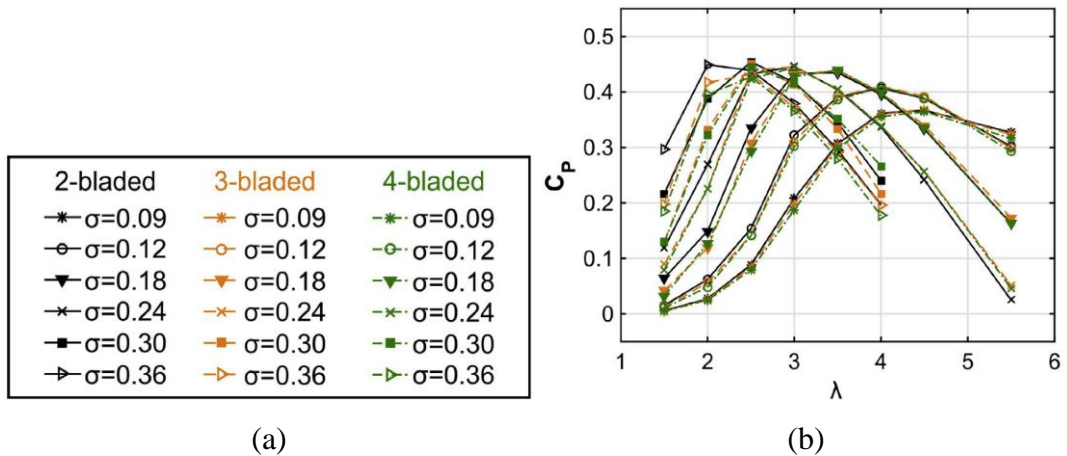
Figure 2.12. The number of blades and the coefficient of the moment [8]

(a)   (b)
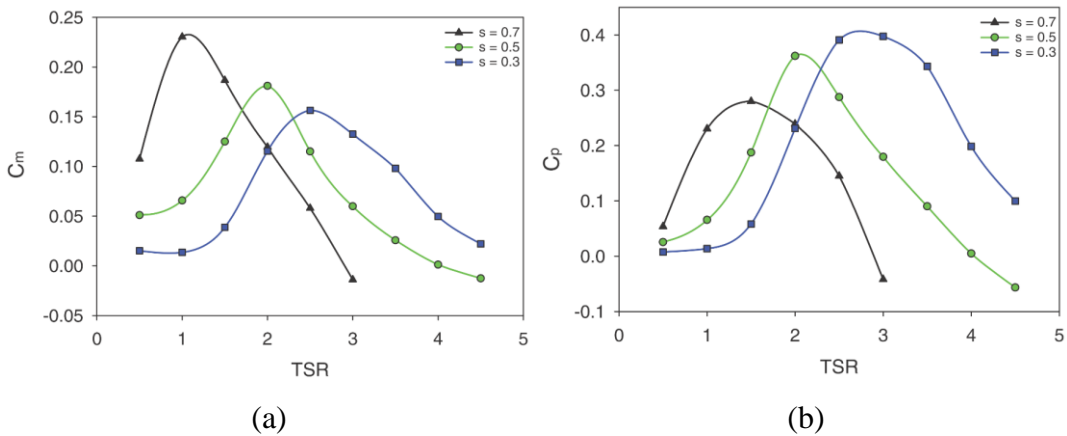
σ	0.7	0.5	0.3
λ_{opt}	1.5	2.0	2.8
C_{Pmax}	0.280	0.362	0.391

(c)

Figure 2.13. The output of the turbine, (a) coefficient of the moment, (b) coefficient of power of each optimum TSR [16].

For another auditor [16] has been conducted H-type Darrieus wind turbine with different turbine solidities, the whole implement is invented by modeling of k-omega SST where is varied in three different solidities of (0.3, 0.5, and 0.7) at velocity inlet 8 m/sec, the result of the research paper is obtained the best configuration at a solidity of 0.3 with TSR of 2.8. Figure 2.13 as shown below are described the results in different solidities ratios of the single H-Darrieus rotor with

the tip speed ratio. There is ultimately for the solidity of 0.7 that is extracted higher of the coefficient of the moment at the low TSR of 0.5.

Another applicant has been performed the configuration that is implemented on the variation of the solidities ratios and the number of blades turbine, it is notified that the whole models were performed with a diameter of H-Darrieus rotor of 2.5 m, inlet velocity of 10 m/sec, and the solidity form as $\sigma = Nc/D$, the outcome of this application has been achieved for the best configuration where is fitted to the parameter at the low TSR such the two, three, and four blades reached the coefficient of power of 7.51%, 14.56%, and 8.07% respectively that is compared to the conventional research [19]. Figure 2.14 as shown below has been describing each of the features of the coefficient of the moment with the range of TSR.
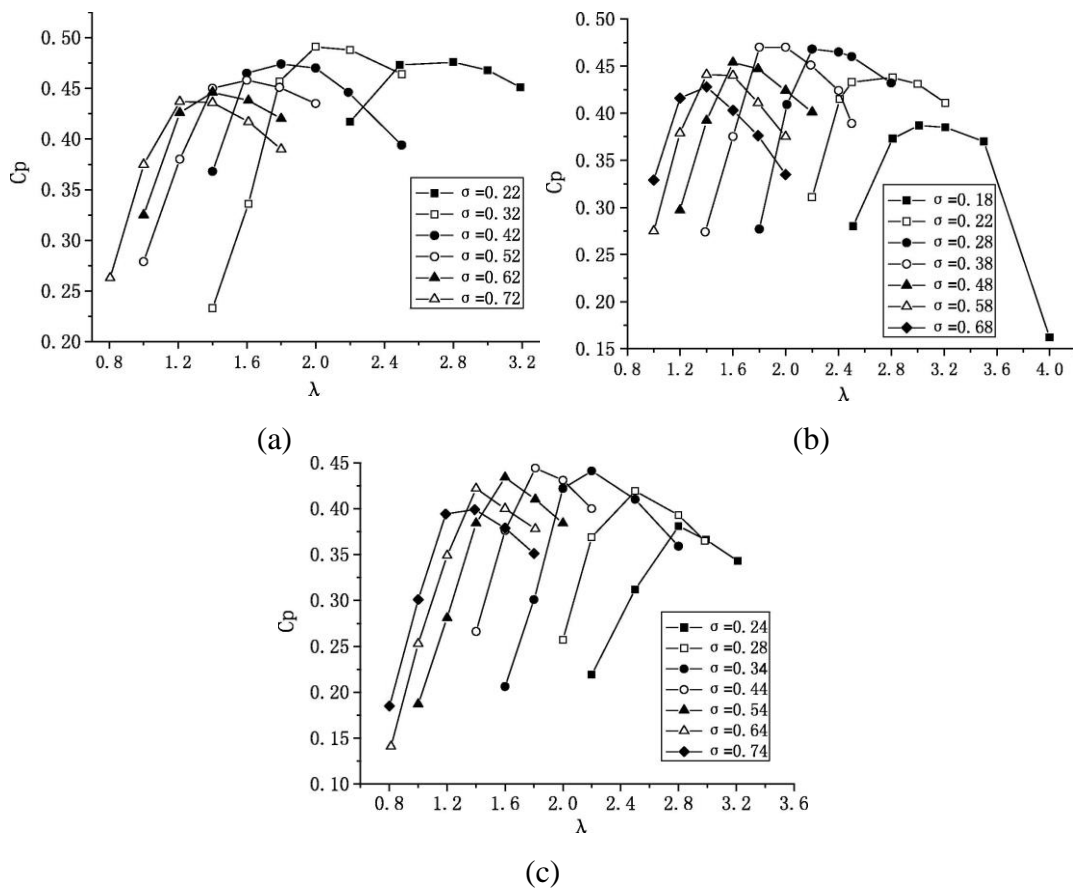
Figure 2.14. C_P via TSR, solidity variation, (a) Two blades, (b) three blades, and (c) four blades [19].

Based on the previous research has been performed the different solidities of the wind turbine, hence it can be notified that while the solidity of the rotor is increased, the coefficient of the moment is increased also at the range of TSR.

The variation of the pitch angle of the turbine is affected by the power coefficient such a small negative pitch angle $\alpha = -2^o$ that can be slightly increased by 6.6 % of the turbine C_P compared to $\alpha = 0$. Besides, the fixed pitch angle also affects the immediate average load and power conservation for VAWT; moreover, the pitch angle shifts found that a change in instantaneous loads and moments between upwind and downwind halves of the turbine. The shift in the instantaneous moment during the revolution for various pitch angles suggests that dynamic pitching might be a very promising approach for further performance optimization [32].

Figure 2.15 is looked forward to the shape of airfoils contained by the high-power coefficient of a TSR. The geometry of the Darrieus rotor is commonly affected by aerodynamics forces. It is an important rule for consideration before investigating turbine to obtain high efficiency, the examination for varying the maximum thickness (12%, 15%, 18%, and 21%) by using CFD technology; also, the power and torque characteristics studied within the power coefficient have found the optimum value following by trend of $C_{P\_NACA\,0018} > C_{P\_NACA\,0015} > C_{P\_NACA\,0021} > C_{P\_NACA\,0012}$, moreover the optimum TSR and operational zone also increase with the decrease in airfoil thickness, additionally, an optimized airfoil thickness is

(a)   (b)
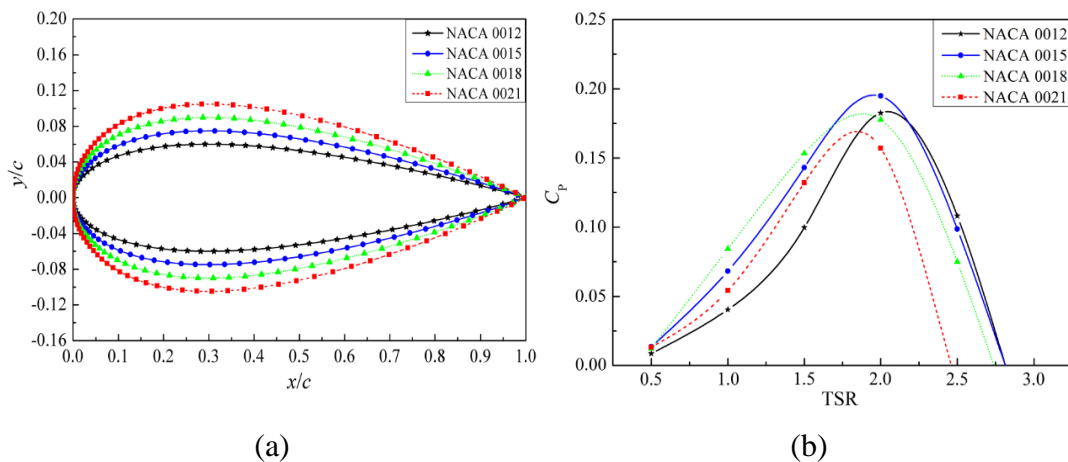
Figure 2.15. The different types of the airfoil, (a) the different shapes of the airfoil, (b) the value C_P of the symmetric airfoil [18].

27

determined to be between 15% and 18% for a relatively high power coefficient and appropriate optimum TSR equal to two, as well as a wider operational zone and a high-efficiency band [18].

The small size of the Darrieus vertical wind turbine has been investigating via Ansys/Fluent by using a SIMPLE algorithm, *SST-kω* turbulence model for this simulation. Meanwhile, the different chambers are NACA-0012, 2412, and 4412 respectively, the pitch angle various between -10° and 10° are discussed; hence, the result showed that the initial acceleration is large at -10° and decreases monotonously as the pitch angle increases from -10° and 10° furthermore, it was notified of NACA-4412 is the best for the self-starting ability of VAWT, finally, the root mean square moment for NACA-2412 are much higher than those of either within pitch angle θ =5° [15]. Figure 2.16 is detailed about the velocity outline on the airfoils of the Darrieus turbine by obtaining high C_{Ms} at the pitch angle of θ=5°.

	(a)			(b)	
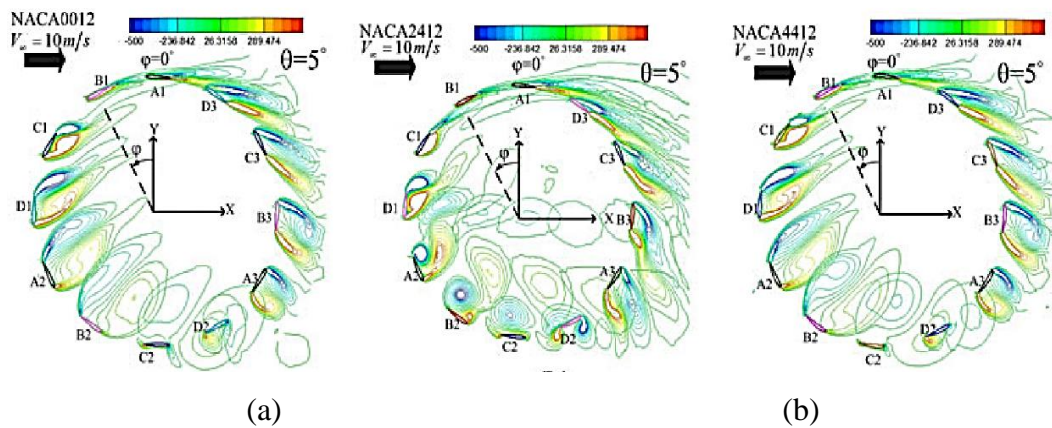
θ	−10°	−5°	0°	5°	10°
NACA0012					
$C_{Mr.m.s}$	0.07696	0.07056	0.09774	0.11543	0.09056
C_{Ms}	0.09363	0.13984	0.16402	0.19564	0.27441
NACA2412					
$C_{Mr.m.s}$	0.09073	0.09941	0.102	0.17339	0.13726
C_{Ms}	0.19357	0.20102	0.20063	0.22406	0.23361
NACA4412					
$C_{Mr.m.s}$	0.10338	0.09699	0.09468	0.09617	0.06906
C_{Ms}	0.1755	0.18811	0.18356	0.204	0.22712

The pitch angle change from −10° to 10° for the blade of different cambers (NACA0012, NACA2412 and NACA4412). The inflow speed is 10 m/s

(c)

Figure 2.16. The velocity profile at V=10 m/sec, (a) the profile of NACA 0012, (b) the outline of NACA2412, (c) the profile of NACA4412, and (d) moment coefficient variations of root mean square [15]

28

2.5 Combined rotors

Since the previous research of Savonius and H-Darrieus rotor has been stated in the previous section. Hence, the statement below will continue to describe the characteristic within the parametric of combined rotors. Also, it will extend some previous researches who have established the proper performance based on the configuration. Therefore, Figure 2.17 is prescribed as the characteristic parameters of the present work.

2-D configuration as shown below also define the specific parameters of the hybrid wind turbine. Each airfoil of H-Darrieus wind turbine divided into 120 deg in a cycle, theta (θ) is an angle where positional between Savonius and H-Darrieus rotor, chord length (*c*) are significant which is relating to the solidity ratio, the stream velocity is inserted flowing from the left side of the boundary of the wind turbine, the turbine is definitely rotated counterclockwise around x-y plan axis.
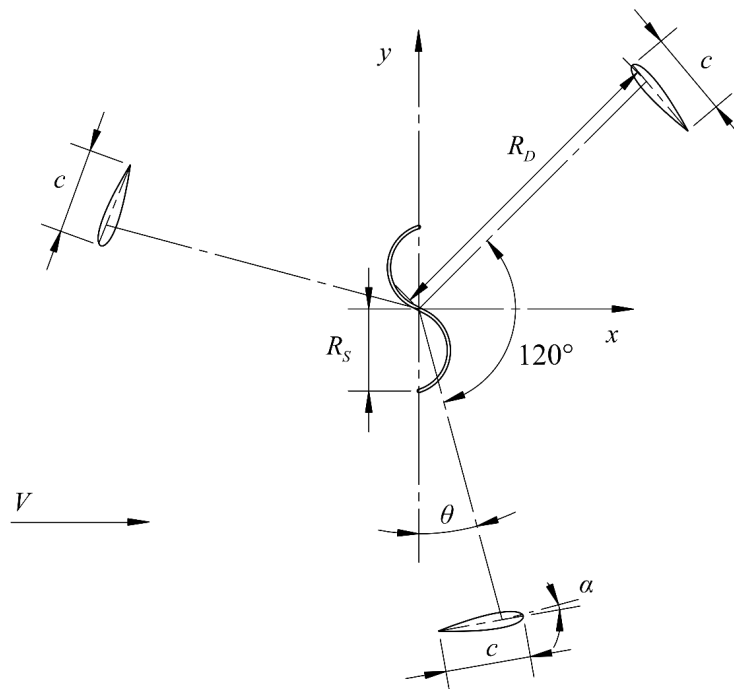
Figure 2.17. Characteristic of the combined rotor.

As the earlier research has been stated on a significant parameter for the combined rotor that is called the radius ratio (KD). The equation as shown below is characterized by the radius of the Savonius over the radius of the H-Darrieus rotor.

The balancing of the KD is an important parameter that makes a combined rotor became more beneficial [17].

$$KD = \frac{Radius\, Savonius}{Radius\, Darrieus} = \frac{R_S}{R_D} \qquad (2.40)$$

Savonius turbine is stated as a self-starting in the omnidirectional of wind speed regimes. The Darrieus rotor also provided a high-power coefficient, but it has low starting torque. High performance of the combined rotor was attributed to the Darrieus rotor for the observed highest relative speed of the combined rotor for the highest pressure and speed drop across the combined rotor at low overlap like 15.37% [33].

Another implement is verified on water channel, the configuration as shown in Figure 2.18 is used for testing on this research, while the progressing is varied on attaching angle (β) by changing β of 0, 45, 90, 135 deg; this research is worked on combined rotors and the result is compared to the single Darrieus and Savonius turbine, the maximum torque is presented when $\lambda = 2.9$ [14].

(a) (b)
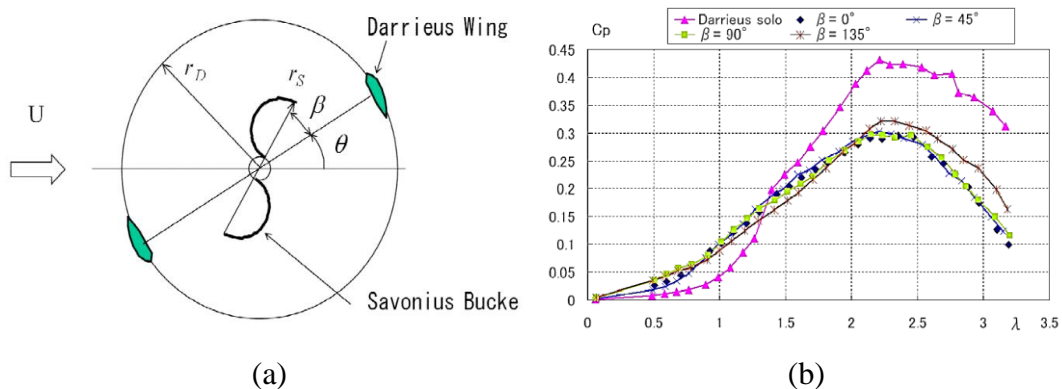
Figure 2.18. The experiment studies combined rotors, (a) the configuration exhibited of varying β, (b) C_P obtained from Darrieus solo and hybrid turbine.[14]

The high starting torque and power exhibited combined rotors, the high performance of combined rotors was assigned to the Darrieus rotor for the observed highest relative speed of the combined rotors and also for the high pressure at low overlap about 15.37 % [25].

Figure 2.21 has been presented of the hybrid rotor. It is investigated good performance but has affected by some parameters such as radius radio (KD) and

attachment angle (θ). Be focusing on the variation of these two parameters, so the optimum value of C_P was 0.363 by attributed within numerical simulation with starting torque below 0.1 Nm at a wind speed of 2 m/sec [20], the archived configuration of the combined rotor of this context aimed at N=2, KD=1/4, θ=0.

Figure 2.19 is the configuration of the hybrid rotor that is investigated on the parameters of the Darrieus-Savonius rotor which are blade number (N) and radius ratio (KD). The value of torque depends on the high radius of the turbine, interaction force from wind speed, and the influence of Stagger angle (θ) in a combined rotor [17].

(a)   (b)
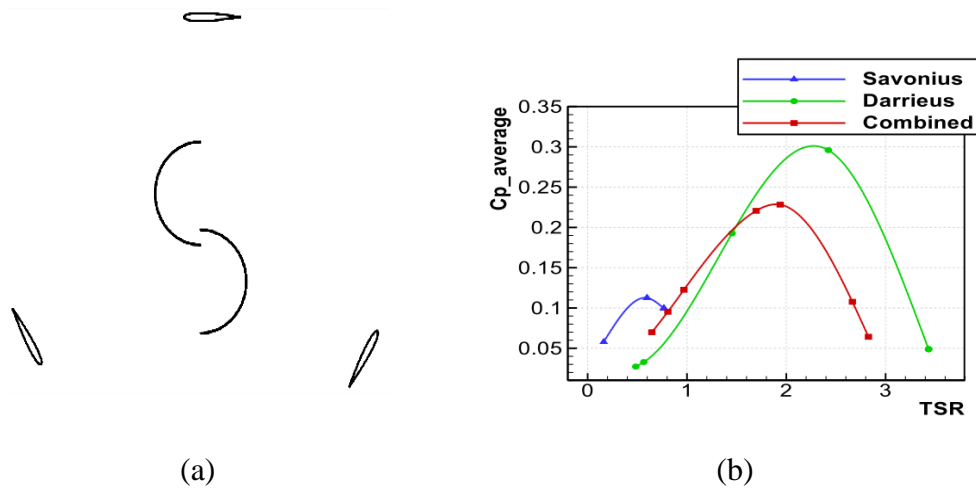
Figure 2.19. The configuration of the combined rotors, (a) configuration utilizes for the model, (b) the power coefficient of the different types of turbines [17]

(a)   (b)
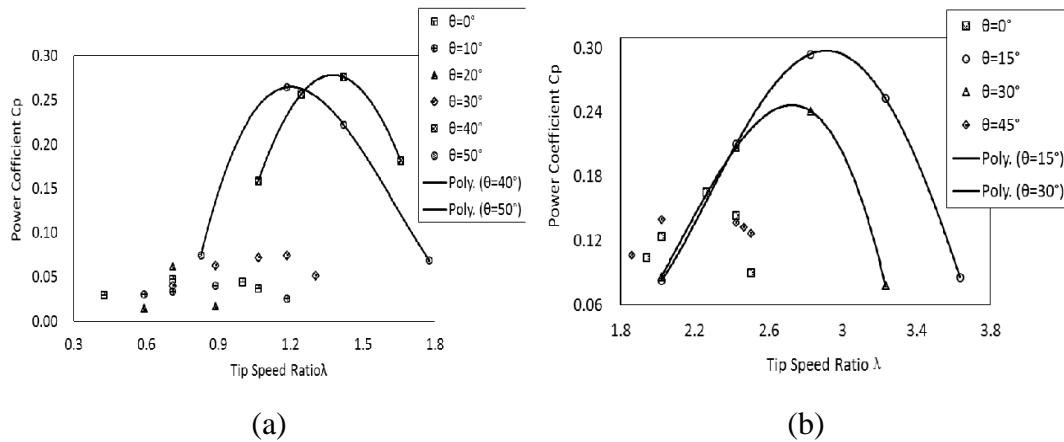
Figure 2.20. The peak C_P of the turbine by different KD and stagger angle (θ), (a) the maximum C_P at θ=40 deg, (b) the maximum C_P at θ=1 [17].

Figure 2.20 is also shown the high value of the C_P of the best two configurations. Darrieus-Savonius combined rotor N=3, KD=0.54, the optimum stagger angle (attachment angle, θ) of 40 degrees and Darrieus-Savonius combined rotor N=3, KD=1/4, the optimum stagger angle of 15 degrees are underworked on this research. The negative torque found when the value of KD is small, the good performance of the turbine already suggested within KD's value should be below 0.5 [20].

(a)   (b)
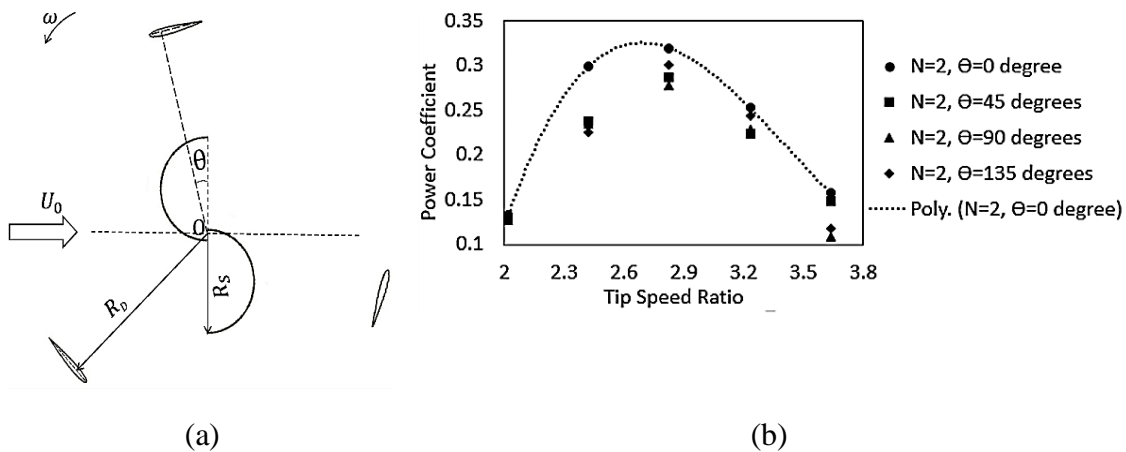
Figure 2.21. The performance of the combined rotor, (a) the hybrid turbine feature, (b) C_P of two airfoil blades combined with two Savonius blades [20].

The combination of both Darrieus and Savonius rotors is implemented by the simulation, however, the result as shown in Figure 2.22. The 2-D, 18 CFD transient simulations were processing on moving mesh. The other parameters value which carried out the turbine high performance such as overlap ratio (ε), arc angle

(a)   (b)
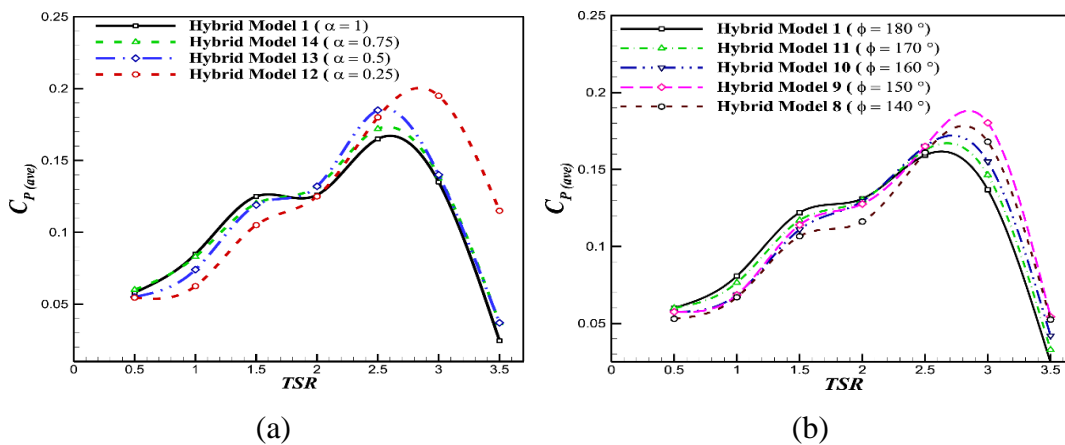
Figure 2.22. Multiple studies of hybrid turbine, (a) C_P value by various α, (b) C_P value by various ϕ.

(α), and curvature (ϕ) of 0.25, 0.25, 150°; the optimum value of the parameter has increased by 12 percentage compared to conventional vertical axis turbines. On the other hand, the turbulent model k-ω, SST applied to predict flow characteristics [26].

Based on Figure 2.23 the power coefficient had comprehended to optimize by the novel configuration of hybrid VAWT, it was found that Darrieus turbine had a high power coefficient (C_P) about 48.4% at a TSR of 2.5, the self-starting has been demonstrated [9].
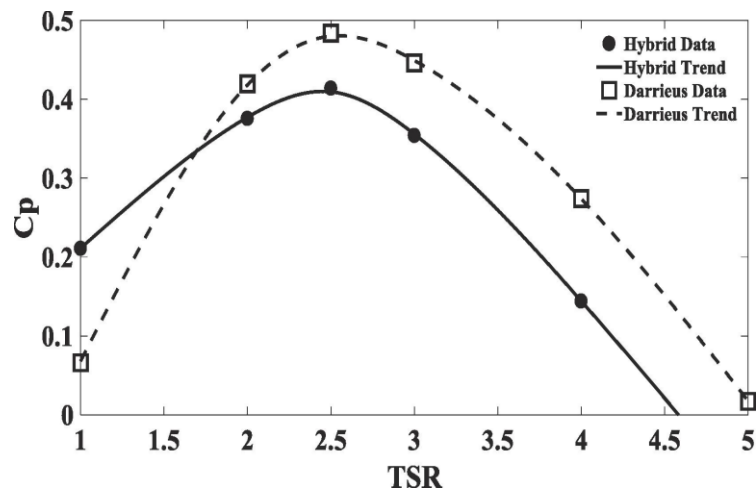
Figure 2.23. The comparison C_P of the hybrid and the Darrieus turbine [9].

According to what the pieces of literature are stated about the combined rotor with many important parameters which are definitely related to the performance of the combined rotor. Furthermore, Table 2.3 is summarized to modify more about efficient parameter by following below:

Table 2.3. The summary of the earlier research histories.

Reference	Geometric and set up the parameter								Other parameters	Observation
	σ [-]	c [mm]	θ [deg]	N_D[-]	N_S [-]	Re [-]	λ [-]	OR [-]		
Y. Kyozuka et al. Feb. 2008 (Exp.) [14]	0.106	100	0, 45, 90, and 135	2	2	-	$\approx$ 0-3.2	-	Stream velocity 0. 6, 0.8, and 1 m/sec	Combined rotor found *Cp* higher at λ=2.9 compared to solo Darrieus rotor
S. Bhuyan and A. Biswas, Aug-2014 (Exp.) [34]	-	100	-	2	2	144×10^5 - 2.33×10^5	1.5 - 2.5	0, 0.10.- 0.2	AR=1, Shaft =15	C_P = 0.34 at λ=2.29, ε=0.15 and Re of 1.92e5

Reference										Notes
Xiaoting Liang et al. May-2017 (Num.)[20]	-	220	0	2, 3, 4	2	-	0.5, 1, - 4	0.1	KD = 0.25	C_P max 0.363, Best approx. with k-ε, Optimum N_D=2, KD=1/4
A. Hosseini and N. Goudarzi, March-2019 (Num.)[9]	0.5	-	-	3	2	1827300	1, 1.5 -2, 2.5, 3, and 4	1.5	KD=0.25	Using model k-ω SST, Maximum C_P of 41.4% at a TSR of 2.5
A. Roshan and A. Sagharichi, Aug-2019 (Num.) [26]	0.5	85.8	-	3	2	-	1.5, 1-3.5	0.1	σ, α, ϕ	Predict flow by k-ω SST, the optimal value parameter α=0.25, ϕ=150 degree and OR=0.25 which increase 12% of C_P

β: Pitch angle, θ: azimuth angle, σ: Solidity, c: chord length, N_D: Darrieus blade number, N_S: Savonius blade number, Re: Reynold number, C_P: Power coefficient, C_t Torque coefficient, OR: Overlap ratio, λ: Tip speed ratio, k: turbulent kinetic energy, ε: dissipation of turbulent kinetic energy, ω: specific rate of dissipation, α: curvature ratio, ϕ: arc angle, C_M: Moment coefficient, AR: Aspect ratio, KD: Radius of Savonius and Darrieus ratio, Num.: Numerical study, Exp.: Experiment

CHAPTER 3
METHOD

This chapter has been presented the configuration of the combined rotor and the turbine blades feature. Furthermore, the computational has been modeled by implementing the method that is fit to this present work, including on the technique in each case of the simulation. In addition, the meshing procedure has been implemented to define the size of the suitable element for the domain contours.

3.1 Hybrid rotor configuration

Many researchers have already done to prescribe parameters that are implemented in the turbine getting high efficiency to the combined rotors, as shown in the literature review section. Although, this present study will be stated to define another characteristic of the combined rotors, which is the Savonius rotor has an ultimate feature of the capability of self-starting.

However, the simulation is performed base on the variations of the H-Darrieus rotor feature that is included two different types of NACA standard airfoil, which is symmetric (NACA-0018) and asymmetric (NACA-2415). The simulation will simulate through various solidities ratio at wind speed inlet of 4 m/sec, while the TSR had been varied as well. The sections below will show the characteristic and meshing technic for the simulation:

3.1.1 Savonius blade

Depend on the earlier researcher had done to determine the best feature for the Savonius turbine [11, 17, 20], meanwhile, this present study will extend more into the Savonius blades by driving into the specific diameter from PVC pipe that has the nominal diameter of 4 inches, in which the bucket angle of 135 deg. In addition, the configuration of the turbine is defined as the zero overlaps ratio as shown in Figure 3.1. The specific dimension of the configuration of the Savonius turbine has been shown in Table 3.1.

Table 3.1. Specification of Savonius turbine.

Blade type	Overlap Ratio (e/D)	Shape factor (p/q)	Rotor diameter (D_S, mm)
Bach-profile arc angle 135°	0	0.2	255
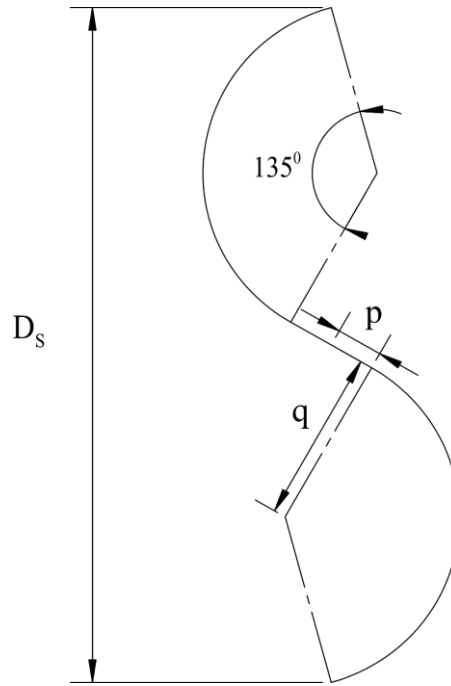
Figure 3.1. 2D-configuration of the Savonius Turbine [11].

3.1.2 NACA airfoil

Airfoil is one of the best features for an aerodynamic force for lift and drag of the wind turbine model, in addition, the previous research is found that airfoil is suitable for investigating Darrieus turbine, hence, this present work will be applied the different shapes of airfoils to define the best concepts and high power coefficient, while attributed into NACA standard, as shown in Table 3.2, Figure 3.2, and Figure 3.3 [35].

Table 3.2. Airfoil configuration data

Airfoil	Chord Length (m)	Maximum thickness (m)	Maximum camber (m)
NACA 0018	0.1	0.018	0
NACA 2415	0.1	0.015	0.002
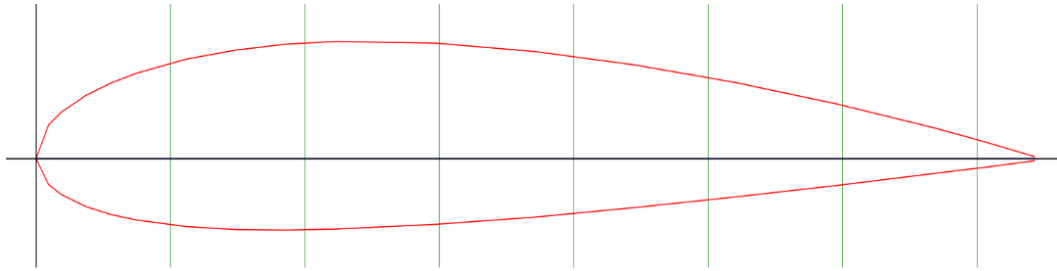
Figure 3.2. Symmetrical NACA-2415 Standard Airfoil
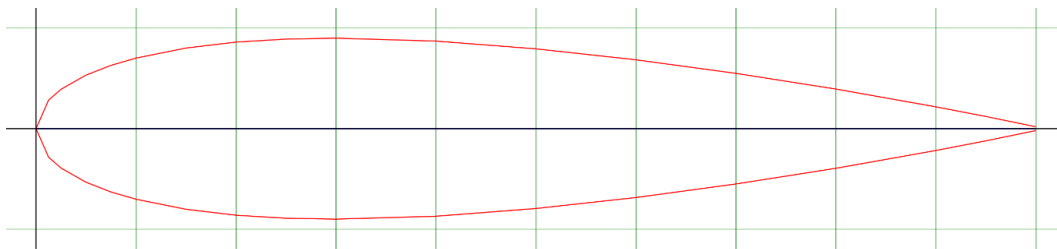
Figure 3.3. Symmetrical NACA-0018 Standard Airfoil

3.1.3 Configuration of the hybrid rotor

H-Darrieus and Savonius are combined together which is called a hybrid turbine. Darrieus rotor will be investigated, consist of three airfoils while it divided the azimuth angle of 120 deg, the attachment angle is 15 deg with the x-axis, and 5 deg of pitch angle. In this case, the model will be studied to compare two-hybrid turbines in the range of the TSR. Also, the variety of the solidities ratios will be performed after the best airfoil shape chosen. Table 3.3 shown the configuration of a hybrid turbine parameters.

Table 3.3. The information of combined rotors

Turbine characteristic	Quantity	
	Darrieus rotor, [10, 15, 18]	*Savonius rotor, V. S. Djanali [11]*
Blade profile	NACA-0018 & NACA-2415	Blade angle 135º
Chord length (m)	0.066-0.266	None
Rotor diameter (m)	1	0.255
Solidity	0.2-0.8	None

Number of blades	3	2
Free stream velocity (m/sec)	4	4
Blade overlap ratio	None	0
KD ratio	0.25	-
Attachment angle (θ, deg)	15	-
The angle of pitch (α)	5°	-
Turbine length (m)	0.5	0.5
Shape factor (p/q)	-	0.2

As more detail of the turbine body configuration which is shown in Figure 3.4 and it is defined for 2-D of the hybrid wind turbine including the specific parameters.
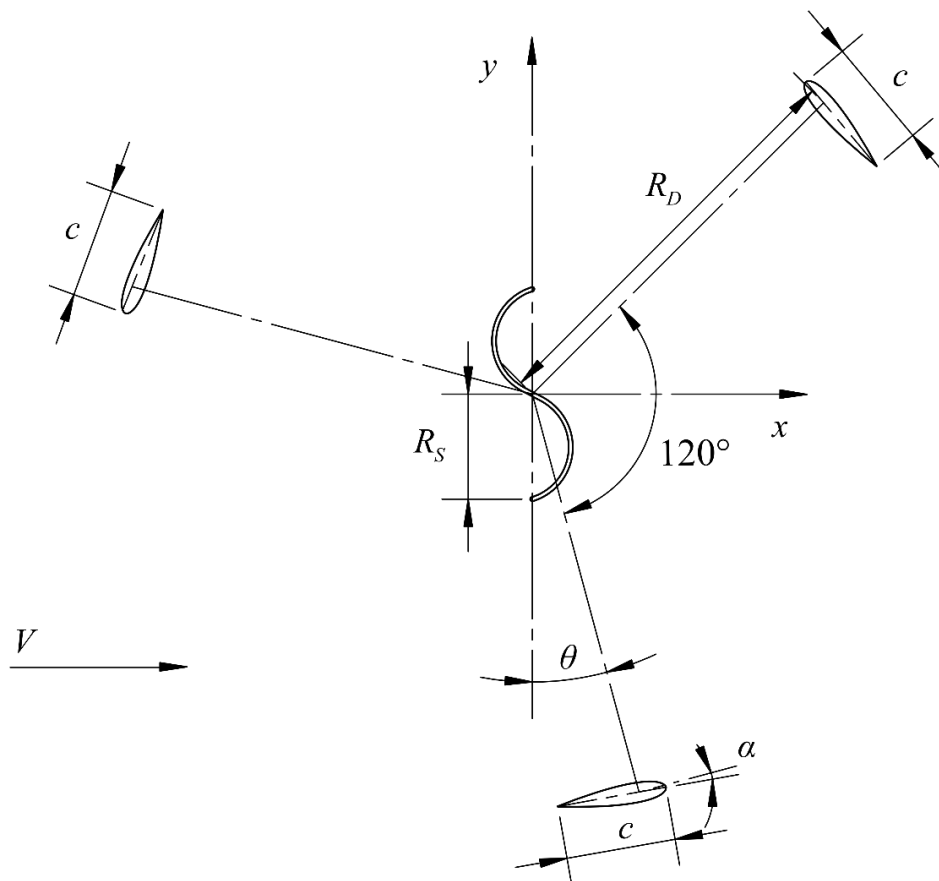
Figure 3.4. Hybrid turbine configuration

3.2 Computational fluid dynamic

The pre-processing contains the input of the flow problem to the CFD program by means of the operator-friendly interface and the subsequent transformation. There are many activities at the pre-processing state.

3.2.1 Mathematical model

The investigating the research goals of this context has been providing in advance CFD techniques, to the simulation is simulated the transient flow of air in the domain of the VAWT. The sliding mesh technique will be applied to rotate the blades of the VAWT. For this purpose, appropriate solver settings and boundary conditions need to be specified.

In general, CFD is the analysis of the systems, including on fluid flow, heat transfer, and referring the phenomena such as chemical reactions based on technical simulation.[36, 37]. The technique is very powerful and spans a wide range of industrial and non-industrial application areas. From the 1960s onwards, the aerospace industry has integrated CFD techniques into the design and manufacture of aircraft and jet engines. Moreover, the method has been practicing on the design of internal combustion engines, combustion chambers of gas turbines and boilers. Also, motor vehicle manufacturers now routinely predict drag and lift forces, airflows in the environment of CFD. Initial validation of such software typically performed using an experimental apparatus such as wind tunnels. CFD is becoming an important software in the design of industrial products and processes.

The conservation of mass, which is defined as the total mass of fluid flow balance, is presented by the mathematical equation below. In general, the conservation equation mostly is derived in three dimensions in contract in this context is applied only two dimensional that related to the scope of the simulation. The differential equation of motion in three directions of a particle form as shown below.

Rate of increase of mass in fluid elements = Net rate of mass into fluid elements

$$\frac{\partial \rho}{\partial t} + \frac{\partial(\rho u)}{\partial x} + \frac{\partial(\rho v)}{\partial y} + \frac{\partial(\rho w)}{\partial z} = 0 \qquad\qquad 3.1$$

$$Div(V) = 0$$

where the density of the liquid is constant.

The above equation in longhand notation written as expression below. This equation describes the net flow of mass out of the element across its boundaries:

$$\frac{\partial u}{\partial x} + \frac{\partial v}{\partial y} = 0 \qquad\qquad 3.2$$

where the equation presented in steady and three-dimensional mass conservation of the continuity in an incompressible fluid flow.

The rate of change of momentum of a fluid particle equals the sum of the forces on the particle is called Newton's second law.[37]

Rate of increase of momentum of the fluid particle = Sum of force acting on the fluid particle

The rate increase of x and y momentum per unit volume of fluid-particle is present by:

$$\rho \frac{Du}{Dt}, \quad \rho \frac{Dv}{Dt}$$

The force that reacted on the fluid divided into two types: first is the surface force, which is including pressure, gravity, and viscous force. Second is body force which content of centrifugal, electromagnetic, and Coriolis force. The x and y-component of the momentum equation given by setting of rate change of x and y-momentum of the fluid particle equal to the total force in the x and y-direction on the element due to surface stresses. The differential equation of motion given below:

$$\rho g_x + \frac{\partial \sigma_{xx}}{\partial x} + \frac{\partial \tau_{yx}}{\partial y} = \rho\left(\frac{\partial u}{\partial t} + u\frac{\partial u}{\partial x} + v\frac{\partial u}{\partial y}\right) \qquad\qquad 3.3$$

$$\rho g_y + \frac{\partial \tau_{xy}}{\partial x} + \frac{\partial \sigma_{yy}}{\partial y} = \rho\left(\frac{\partial v}{\partial t} + u\frac{\partial v}{\partial x} + v\frac{\partial v}{\partial y}\right) \qquad\qquad 3.4$$

These equations of motion are called the Navier Stokes equations. The equations are greatly simplified when applied to incompressible flow with constant viscosity. Under these conditions, it can be simplified the fluid motion.

$$\rho\left(\frac{\partial u}{\partial t}+u\frac{\partial u}{\partial x}+v\frac{\partial u}{\partial y}\right)=\rho g_x-\frac{\partial p}{\partial x}+\mu\left(\frac{\partial^2 u}{\partial x^2}+\frac{\partial^2 u}{\partial y^2}\right) \qquad 3.5$$

$$\rho\left(\frac{\partial v}{\partial t}+u\frac{\partial v}{\partial x}+v\frac{\partial v}{\partial y}\right)=\rho g_v-\frac{\partial p}{\partial y}+\mu\left(\frac{\partial^2 v}{\partial x^2}+\frac{\partial^2 v}{\partial y^2}\right) \qquad 3.6$$

3.2.2 The domain of VAWT and meshing

When a time-accurate solution for rotor-stator interaction (rather than a time-averaged solution) desired, the sliding mesh model is applied to compute the unsteady flow field. The sliding mesh model is of an accurate method for simulating flows in multiple moving reference frames, but also the most computationally demanding. The operating sliding mesh is a procedure two or more cell zones are used. For combined rotor VAWT, each cell zones bound by at least one interface zone. The rotation zone will be rotated relative to the other zones long the mesh interface. The interface zones of adjacent cell zones are associated with one another to form a mesh interface. The sliding mesh model allows adjacent meshes to slide relative to one another. In doing so, the mesh faces do not need to align on the mesh interface. At the boundary between two sub-domains, the diffusion and other terms in the governing equations in one sub-domain require values for the velocities in the adjacent sub-domain. The solver used in the present study enforces the continuity of the absolute velocity to provide the correct neighbor values of velocity for the sub-domain under consideration. When the relative velocity formulation is used, velocities in each sub-domain had computed relative to the motion of the sub-domain [38].

The overall dimension for the simulation as shown in Figure 3.5, which is a domain for the CFD model. This configuration has drawn in the Solidwork program, then it has been exported to the solver. The present model consists of three airfoil blades of the H-Darrieus rotor. Meanwhile, the two blades are termed Savonius turbine. The Savonius rotor is located at the center of the Darrieus rotor. There are many models in this present study, the amount of it will be stimulated by

42

various TSRs = (0.5- 4). The radius of the H-Darrieus rotor is R_D =500 mm and the radius of Savonius as pursued by the standard of PVC pipe which has nominal diameter $D_{nominal}$ = 101.6 mm or R_S =50.4 mm. The domain simulation is recognized as a rotating and fixed domain. The inlet domain has defined as the velocity inlet and the outlet has identified as gauge pressure, and the Slip walls are stated as a stationary wall at specified shear of 0 pascals.
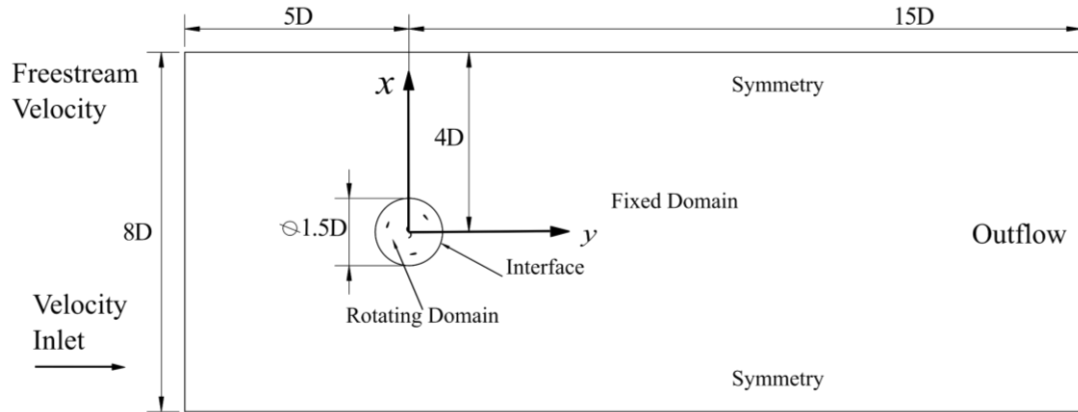
Figure 3.5. 2-D for the simulation domain.

In general, the meshing body is a significant part of the simulation. Based on the option technique the domain will be divided into two different regions. The first zone is controlled by a fixed-domain that is set as the global sizing function. It defined cell size was 25 mm square length. Second, being as the core rotating-domain of H-Darrieus and Savonius express cell size as 5 mm. Moreover, the cell near the wall of the turbine is suggested to use the inflation option, while y plus value is estimated to 1.

Figure 3.6 is shown about the diagram of the boundary layer of fluid flow on the plate flat. In chapter 7 of the immerse body, this statement is described as the external fluid flow over the immerge body [2].

The boundary layer thickness as the reference shown above where is defined as the relationship with local Reynolds number Re_x.

$$\frac{\delta}{x} = \begin{cases} \dfrac{5}{Re_x^{1/2}} & \text{Laminar} \\ \dfrac{0.16}{Re_x^{1/2}} & \textit{Turbulent} \end{cases} \qquad 3.7$$

Reynolds number formula for computing the Reynolds value on each blade of the wind turbine:

$$\mathrm{Re}_x = \frac{\rho V x}{\mu} \qquad\qquad 3.8$$

where Re_x is called the local Reynolds number of the flow along the blade's surface, ρ is the air density, $x=L$ characteristic length (chord length, the diameter of Savonius turbine), μ is the viscosity of the fluid.
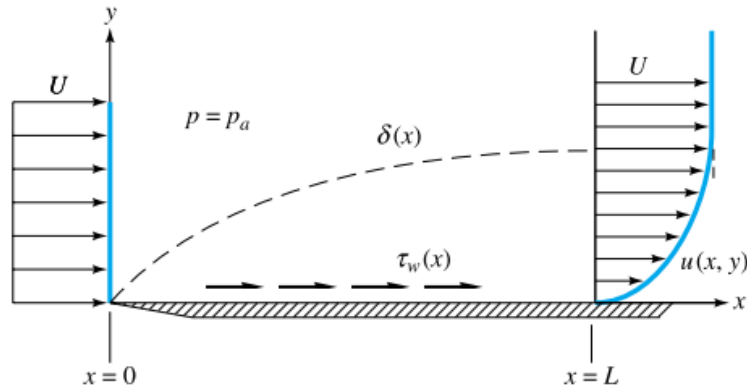
Figure 3.6. Boundary layer on the plate. [2]

As another equation of wall shear stress that is validated for either laminar or turbulent:

$$\tau_w = \rho U^2 \frac{d\theta}{dx} \qquad\qquad 3.9$$

where θ is perform of the momentum thickness of the boundary layer, was derived in 1921 by Kármán.

The skin-friction Coefficient is c_f

$$c_f = \frac{2d\theta}{dx} \text{ or } c_f = \frac{2\tau_w}{\rho V^2} \qquad\qquad 3.10$$

Logarithmic law of the boundary lay

$$\frac{u}{u^*} \approx \frac{1}{k} \ln \frac{yu^*}{v} + B \qquad u^* = \sqrt{\frac{\tau_w}{\rho}} \qquad\qquad 3.11$$

where $k=0.41$ and $B=5$. At the outer edge of the boundary layer, $y=\delta$ and $u=V$, as shown in the equation above

$$\frac{V}{u^*} = \frac{1}{k} \ln \frac{\delta u^*}{v} + B \qquad\qquad 3.12$$

As the skin friction is defined that:

$$\frac{V}{u^*} \equiv \sqrt{\frac{2}{c_f}} \qquad \frac{\delta u^*}{v} \equiv \mathrm{Re}_\delta \sqrt{\frac{c_f}{2}} \qquad\qquad 3.13$$

The skin-friction law for turbulent flow:

$$\sqrt{\frac{2}{c_f}} \approx 2.44 \ln \left[\mathrm{Re}_\delta \sqrt{\frac{c_f}{2}} \right] + 5 \qquad\qquad 3.14$$

The Power-law approximation

$$c_f \approx 0.02 \, \mathrm{Re}_\delta^{-1/6} \qquad\qquad 3.15$$

The turbulent profile can be approximate by Prandtl's one-seventh-power law:

$$\left(\frac{u}{V} \right) \approx \left(\frac{y}{\delta} \right)^{1/7} \qquad\qquad 3.16$$

It is presented the momentum thickness for the power law of the turbulent profile

$$\theta \approx \int_0^\delta \left(\frac{y}{\delta} \right)^{1/7} \left[1 - \left(\frac{y}{\delta} \right)^{1/7} \right] dy = \frac{7}{72} \delta \qquad\qquad 3.17$$

Based on the equation of the skin friction coefficient, it can be substituted to define the result as shown below:

$$c_f = 0.02 \, \mathrm{Re}_\delta^{-1/6} = 2 \frac{d}{dx} \left(\frac{7}{72} \delta \right)$$

$$\Leftrightarrow \mathrm{Re}_\delta^{-1/6} = 9.72 \frac{d\delta}{dx} = 9.72 \frac{d(\mathrm{Re}\,\delta)}{d(\mathrm{Re}_x)} \qquad\qquad 3.18$$

At $\delta=0$ and $x=0$, it was obtained that:

$$\Rightarrow \begin{cases} \mathrm{Re}_\delta \approx 0.16 \mathrm{Re}_x^{6/7} & or \quad \dfrac{\delta}{x} = \dfrac{0.16}{\mathrm{Re}_x^{1/7}} \Rightarrow c_f = \dfrac{0.027}{(\mathrm{Re}_x)^{1/7}} \\ c_f = 0.02 \, \mathrm{Re}_\delta^{-1/6} \end{cases} \qquad 3.19$$

So $\tau_{wall} = \dfrac{C_f \rho V^2}{2}$ $\qquad$ 3.20

- Velocity friction of turbine U_f

$U_f = \sqrt{\dfrac{\tau_{wall}}{\rho}}$ $\qquad$ 3.21

- The first layer thickness near the wall Δs

$\Rightarrow \Delta s = \dfrac{y^+ \mu}{U_f \rho}$ $\qquad$ 3.22

where: y^+ : non-dimensional parameter.

| (a) | (b) | (c) |
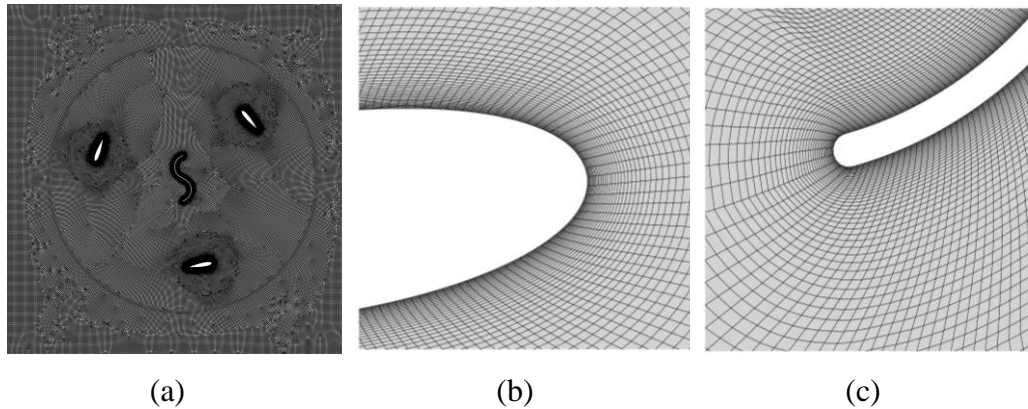
Figure 3.7. Meshing configuration, (a), meshing of the rotate domain(b) the inflection mode of airfoil, (c) distance order of the cell near the wall of the Savonius rotor.

Depending on what these formulations stated about the distance of the first layer obtained to pursue on the Darrieus blades about 0.07 mm and Savonius of 0.04 mm. The main idea for simulation is the procedure sizing the cell grid near the wall, so Figure 3.7 is shown the grid distance near the wall of the turbine. However, it's not only considered cell grids near the wall but also based on the overall flow domain of the turbine, also the structure mesh is significant to apply.

3.3 Meshing verification

The meshing quality is one of the accuracies for numerical simulation. The current study has been tested on the grid quality by shown in Table 3.4. This value cell grid is verified by 4 models; in which it arranges by the number of the cell

elements from coarse to fine mesh. Also, the models have been simulating at a TSR of 2.75 with a wind velocity of 4 m/sec. Therefore, the value of y plus is observed and identified based on Table 3.4. Therefore, the entire models are observed that the higher or the lower number of cell elements have not extracted the optimum value of C_M. A model of the grid number (1,162,322) was driven the value of y plus became about 4 and stable C_M of 0.071. Thus, it is a suitable model that can be applied to future models. The high value of C_P is obtained respect to the value of y plus respectively [39].

Table 3.4. Grid independent test

Number of elements	Maximum y^+ value	Average C_M	Relative errors
834,615	3.69	0.059	-
1,162,322	3.85	0.071	15.76%
1,330,896	3.95	0.071	0.07%
1,550,773	3.58	0.072	2.15%

Also, Figure 3.8 is exhibited by the range of meshing independency. Meanwhile, it is established the medium mesh is not definitely changed of the C_M value while this test is provided the turbine rotating in 5 rotations (1800 deg).
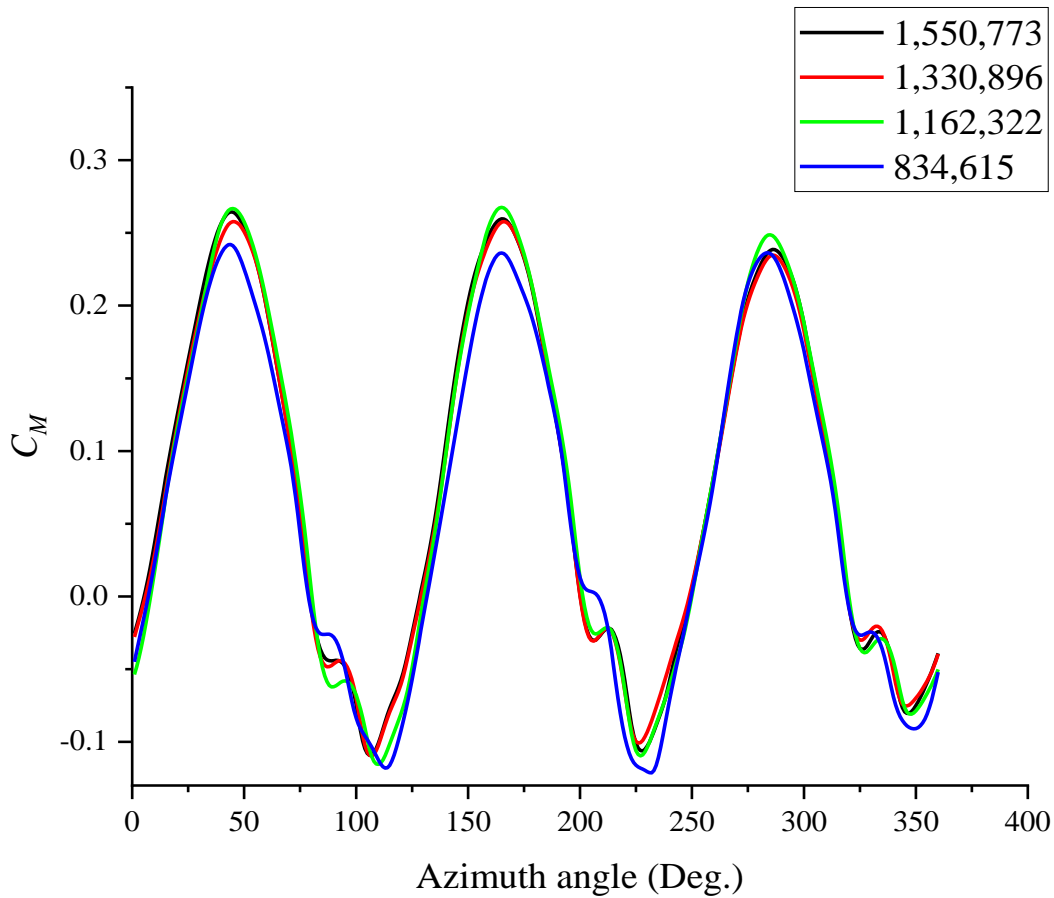
Figure 3.8. C_M vs Azimuth angle, a graphic of independency test

3.3.1 Fluent solver setup

The incompressible fluid flow, Reynold Average, Navier-Stokes (RANS) solved in discretized form. This setup refers to the linear dependence of velocity and pressure. Thus pressure-velocity is required to predict the pressure distribution in the flow domain with reasonable accuracy.

RANS equation is solved by using the SIMPLE pressure-velocity coupling scheme. Pressure interpolation scheme and upwind spatial discretization schemes by 2nd order. The pressure gradient term will be calculated by using the pressure distribution from the previous iteration or an initial guess. The wall side of the domain employed on the sides of the domain, along with constant inlet velocity and outer pressure. A non-slip condition used on airfoils and Savonius turbines.

The material for the whole simulations are identified as air for the boundary domain, in which it has the property of air density of 1.225 kg/m^3, the viscosity of 1.7894x10^{-5} kg/ms, and the reference values computing from the inlet condition, area definitely changing follow by the outer area of H-Darrieus rotor (m^2), depth equal to1 m, and length of 0.5 m.

3.3.2 Turbulent model

The suitable model indicates for the simulation is the 2-equation shear stress transition turbulence SST k-ω. As the model has already suggested that it is provided superior performance for zero pressure gradient, adverse pressure gradient of the boundary layer, and free shear layer. Therefore, it is supposed to be significant for VAWT. The results demonstrate the good capabilities of the transition SST turbulence model compared to the classical fully turbulent models [40].

The main problem for the application of the simulation is precise on the selection method for the entire model. However, many earlier pieces of research have been tested every different model in each method such as Reynolds Average Navier Stock Equation (RANS), Large Eddy Simulation (LES), and Direct Numerical Simulation (DNS). Indefinitely, for wind turbine has been designated as a suitable method for testing with the simulation to establish with the experimental. There are numerous of turbulent models that have been performed on H-Darrieus wind turbine, the analyze had tried to compare most of the turbulent model with the experiment of the previous research,

In recently, there are many models for performing the numerical simulation. Also, the pervious researches have been recommended the suitable algorithm to model on CFD. Specially, the algorithm for modeling of wind turbine is definitely chosen of k-omega SST. According to Figure 3.9 is shown the results obtained from the comparison of the turbulent models, however, two models have chosen for the suitable model for a wind turbine is that k-epsilon Realizable and k-omega SST model [13].
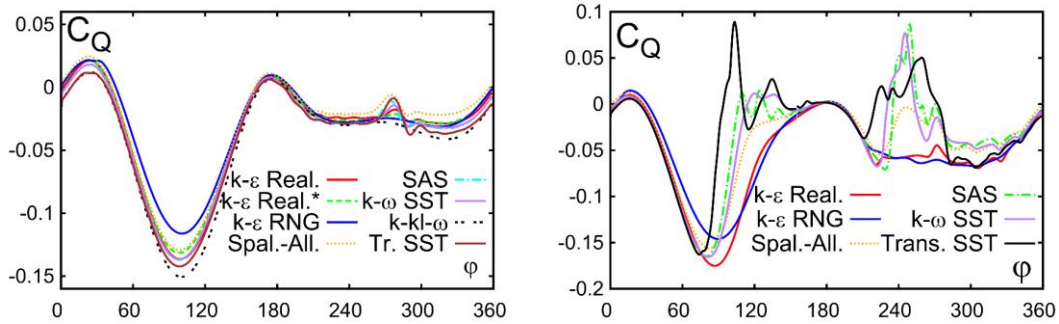
Figure 3.9. The coefficient of the moment with azimuth angle, comparison of turbulent models of H-Darrieus rotor [13].

3.3.3 Boundary conditions

In general, 2-D of wind turbine simulation is separated into two domains such as fixed and the rotating domain. The boundary condition of the wall inlet is specified by the wind inlet that reminded to be constant as 4 m/sec. The pressure also defined as an atmospheric condition at the outlet wall where marked into zero-gauge static pressure. Moreover, all the walls of the flow domain are set as non-slip boundaries, it means that the flow does not slip on the surface of the wall. Besides, the interface between rotating and fix domains is defined as rotating rotation. The boundary condition in Table 3.5 is required to input by the designer or default setting from a commercial solver program.

Table 3.5. Condition and boundary types

Boundary Name	Boundary Type	Boundary condition
Inlet	Inlet velocity	4 m/sec
Outlet	Outlet pressure	0-gauge pressure
Symmetrical sides	Stationary walls	No shear stress (0 Pascal)
Darrieus (Airfoils)	Rotating wall	No-slip
Savonius	Rotating wall	No-slip
Outer domain	Fixed condition	Interior
Inner domain	Rotated condition	interior

3.3.4 Optimal time step

Another useful to be considered by controlling the time step for the simulation, it is also modified to express the converge solution or stabilization of simulation. For the combined rotor, the Darrieus rotor is the main for producing torque coefficients. Meanwhile, it is the key to take account to calculate the time step by following the Darrieus rotor [26]. Table 3.6 as shown below is identified the time step procedure for the whole simulation. However, it is calculated based on the angular velocity of the turbine, TSR, and degree of the step rotation.

$$\text{Total number of degrees rotating per second} = \frac{360N}{60} \qquad 3.23$$

Let the *degree of the domain* as the degree is rotated per time step

$$\text{Time step} = \frac{\text{degree of domain}}{\text{deg}} \qquad 3.24$$

The purpose of this calculation is to define the total number of the time step and time step size in order to push the turbine rotated a degree per time step.

Table 3.6. The time step size consistent with wind velocity

TSR	ω (v=4 m/sec)	Time step (sec)
0.5	4	0.0044
1	8	0.0022
1.5	12	0.0015
2	16	0.0011
2.5	20	0.0009
3	24	0.0007
3.5	28	0.0006

The summery of setting up for some specific values in ANSYS fluent. Table 3.7 as shown below is explained by the parameters that require the user to input.

This proposed research will perform in different characteristics of the H-Darrieus rotor that is formed as different of the solidities ratios. The research flow

chart is a flow chart which is defined as the process of the simulation. It is an important guideline to define the final result of the simulation as shown in Figure 3.10.

Table 3.7. Inputting parameter on CFD

Parameter	Value & description
Solver	Transient (implicit)
Viscous model	k-ω (2 Eq.) SST-model
Velocity inlet	4 m/sec
Turbulent intensity	5%
Turbulent length scale	0.0153 m
Solution method	SIMPLE
Equation order (Pressure, Momentum, Turbulent kinetic energy, Specific dissipation rate)	2nd-order upwind

```
                          ┌─────────────┐
                          │    Start    │
                          └──────┬──────┘
                                 │
                          ╱──────────────╲
                         ╱ Define and data╲
                         ╲   collection   ╱
                          ╲──────────────╱
                                 │
                          ╱──────────────╲
                         ╱ Select airfoil and╲
                         ╲ Savonius turbine  ╱
                          ╲──────────────╱
                                 │
                          ╱──────────────╲
                         ╱ Design 2D feature╲ ◄──────────┐
                         ╲   of turbine    ╱             │
                          ╲──────────────╱               │
                                 │                       │
    ┌──────────┐          ╱──────────────╲               │
    │ Database │         ╱ Import *iges file╲            │
    └────┬─────┘         ╲   to Fluent    ╱              │
         ┊                ╲──────────────╱               │
         ┊                       │                       │
         ┊                ┌──────────────┐               │
         ┊                │Meshing algorithm│            │
         ┊                └──────┬───────┘               │
  ┌──────────────┐               │                       │
  │- Calculate TSR│       ┌──────────────┐               │
  │-Calculate turbulent┊┈►│Set up CFD software│          │
  │length scale   │       └──────┬───────┘               │
  │- Calculate time step│        │                       │
  └──────────────┘        ┌──────────────┐               │
                          │   TS=TS+1    │ ◄───────┐     │
                          └──────┬───────┘         │     │
                                 │                 │     │
                          ┌──────────────┐         │     │
                          │CFD simulation│         │     │
                          └──────┬───────┘         │     │
                                 │                 │     │
                          ╱──────────────╲         │     │
                         ╱ Reach iteration ╲───────┘     │
                         ╲                ╱              │
                          ╲──────────────╱               │
                                 │                       │
                          ╱──────────────╲               │
                         ⟨   CFD result   ⟩              │
                          ╲──────────────╱               │
                                 │                       │
                          ╱──────────────╲               │
                         ╱  Check torque? ╲──────────────┘
                         ╲                ╱
  ┌──────────────┐        ╲──────────────╱
  │TSR: Tip Speed Ratio│          │
  │TS: Time Step  │        ┌──────────────┐
  │Cp: Power coefficient│  │Extract torque to excel software│
  └──────────────┘        └──────┬───────┘
                                 │
         ┌──────────────┐  ┌──────────────┐  ┌─────────┐
         │Calculate final Cp├►│Compare model├►│   End   │
         └──────────────┘  └──────────────┘  └─────────┘
```
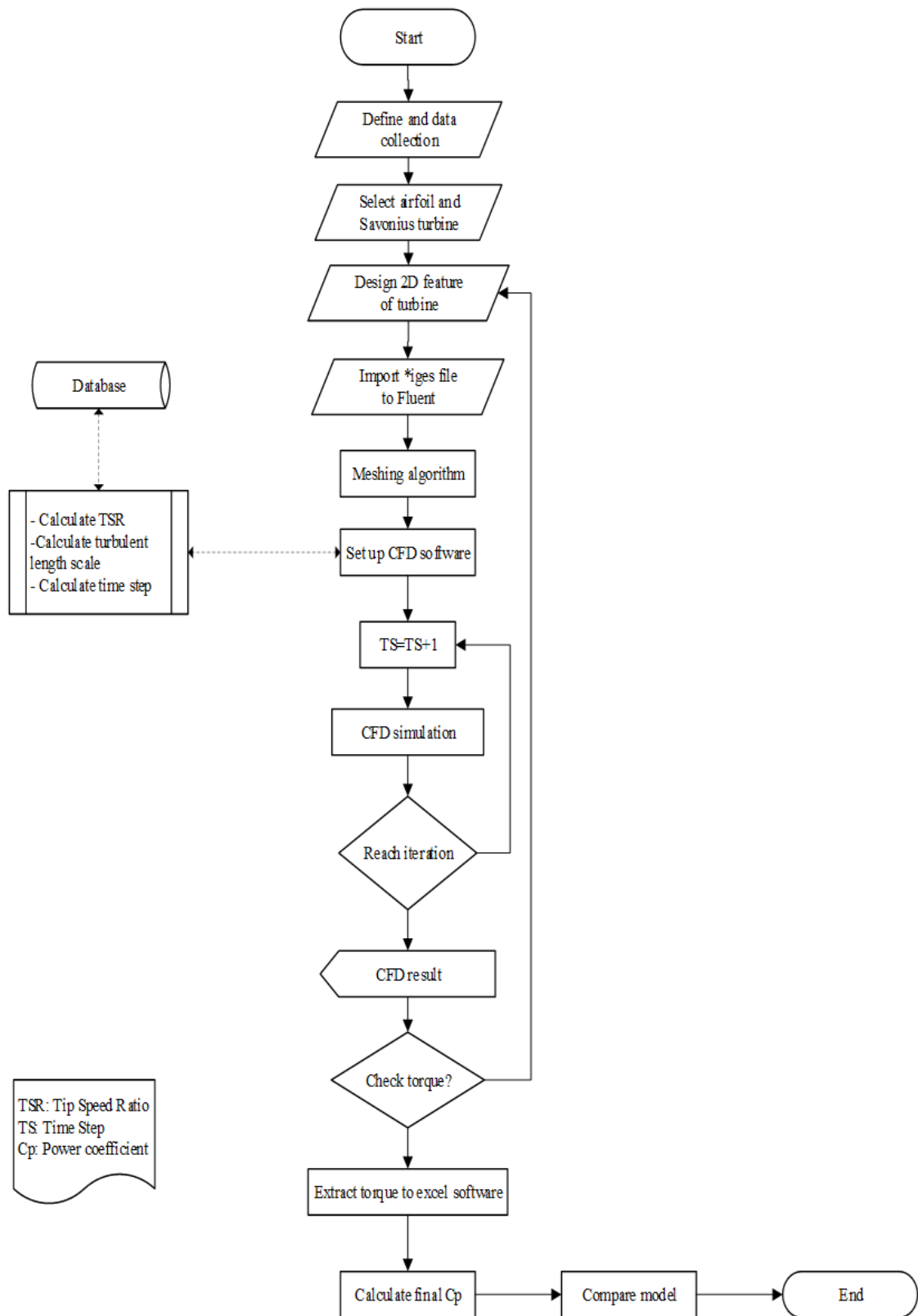
Figure 3.10. The flow chart that is defined as the process of the simulation

53

CHAPTER 4
RESULT AND DISCUSSION

This chapter will be throughout the entire discussion of the result in each case of this present work. The first of this section has been described the validation outcome to the other research (single-Darrieus and combine rotor). Second, the present research is focused on the effect of the airfoil shape by explaining including with the performance graph and turbine aerodynamic contours. At the final, it is explored the performance effect by the solidity ratio of the combined rotor form by the Darrieus rotor.

4.1 Validation

An implemented on single-Darrieus through varied solidities ratio is chosen for validation to this present research. For this model were performed by 2-D CFD simulation, the characteristic was described in Table 3.3. Previous research on single-Darrieus through varied solidities ratio with a wind velocity of 4.7 m/sec by Xiaojing Sun [41] is chosen for validating this present research. The comparison will be investigated by plotting the turbine performance (C_P) which is different ranges of the TSR $(0.5 \leq \lambda \leq 4)$. Ying-bin Liang [42] has been performed the numerical simulation on a small scale of the wind, also this implementation has varied some parameters (number of turbine blades) to define the characteristic optimum of the coefficient of the power and aerodynamic performance. An impressing on this research is that the inlet velocity about 4.7 m/sec, the diameter of the wind turbine was 0.6 m while the suitable blade feature for producing high lift to drag has chosen by NACA-0018 for the entire model. Habtamu Beri and Yingxue Yao [43], unsteady flow analysis of vertical axial wind turbine by comparing the result of double multiple stream tube model with the CFD simulation, also, this implementation has been used the feature of the airfoil of NACA-0018 at the low wind speed of 4 m/sec. Moreover, the simulation has modified the airfoil chord length of 0.2 m including on the turbine radius of 2 m.

The simulation results have been dominated at the low TSR, the H-Darrieus rotor had demonstrated lower C_M than the hybrid rotor. In contrast, at the high TSR, it is definitely an H-Darrieus rotor had established higher C_P than a hybrid rotor. Meanwhile, Liang Xiaoting [20] has been performed by the configuration such diameter of the combined rotor of 1.5m and Re of 9.98×10^5, approximated of the stream velocity V=9.72 m/sec. Table 4.1 is the line data of the present work that is compared to the other researches by matching its performance of the C_M & C_P with a range of TSR. Figure 4.1 is illustrated to distinguish the range value of the C_M based on the range of the TSR whereas those turbines produced the performance in which similar. But the curve of the single-Darrieus has slightly increased at the high of the TSR than the combined rotor. Figure 4.2 was the characteristics of the coefficient of power of the five different types of small wind turbines including the characteristic of the present study as well. Based on these the graphics of the turbine performance, the combined rotor has developed the capability of self-starting, the Savonius turbine locating at the middle was generated much of drag forces by the large among of the surface interaction to the fluid flow at the low range of the TSR. At the optimum TSR, the combined rotor has occurred some effect to the region that less provides a better fluid interaction between Darrieus and Savonius rotor. For the single of H-Darrieus rotor hard to start the turbine rotating at the low range of TSR according to the turbine has produced low of the performance. According to the earlier researches of the H-Darrieus rotor, which is found that at the lower of the TSR, low of the stream velocity, conducted the shaft of the turbine hard to rotate. But at higher range of TSR, it has generated higher performance than the combined rotor.

Table 4.1. The C_M and C_P comparison of the turbine performance.

C_M /TSR	0.5	1	1.5	2	2.5	3	3.5	4
Single Darrieus [41]	-	-	0.100	0.180	0.178	0.127	0.069	0.013
Single Darrieus[42]	-	0.030	0.060	0.110	0.156	0.117	0.071	0.028
Single Darrieus[43]	-	-	0.065	0.120	0.142	0.107	-	-

|							
Single-Darrieus Present study	0.011	0.011	0.0047	0.114	0.153	0.095	0.043	0.001
Combined rotor (Num.) [20]	-	-	-	0.05	0.1	0.09	0.02	-
Combined rotor present study	0.021	0.007	0.100	0.123	0.145	0.089	0.031	0.0001
C_P/TSR	**0.5**	**1**	**1.5**	**2**	**2.5**	**3**	**3.5**	**4**
Single Darrieus [41]		-	0.15	0.36	0.445	0.38	0.24	0.05
Single Darrieus[42]	-	0.03	0.09	0.22	0.39	0.35	0.25	0.11
Single Darrieus[43]	-	-	0.097	0.24	0.355	0.32	-	-
Combined [20]				0.07	0.23	0.3	0.15	
Combined rotor present study	0.011	0.007	0.151	0.248	0.364	0.269	0.112	0.004
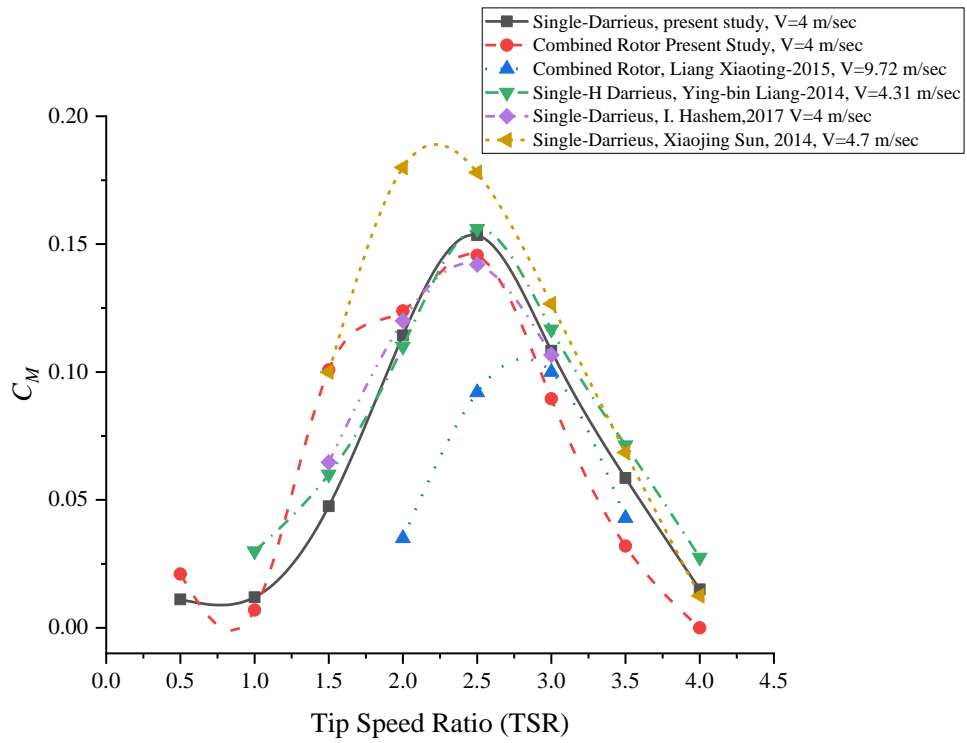
Figure 4.1. Cm via TSR, the graphic of the coefficient of moment exhibited the data validation of the combined rotor to the other previous research.
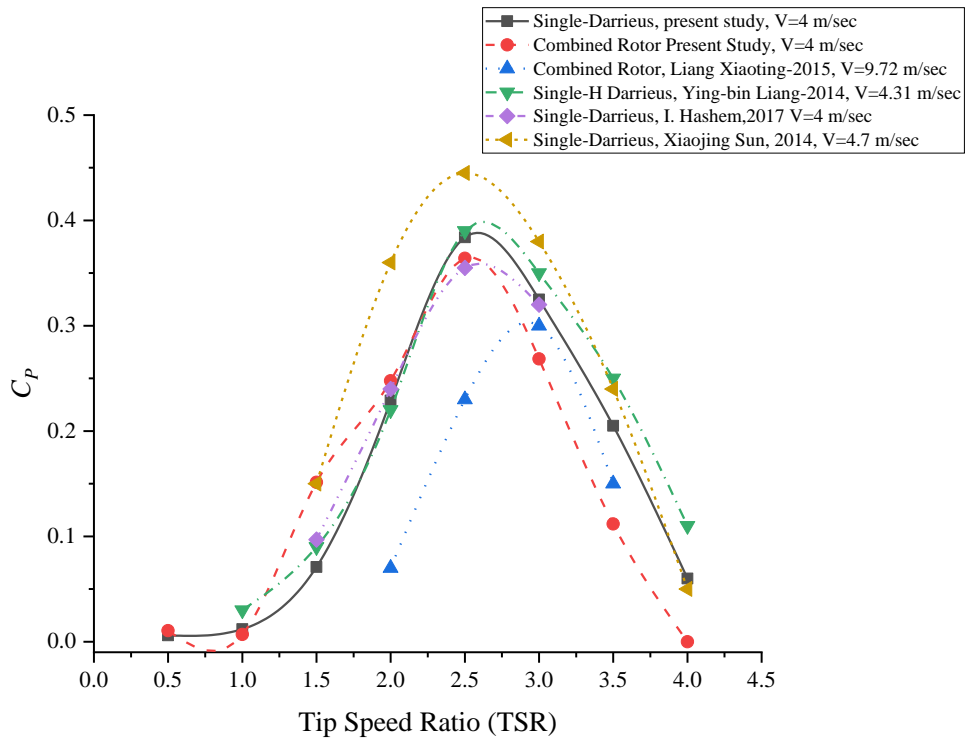

Figure 4.2. The coefficient of the power generated to compare the turbine performance.

Another section below will describe the feature of the combined rotor and single H-Darrieus rotor:

4.2 Characteristic of the combined rotor

The establishment of the single-Darrieus rotor and combined rotor are proposed in a direction that is defined as the best performance of those turbines. The two features of these two turbines are finished to simulate and found a peak configuration, which is clarified by solidity of 0.4. Figure 4.3 as shown below has described the graphic of the coefficient of the moment via azimuth angle at the TSR of 2.5. Also, there is exhibited the maximum producing the C_M at 50 deg, 175 deg, and 300 deg of the turbine rotating. As it notified that at 110 deg both turbine have different conducting of their performance; the single-Darrieus rotor generated higher performance than the combined rotor, in which there is an indication to the combined rotor reducing the performance at the optimum of the TSR by the Savonius rotor. Meanwhile, the pressure and velocity contours of the single-Darrieus and combined rotor has demonstrated the effect between turbine blades by shading and high vortex interaction while the operation. Figure 4.4 is illustrated the velocity contours and velocity instantaneous streamlines of the single-Darrieus rotor that was less of the turbine blades shading and wake motions if it has compared to the combined rotor as shown by Figure 4.5. Also, there are analyzed the vortex characteristic by the streamlines along with the turbine blade. Figure 4.6 and Figure 4.7 are extending to compare the pressure coefficient and pressure instantaneous streamlines of both turbines. Therefore, there are established the interaction of the aerodynamic performance to each of the rotors. Hence, based on the color map of the pressure coefficient, the single-Darrieus has a wide of the fluid flow on the turbine but the combined rotor has a poorer space and much of vortex in the turbine region. In supposition, the combined rotor conducted performance lower than the single-Darrieus rotor at the optimum of the TSR because of the bothering and effectiveness of the Savonius rotor. In suggestion, the combined rotor should be used at the first starting, low wind speed region, and lower of the TSR as shown in Figure 4.58.
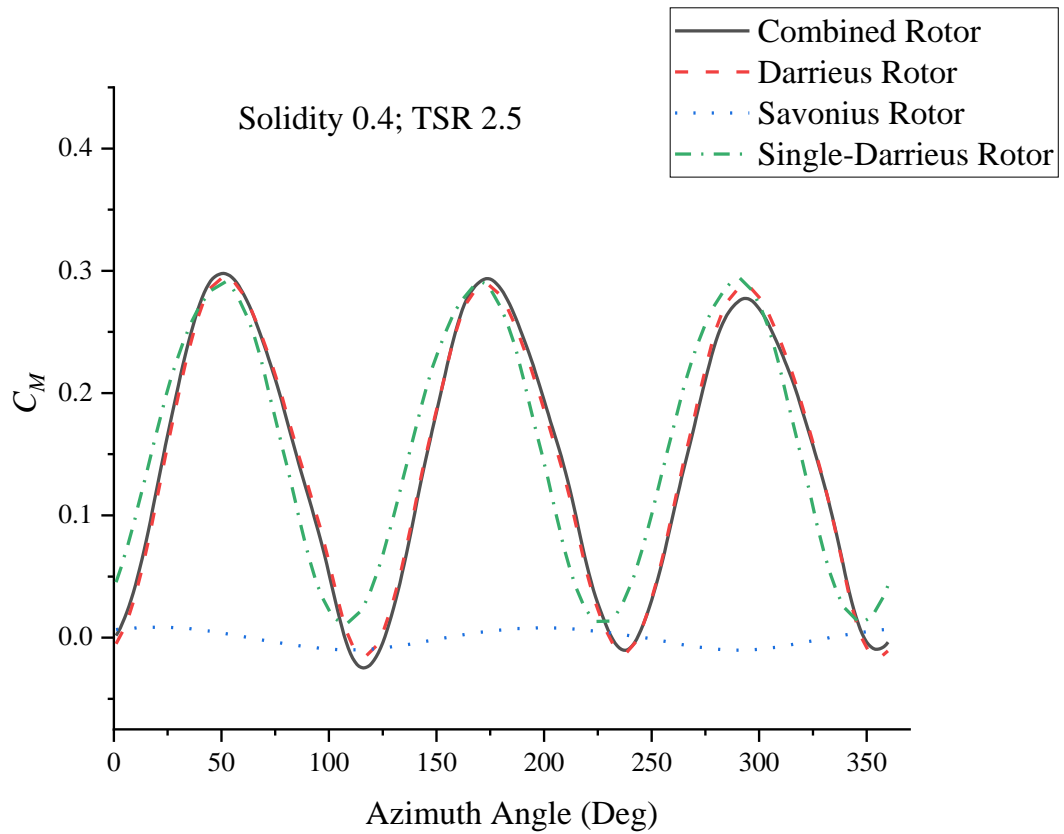
Figure 4.3. The coefficient of the moment comparison between the combined rotor and single-Darrieus rotor.
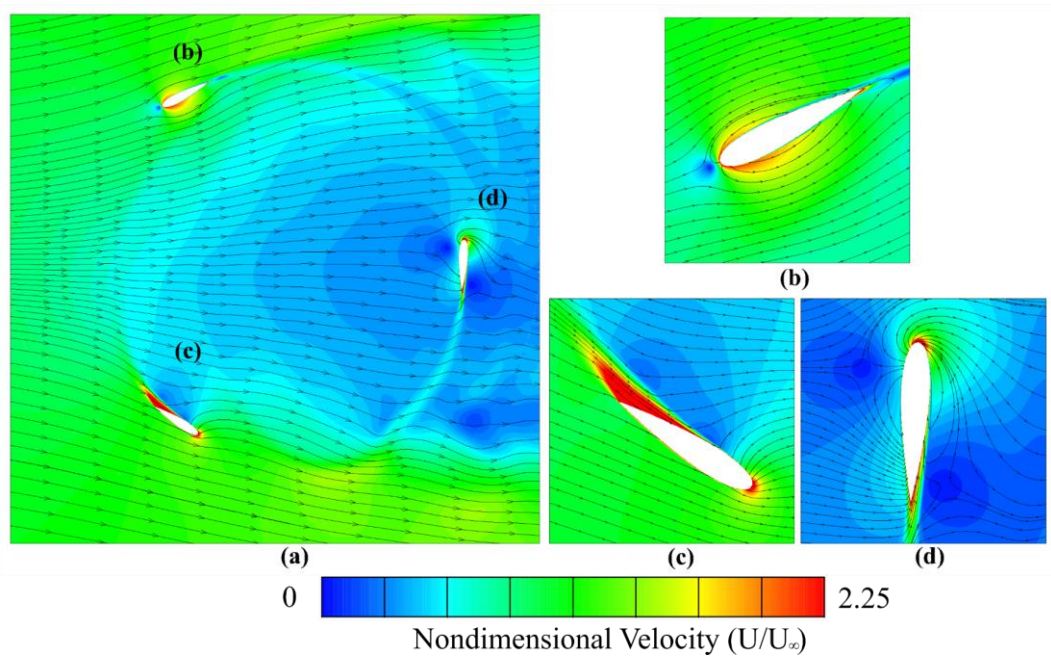
Figure 4.4. The velocity contours and instantaneous streamlines of the single-Darrieus rotor at the TSR of 2.5, rotating 110 deg of the azimuth angle.

Figure 4.5. The velocity contours and instantaneous streamlines of the combined rotor at 110 deg of the azimuth angle, the solidity of 0.4 with the optimum TSR of 2.5

Figure 4.6. Pressure coefficient contours and the instantaneous streamlines through the single-Darrieus rotor blades with the TSR of 2.5, rotating 110 deg of the azimuth angle.
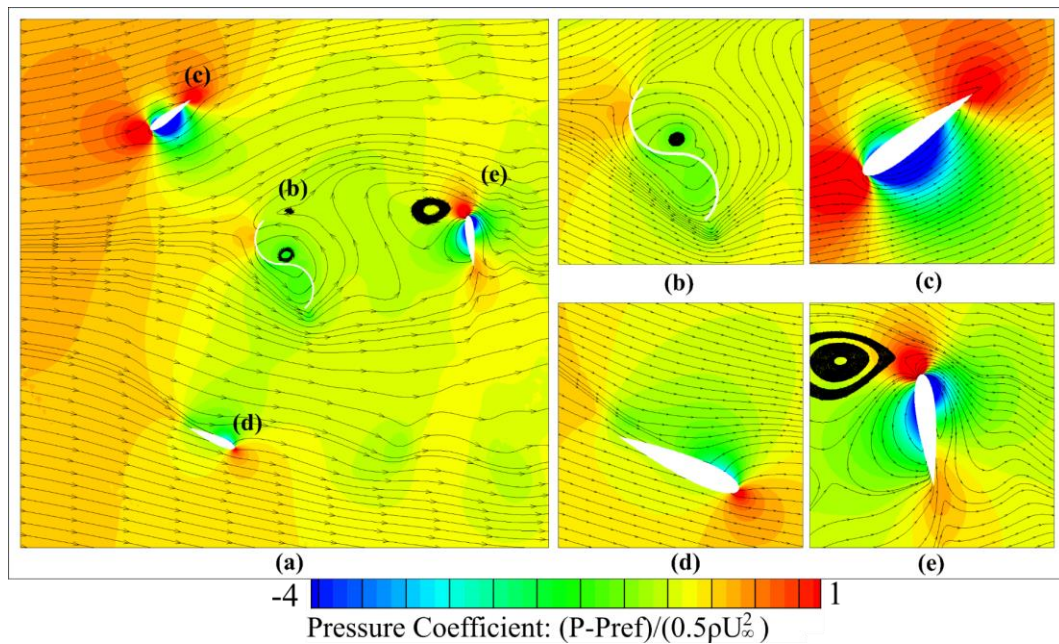
Figure 4.7. The pressure contours of the combined rotor and pressure instantaneous streamline along with the turbine blades at the TSR of 2.5, rotating angle of 110 deg.
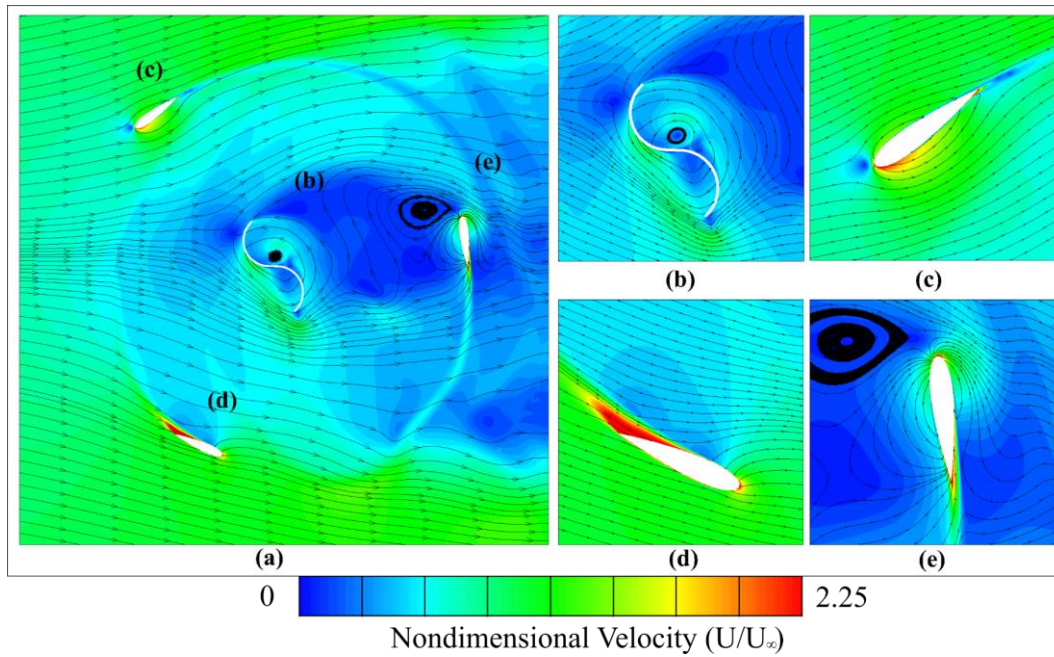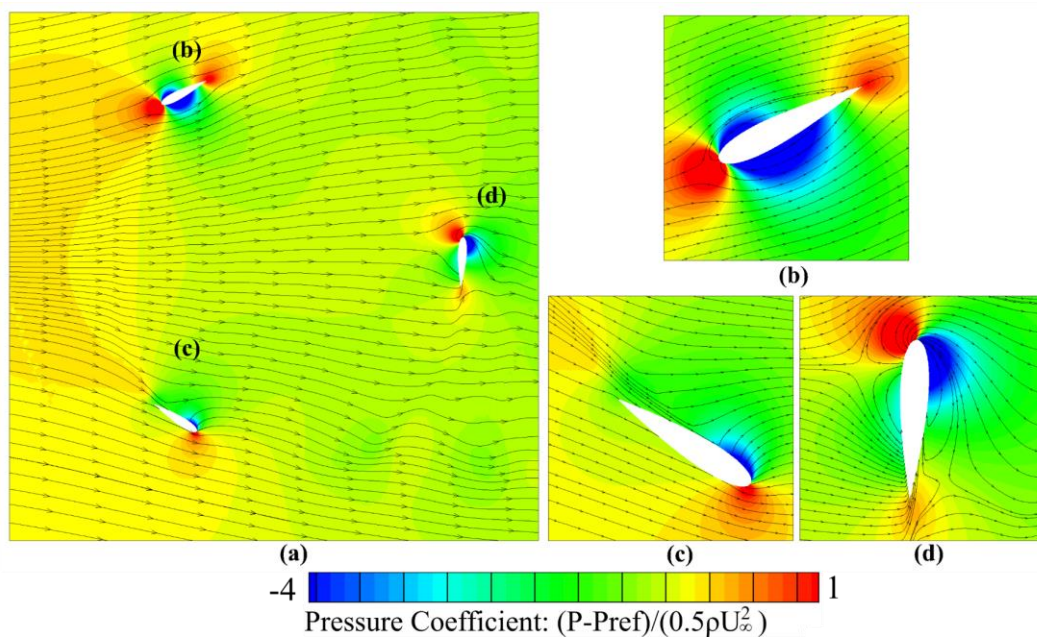
4.3 The effect of Airfoil shape of Combined rotor

Based on the shape of the airfoil, it is significant to analyze the aerodynamic performance along with the shape between symmetric and asymmetric airfoil. Impressed to the symmetric is the type of qualify the shape above and upper is equivalent. As neither of the symmetric airfoils is satisfied by another airfoil where is asymmetric type. Definitely, as shown in Figure 4.8, the wing blades of the turbine have provided lift by conducting the above pressure lower than the pressure below of the wing blades. Also, the asymmetric one is significant to provide higher net force than symmetric airfoil. In addition, the satisfaction on the above feature of the asymmetric airfoil was produced better pressure relationship than symmetric.

Figure 4.8. The configuration of fluid flow around symmetric and asymmetric airfoil form as instantaneous streamlines.

In this section, the expected result has been exhibited of different shapes of airfoils as the hybrid rotor. The implementation is performed by a constant inlet velocity of 4m/sec, TSR of 2.75, and solidity of 0.3. Based on Figure 4.9 is described the coefficient of moment with azimuth angle. At zero position of the turbine located on x-axis parallel with the axis of the Savonius turbine where C_M approximates to zero. Another observation on the C_M graph is shown that at 50 deg of the rotation has been defined higher of C_M value. Between symmetric and asymmetric are obtained in different aerodynamic performance. For modification, Table 4.2 is clarified the value of the coefficient of the moment at the optimum TSR of 2.75.
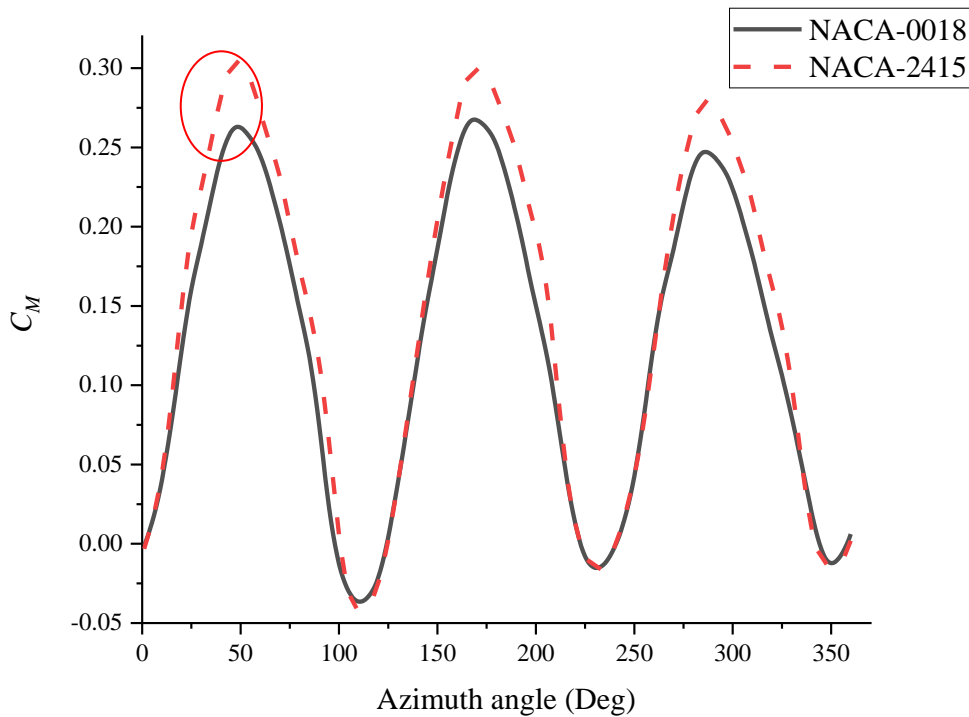

Figure 4.9 The graph of the coefficient of the moment at TSR of 2.75

62

Eventually, the first models of the combined rotor of various shapes of the airfoil have been completed. As another evidence according to Figure 4.10 is clarified about the different constant values of the coefficient of moment at a wind velocity of 4m/sec. Moreover, the graph is ascertained that the maximum C_M with a TSR of 2.75. Also, Figure 4.11 is notified that the symmetric airfoil of the hybrid rotor has conducted lower C_P than asymmetric about 10%. As many reasons are exhibited that the asymmetric is better to conduct the coefficient of performance value. Indefinitely, by using numerical to design such as a computer program, it is the facility to perform shape behavior of asymmetric. But for manufacturing of asymmetric airfoil is implausibly to build, Additionally, between NACA-2415 and NACA-0018 are different constitute lower of C_P. In the suggestion, the symmetric airfoil should be used for constructing the real prototype as well as its benefits such as shape facile for manufacturing, low cost constructing, simple configuration than asymmetric, and smaller different performance between asymmetric. For this reason, the implementation of the further models will choose the symmetric airfoil to develop in another testing. So, the present study will apply with another configuration that is conducting with the solidities ratios.
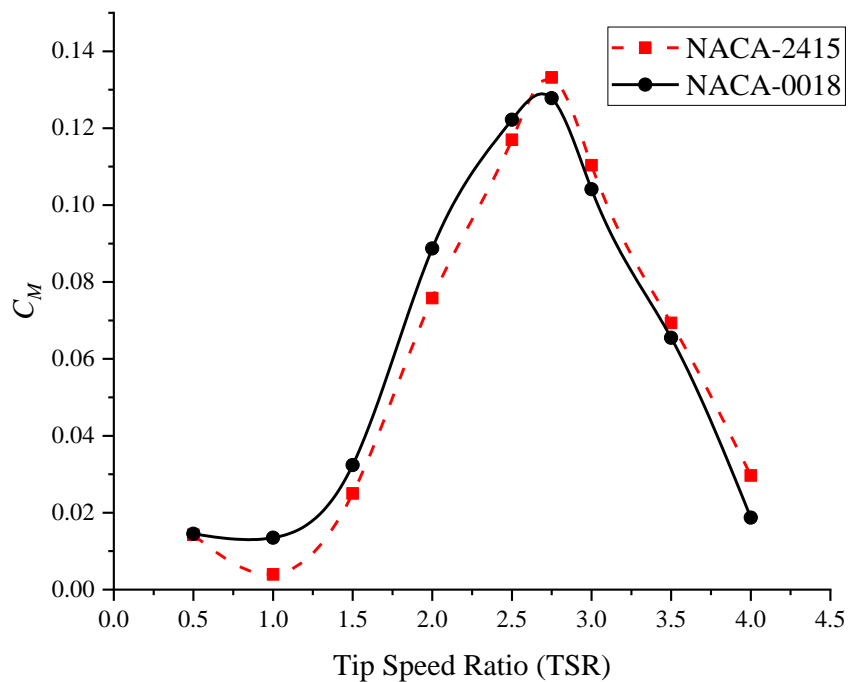

Figure 4.10. The coefficient of the moment of the hybrid turbine in different airfoil types
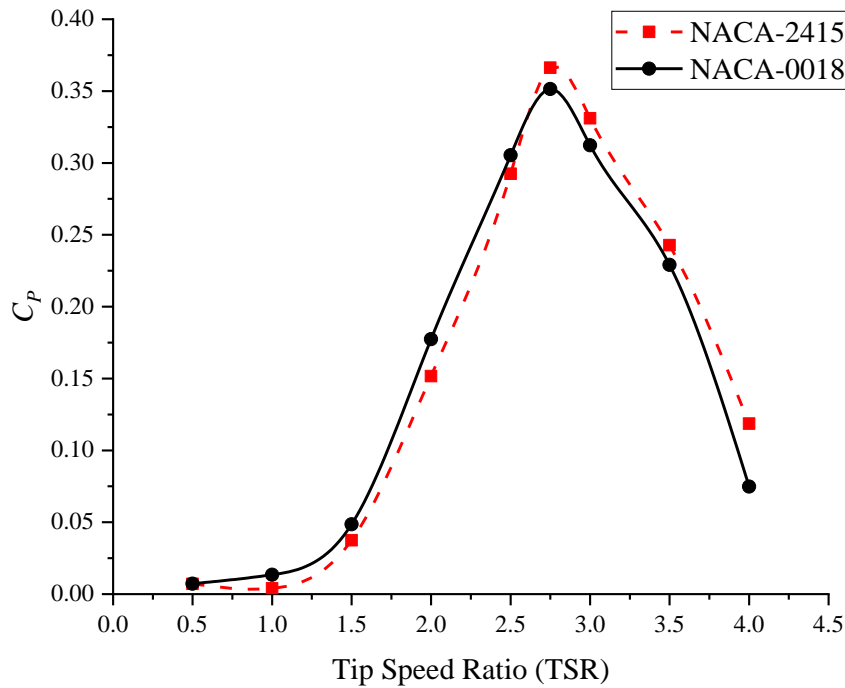
Figure 4.11. The graph of the coefficient of the moment of the combined rotor in different airfoil shapes.

Figure 4.12 as shown below is the velocity contours which are ranged by asymmetric and symmetric airfoil of the combined rotor. Also, there are velocity streamlines through the turbine blades. Moreover, those contours are prescribed the aerodynamic performance as shown by the color map of the velocity magnitude where effected on the turbine's blades surface. Figure 4.13 is presented about the pressure contours of the combined rotor of the symmetric and asymmetric airfoil at 50 deg of the azimuth angle. Likewise, among these contours established the pressure coefficient streamlines over the turbine blades. In conclusion, the asymmetric airfoil is produced better aerodynamic performance and drag force than symmetric airfoil.

Table 4.2 the summary result of those types of the combined rotor at TSR of 2.75

Airfoil	C_M	C_P
NACA 0018	0.12	35.14%
NACA 2415	0.13	36.62%
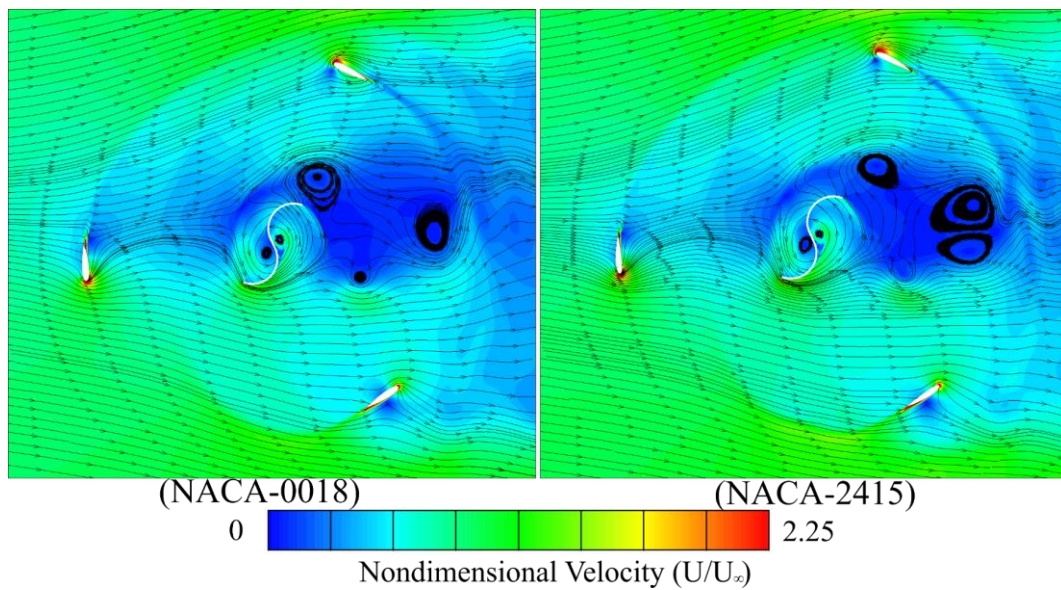
Figure 4.12. The velocity contours of the combined rotor of the asymmetric airfoil and symmetric airfoil at the TSR of 2.75 within velocity instantaneous streamlines along with blades turbine, the rotating position of the azimuth angle of 50 deg.

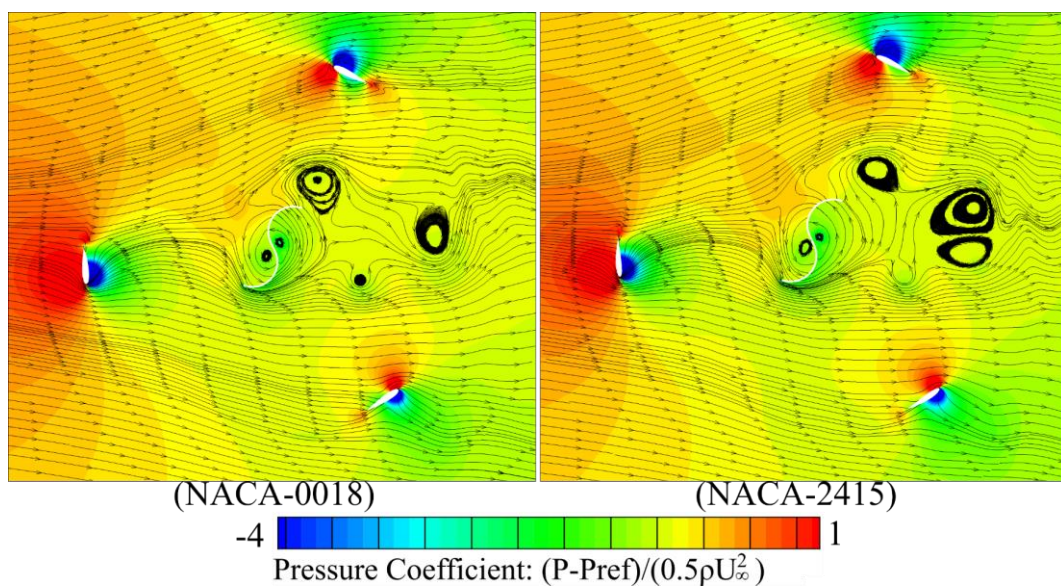Figure 4.13 The pressure contours of the combined rotor of the asymmetric airfoil and symmetric airfoil, presenting at a TSR of 2.75, velocity instantaneous streamlines along with blades turbine

In summary, the effect of the shape between symmetric and asymmetric airfoil is caused by above and below surface of the both airfoil where was conducting the lift and drag force significant differences. For this reason, the

asymmetric shape has a major conducted better aerodynamic by improving higher lift from the above surface than symmetric.

4.4 The effect of solidity ratio

In the literature reviews section [8, 16, 19] are definitely proved the suitable solidity for a single H-Darrieus rotor. However, in this present study will explain to another parameter of the combined rotor, it was called the solidities ratios. The solidity ratio is focused on the changing of the chord length of the H-Darrieus rotor which is described in Table 4.3 as shown below by determining the difference of the solidities ratios and the chords length value.

The simulation has completed while the outcome of the solidity performance also generated. Based on Figure 4.56 as illustrated below is that clarified about the different of solidities ratios with the range of the TSR. Also, it is characterized while the solidity ratio is increased, the performance (C_M) is increased at the low range of the TSR. High solidity ratio ($\sigma=0.8$) reach maximum C_M at TSR=1, low solidity ratio ($\sigma=0.2$) determined the peak C_M at TSR=3.5. Thus, the graph as shown in Figure 4.56 is the achievement of the C_M establishing by high solidity ratio at the low of the TSR, it might be recommended to determine the self-starting problem of the combined rotor as well. Only the C_M is not enough to represent the realization performance in which of the solidity range. Hence, another modification is that the coefficient of power (C_P) as exposed by Figure 4.57. The curve performance in Figure 4.57 is significant to propose the best characteristic for the combined rotor of the present study. Definitely, paying attention to the C_P graph, it is performed and compared the performance by generating C_P within the range of the TSR. At the lowest and highest of the solidity ratio, the combined rotor is not better generated the best performance. Except, the medium of the solidity ratio value the turbine is obviously regenerated higher C_P than the conventional of the turbine characteristics. As a further observation on Figure 4.57, the higher of the solidity ratio cannot operate at the high range of the TSR because of the obstruction within the incoming free stream flow past the turbine forming as the fluid flow through a cylinder, where the fluid incoming is separated to the sides

instead of passing through the rotor, therefore, the high solidity ratio has led the C_P decreasing at a high rotational speed.

In contrast, the reason why lower solidity is conducted the low performance because the lower solidity ratio has a short length of the airfoil chord or small among the surface interaction to produce the drag force for the turbine rotating. But, based on the graph result of the present work the low solidity has distinguished the Savonius rotor inside extremely developed the torque performance at some azimuth angle because the low solidity has widely fluid flow through each blade turbine.

The medium range of the solidity ratio (σ=0.4) produced higher C_P while the turbine operated at the optimum of the TSR=2.5, occasionally larger of high of the performance as well.

In summary, an observation of the C_M figures of the turbine performance by varying the solidity ratio, the coefficient of the moment is slightly decreased at the high range of the TSR. It can be seen that in order of C_Ms are decreased at the range of increase of the solidity ratio. Finally, the present numerical result establishes that C_P maximum relatively larger operating range of TSR.

Table 4.3 The variation of solidities value as different chord lengths

No	Solidities	Chord length (mm)
1	0.2	66.7
2	0.3	100
3	0.4	133.3
4	0.5	166.7
5	0.6	200
6	0.7	233.3
7	0.8	266.7

4.4.1 Solidity of 0.2

The solidity of 0.2 is the lowest value amount of the solidity ratio. The coefficient of the moment graph has described the fluctuation of maximum and

minimum at the specific azimuth angle per rotation at a TSR of 3.5 as shown in Figure 4.59. However, at the low solidity where is less of the surface interaction to the fluid flow past the turbine and it is demonstrated the low of the performance that compares to the conventional solidities. Based on, Figure 4.14, Figure 4.15, and Figure 4.16 are modified of the turbine rotating about 0 deg, 50 deg, and 100 deg respectively. Also, there are clarified the instantaneous streamlines velocity around the turbine blades. In case, at the lowest of the C_M is defined where the Savonius turbine located parallel to the x-axis. In addition, the maximum of the C_M is presented when the turbine is presented at 50 deg. In contrast, the turbine has produced a minimum of C_M while the turbine is rotated at 100 deg. Moreover, Figure 4.17, Figure 4.18, and Figure 4.19 are declared the highest and lowest pressure coefficient on the circumference of the blades turbine by presenting with the color map of the contours. Also, there are exhibited the instantaneous streamline pressure where are interacted on the surface of the turbine blades.

The suggestion of this configuration is that better producing rotating torque at the lower of the TSR because it has demonstrated that the Savonius rotor has generated positive torque, and while the turbine operating has wide interaction of each turbine blade within the fluid flow past the turbine.
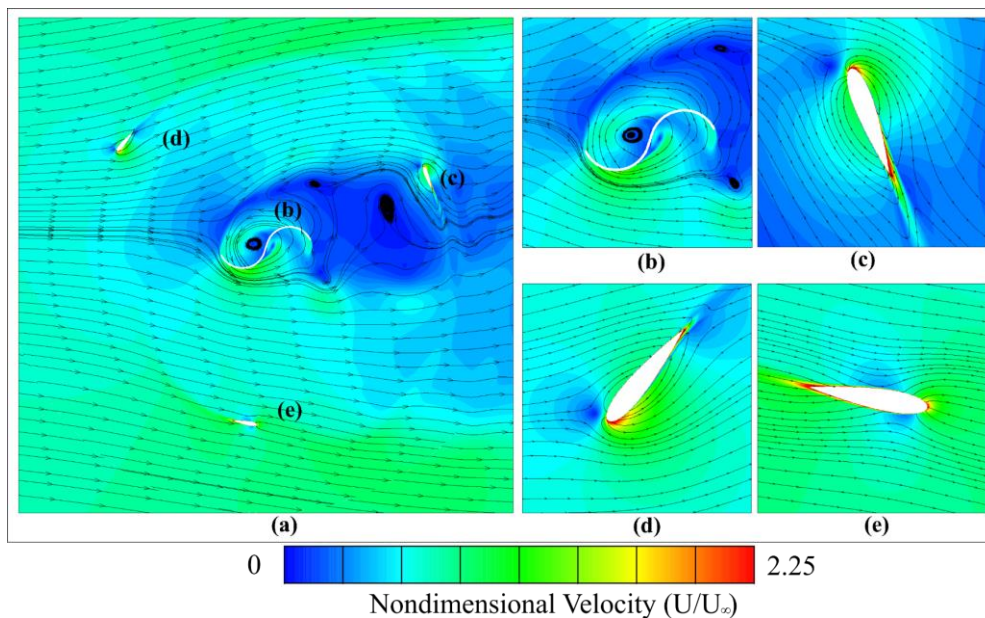

Figure 4.14. The velocity contour of the turbine of solidity 0.2 at 0 deg with a TSR of 3.5, (b), (c), (d), and (e) are the contours of the fluid interaction with the turbine blades.

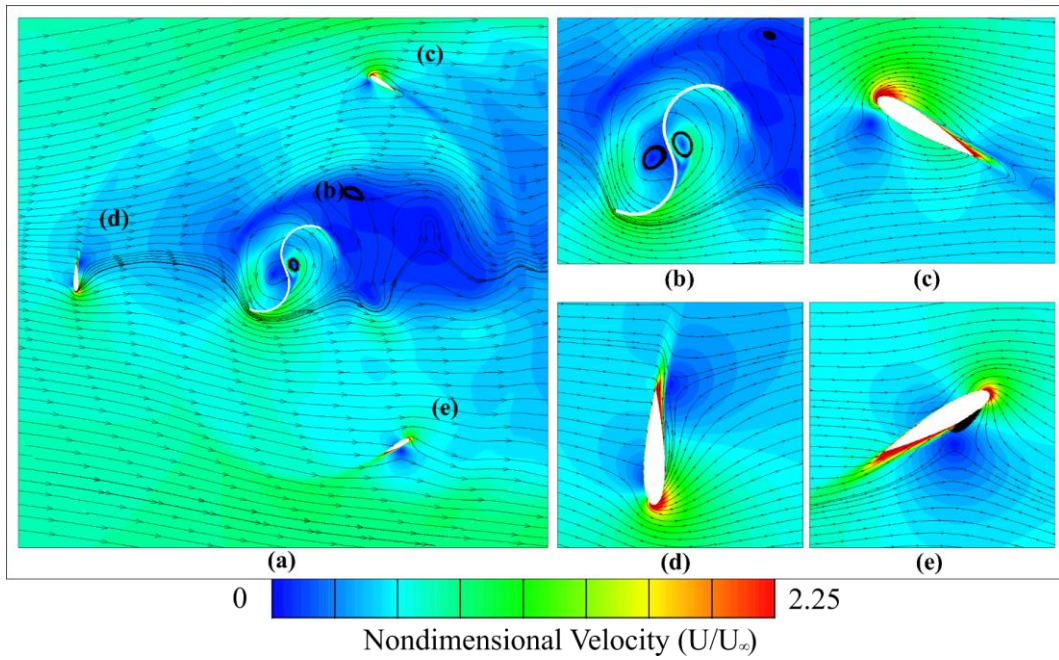Figure 4.15. The velocity outlines at 50 deg of the combined rotor, (b), (c), (d), and (e) are the contours of the fluid interaction and instantaneous streamlines velocity over the turbine blades.
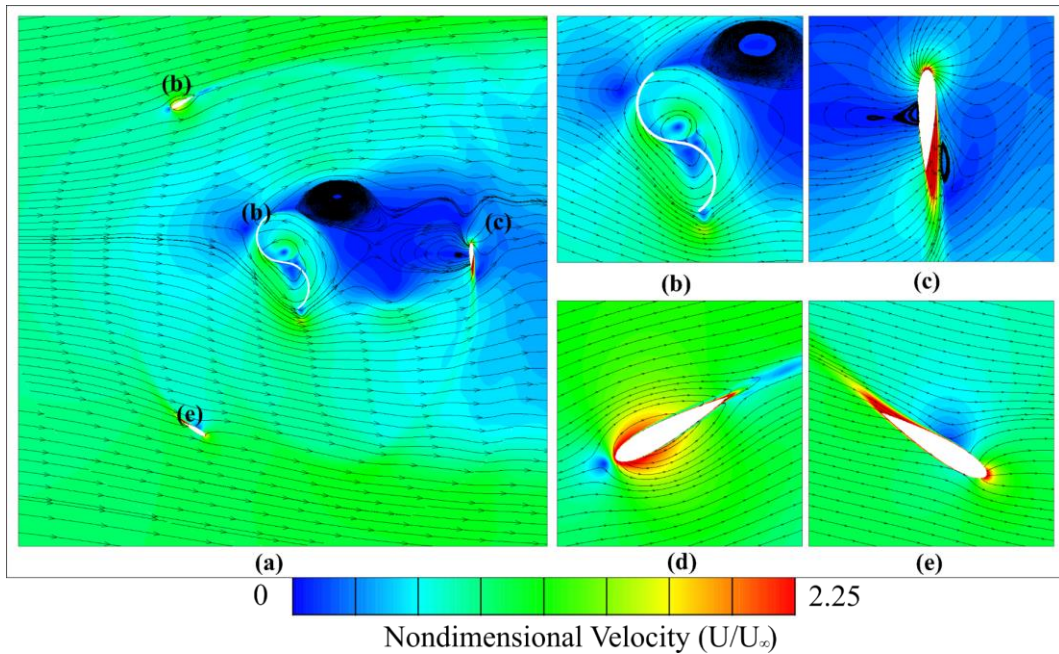
Figure 4.16. The velocity profile at 100 deg of the turbine rotating, (b), (c), (d), and (e) are the contours of the magnitude velocity and instantaneous velocity streamline around the turbine blades.

Figure 4.17. The pressure contour at 0 deg, (b), (c), (d), and (e) are the profile of the pressure coefficient and instantaneous streamlines pressure interaction with the turbine blades.
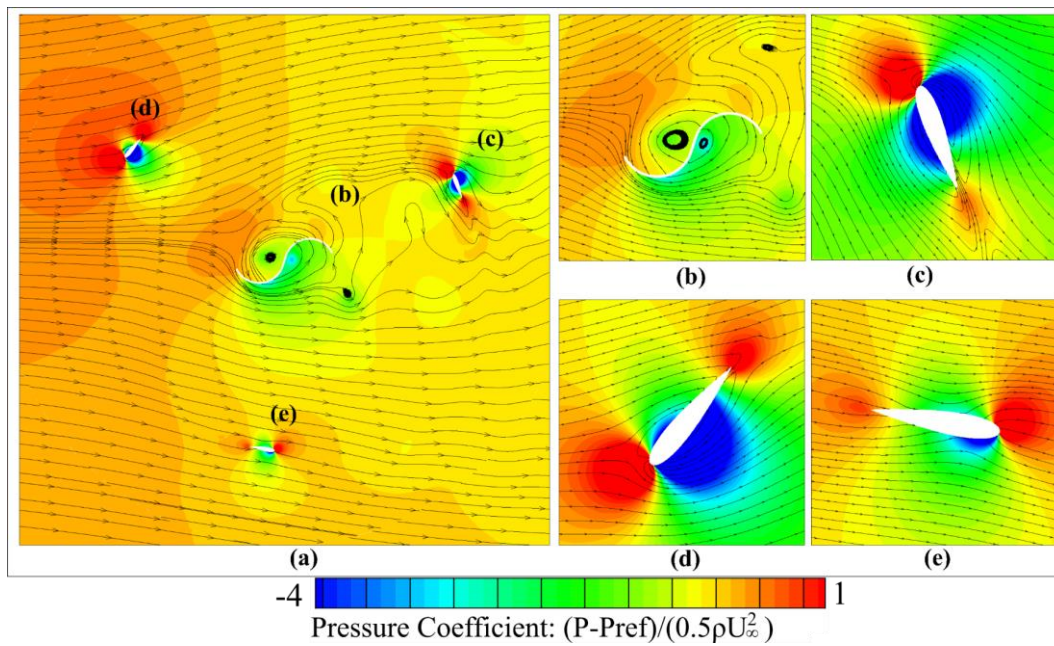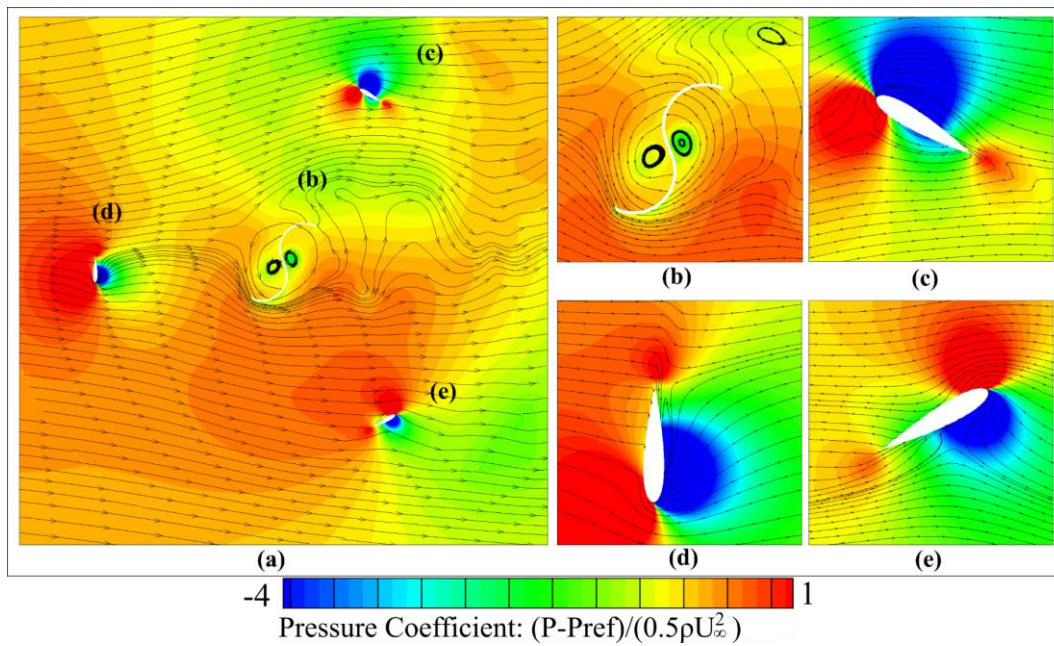

Figure 4.18. The pressure profile at 50 deg of the turbine rotating, (b), (c), (d), and (e) are the contours the pressure coefficient and pressure instantaneous streamlines interaction with the turbine blades.
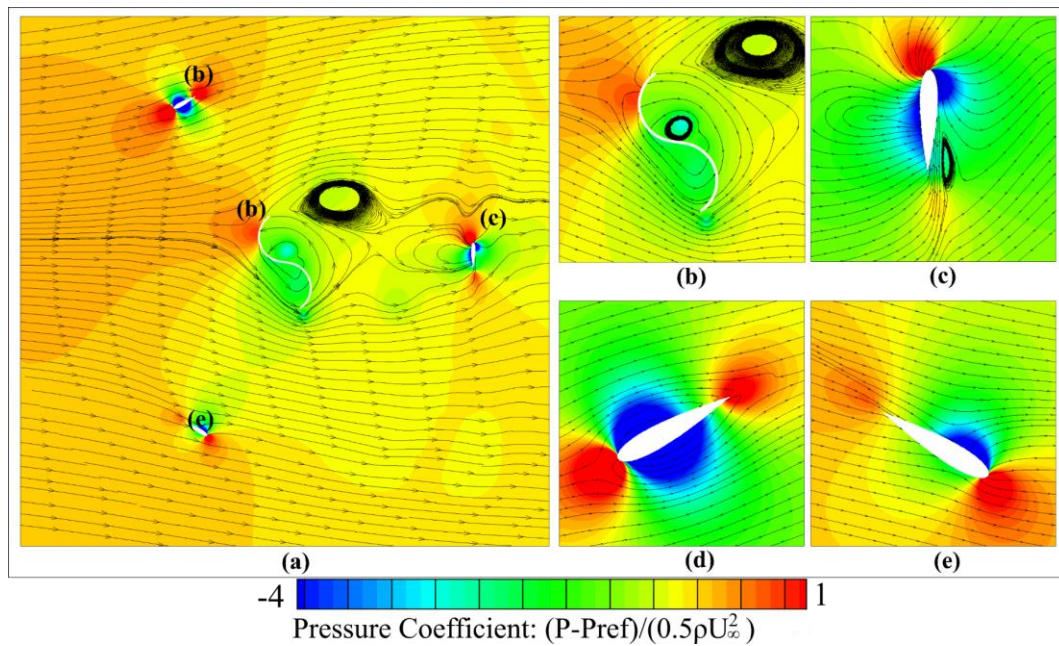
70

Figure 4.19. The pressure outline at 100 deg of the turbine rotating, (b), (c), (d), and (e) are colorized the pressure coefficient and pressure instantaneous streamlines around the turbine blades.

4.4.2 Solidity of 0.3

The combined rotor for the solidity of 0.3 is modified of the chord length equal to 100 mm. It is clarified the best aerodynamic characteristic which is stated by the previous study. Also, this present work has been performed to add the Savonius turbine in the middle of the Darrieus turbine. The result as shown in Figure 4.59 is established the increase of the C_M higher than the hybrid turbine of solidity 0.2. Further, it is simplified the higher and lower C_M value at the specific position of the turbine rotation. At 50 deg the turbine is conducted the optimum performance because the turbine blades produced the lower shading and less vortex. The opposite, at 0 and 100 deg the airfoil **(c)** has been shaded by the Savonius turbine form into the vortex, so that is the reason for reducing the turbine performance. Definitely, the entire turbine has been reduced the performance. Figure 4.20, Figure 4.21, and Figure 4.22 are established the velocities contours and velocity instantaneous streamline. Basically, the velocity contours have been represented color map which is detailed the fluid interaction to blades turbine and streamline flow around each blade of the turbine. Besides, Figure 4.23, Figure 4.24,

and Figure 4.25 are prescribed the color map of the pressure coefficient contours and pressure instantaneous streamline.

In summary, the solidity of 0.3 investigated a suitable configuration to produce a better performance at the optimum TSR. Also, the lower of TSR, the turbine has enough space for the fluid flowing along with the turbine blade. The rear of the blade turbine has not much obstructed from the upstream flow, meanwhile, the shading region and fluid wake motion have been reduced. There are many reasons that this configuration has implemented better performance. But in the suggestion, it is not either of the selected configurations in the further model if it compared to the conventional study.

Figure 4.20 The velocity profile at 0 deg of the turbine azimuth angle, (b), (c), (d), and (e) are colorized of the magnitude velocity and velocity instantaneous streamlines around the blades turbine
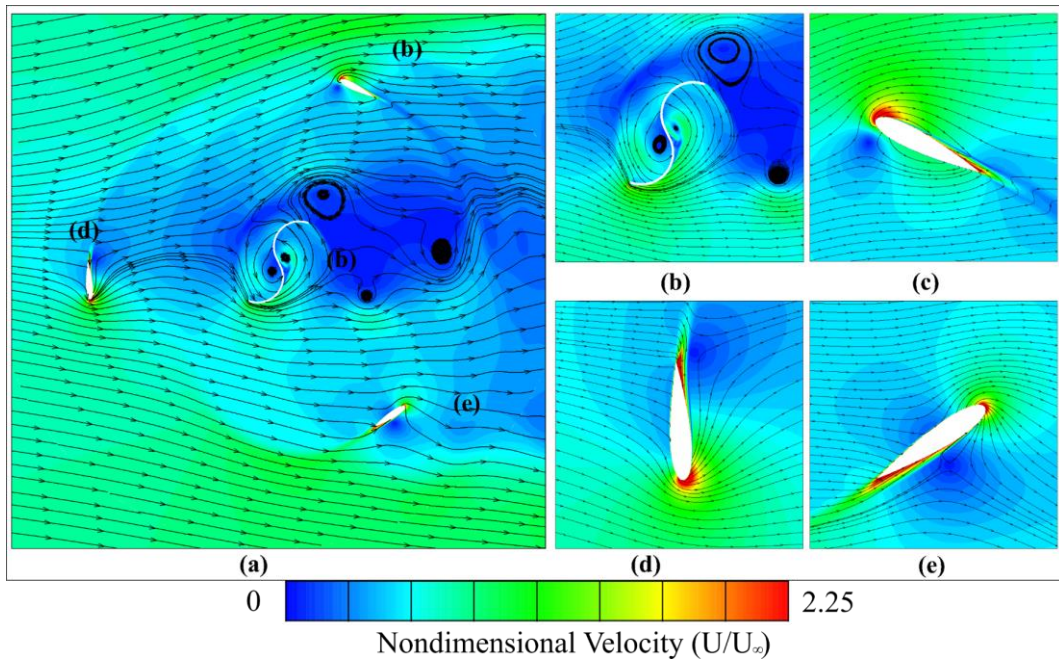
Figure 4.21 The velocity contour at 50 deg of the turbine rotating, (b), (c), (d), and (e) are the contoured of the magnitude velocity color and velocity instantaneous streamlines on all sides the blades turbine
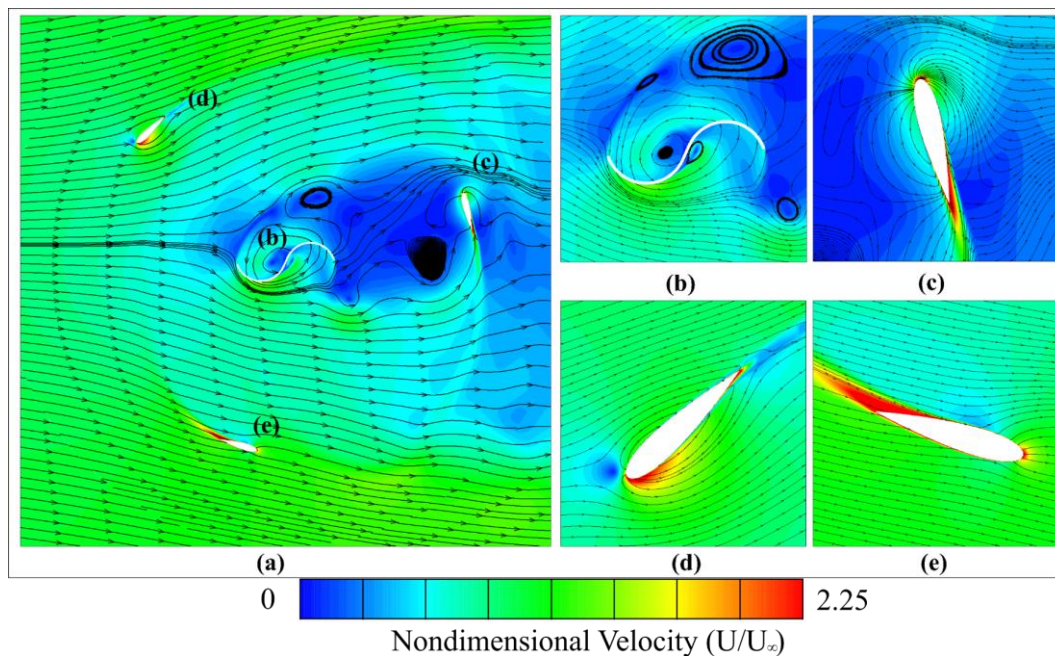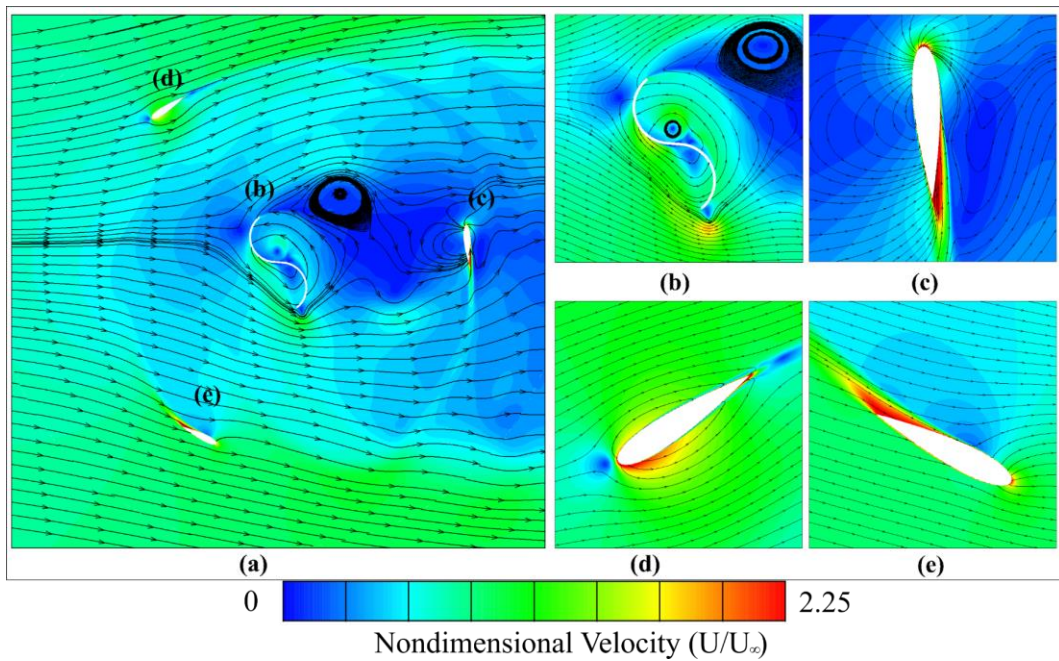

Figure 4.22 The velocity profile at 100 deg of the turbine rotated, (b), (c), (d), and (e) are of the magnitude velocity and the instantaneous streamlines velocity close to the blades turbine.

Figure 4.23 The pressure contour at 0 deg of the turbine rotating, (b), (c), (d), and
(e) are colorized the pressure coefficient and pressure instantaneous
streamlines around the blades turbine

Figure 4.24 The pressure outline at 50 deg of the turbine rotated, (b), (c), (d), and
(e) are the pressure coefficient and pressure instantaneous streamlines
in circumference the blades turbine.

Figure 4.25 The pressure contour at 100 deg of the turbine rotated, (b), (c), (d), and (e) are the pressure coefficient contours and pressure instantaneous streamlines around the blades turbine
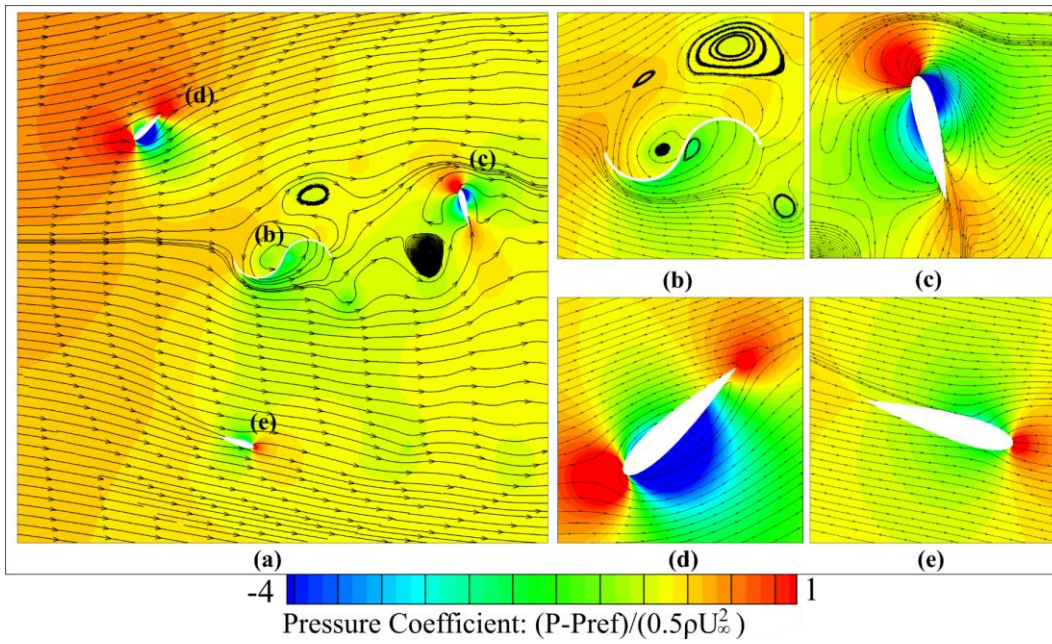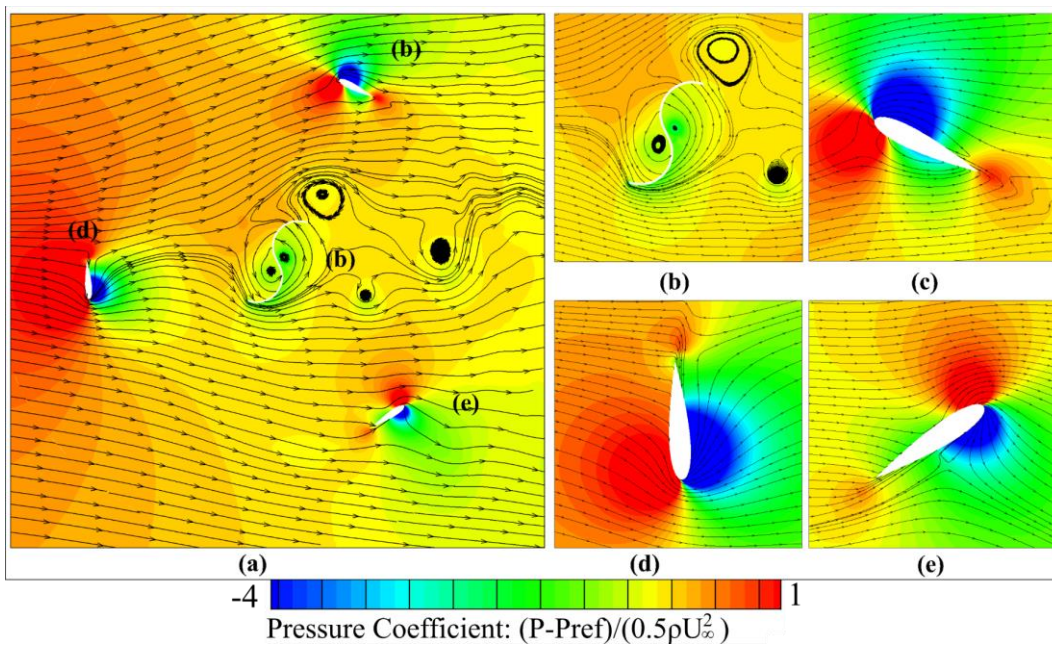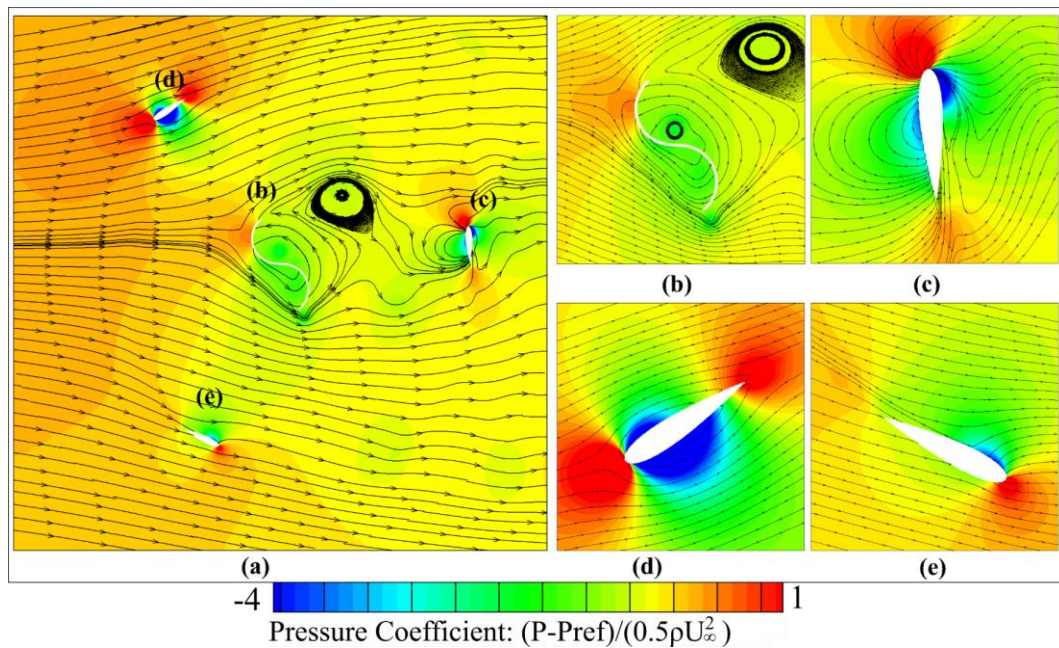
4.4.3 Solidity of 0.4

The third testing on the solidity of 0.4 of the combined rotor which is modified the airfoil chord length of 133.33 mm. Based on the performance graph as shown in Figure 4.57, the solidity of 0.4 is the best performance compared to conventional analysis. Figure 4.49 as presented below is a graphic of the optimum performance for the turbine rotating in a circle. Also, it is defined as the optimized value of the performance in each position of the turbine rotation. Figure 4.26, Figure 4.27, and Figure 4.28 are illustrated the velocity magnitude of fluid interaction over the combined rotor, and there are offered the velocities instantaneous streamlines around the turbine blades. Figure 4.29, Figure 4.30, and Figure 4.31 are appeared the pressure coefficients and pressure instantaneous streamlines nearby the surface of the blades turbine. The observation on the color map of the turbine contours is indicated that higher pressure or velocity is situated near the blade and low shading between each of the turbine blades. Definitely, the performance of the combined rotor has been changing in every different azimuth angle, for example, the optimum C_M is demonstrated at the azimuth angle of 50 deg by indicating with low shading

fluid flow and less vortex point. Moreover, the pressure contours at the high of the performance (50 deg) have demonstrated high-pressure regions such as blade (**d**) of the turbine rotating position. Mostly, the streamlines are mainly used for the analysis of the fluid flow characteristic such as wake motion, shading region, and fluid flow interaction on the turbine blades. For the evidence the pressure and velocity contours of this present work, which are less producing performance by showing that there are many wakes of fluid motions, and shading regions of the downstream blade.

In summary, this configuration (σ=0.4) is generated higher performance by comparing it to the conventional configuration. Therefore, it was better to produce the performance relatively established the best interaction between fluid flow past the turbine. Extremely, it is the optimum feature for using in further research and improving the performance, applying to the future simulation and prototype of the application.

Figure 4.26 The velocity contour at 0 deg of the turbine azimuth angle, (b), (c), (d), and (e) are the profile of the magnitude velocity and instantaneous streamlines velocity along with the blades turbine.

Figure 4.27 The velocity contour at 50 deg of the turbine rotated, (b), (c), (d), and (e) are the magnitude velocity profiles and velocity instantaneous streamlines around the blades turbine

Figure 4.28 The velocity contour at 100 deg of the turbine rotated, (b), (c), (d), and (e) are the magnitude velocity profile and velocity instantaneous streamlines around the blades turbine.
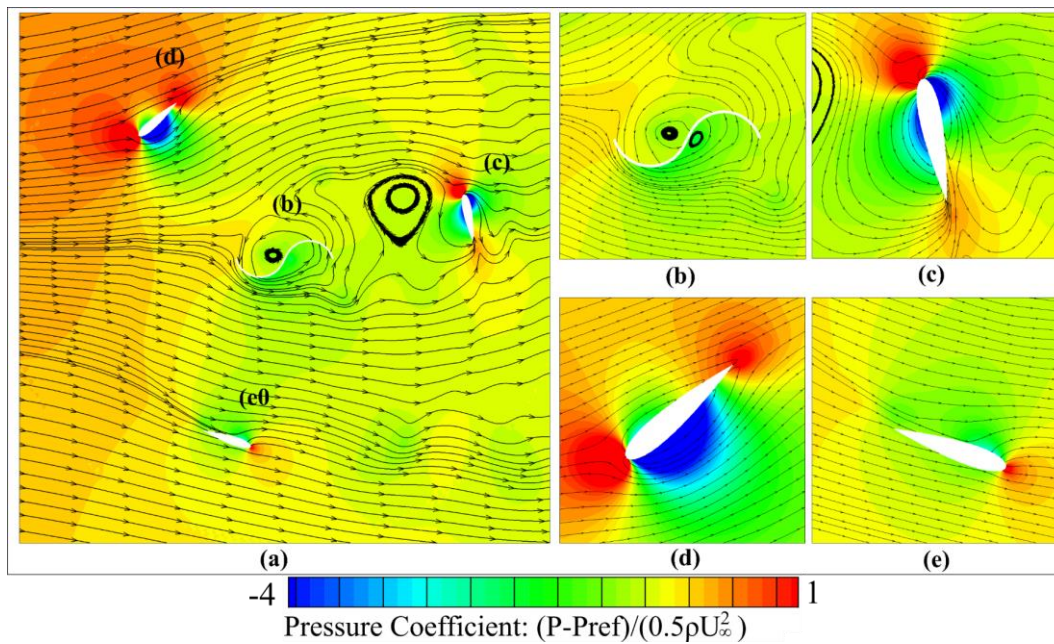
Figure 4.29 The pressure contour at 0 deg of the turbine rotated, (b), (c), (d), and (e) are the outlines of the pressure coefficient and pressure instantaneous streamlines close to the blades turbine.
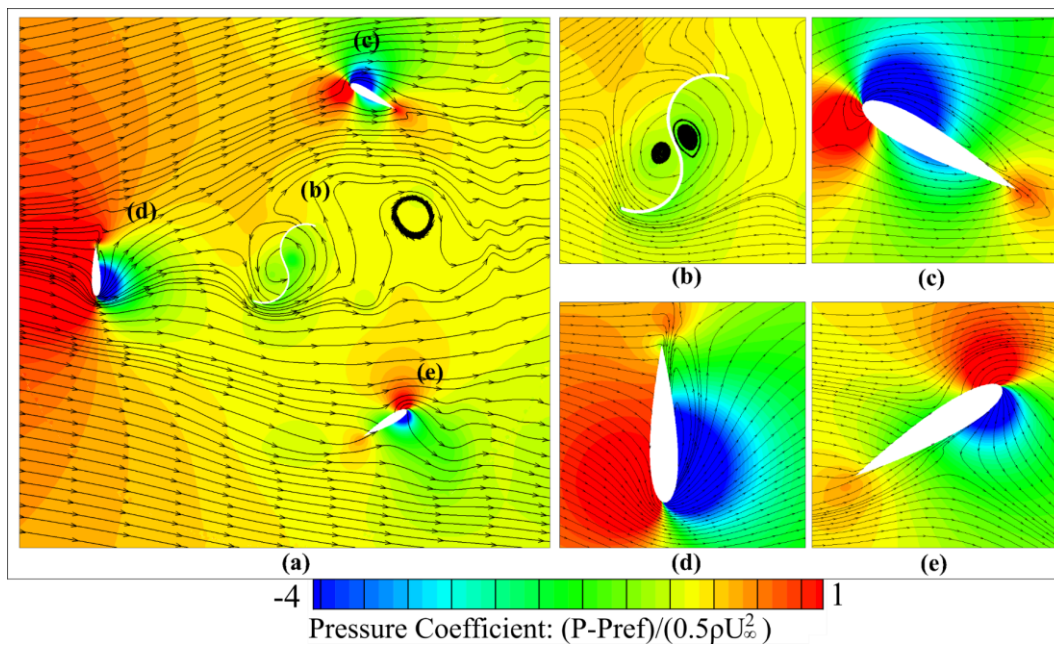
Figure 4.30 The pressure profile at 50 deg of the turbine rotated, (b), (c), (d), and (e) are the pressure coefficient contours and pressure instantaneous streamlines close to the blades turbine
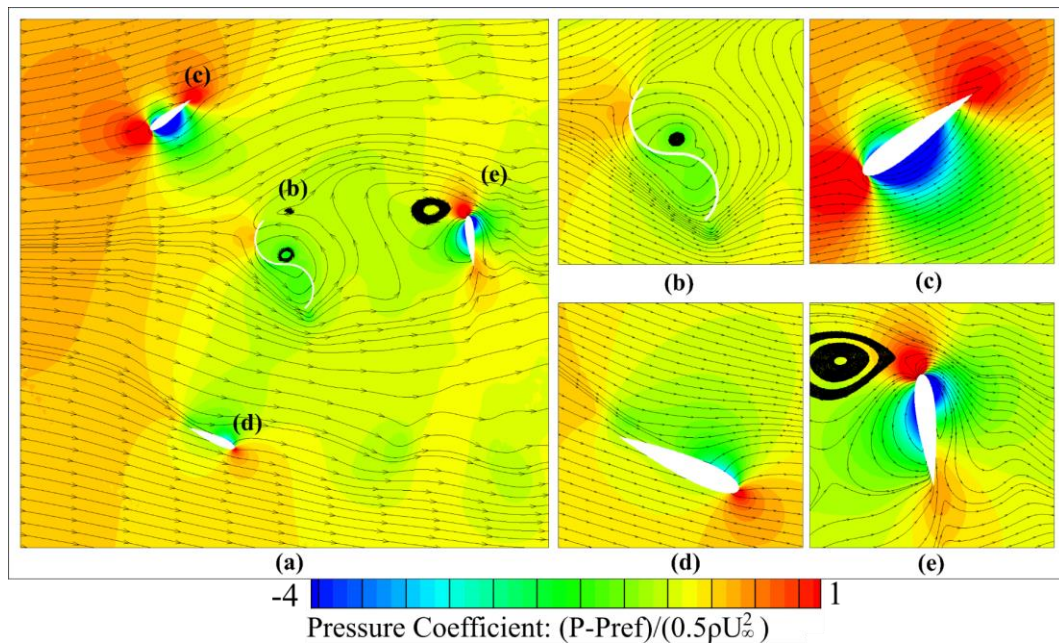
Figure 4.31 The pressure profile at 100 deg of the turbine azimuth angle, (b), (c), (d), and (e) are the pressure coefficient contours and pressure instantaneous streamlines close to the blades turbine

4.4.4 Solidity of 0.5

The combined rotor of the solidity of 0.5 is demonstrated higher C_M than the previous analysis of the solidity = (0.2-0.4) with the low TSR as shown in Figure 4.56. The description of this case is not different from the previous case, for instance, Figure 4.59 is exemplified the C_M value with the characteristic of a full rotation of the wind turbine. Also, each turbine contours are shown in Figure 4.32, Figure 4.33, and Figure 4.34 which are determined the position conducting the higher and lower C_M value. Furthermore, there are explained the flow representative with the instantaneous streamline over the turbine blades. Especially, the color map is colored to indicate the shading and vortex zone. Figure 4.35, Figure 4.36, and Figure 4.37 are presented with the pressure coefficient color map and instantaneous streamlines. In conclusion, this model is defined as the higher C_M when the turbine rotated at 50 deg, 175 deg, and 300 deg but, lower of the C_M was at 0 and 100 deg, 240 deg, and 360 deg. Based on those velocity and pressure contours are conducted much of wake motion and shading region. The Savonius turbine has been shaded by the large length of the chord of the Darrieus rotor. But, it is better fluid interaction that is occurred at the low of the TSR.
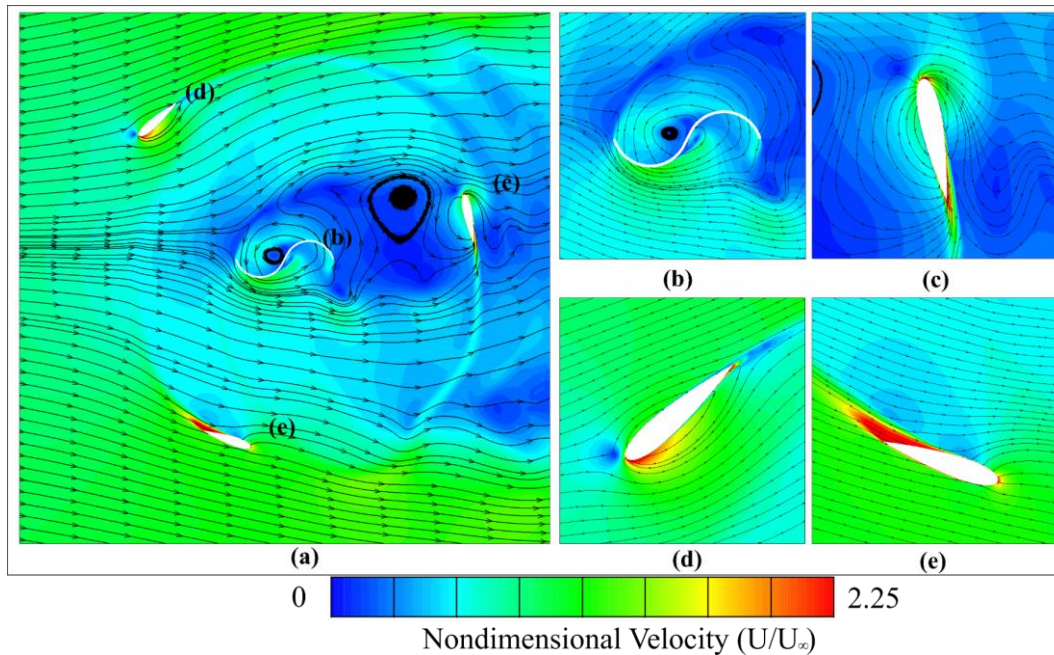
79

Figure 4.32 The velocity contours at 0 deg of the turbine rotated, (b), (c), (d), and (e) are the contours of the magnitude velocity and the instantaneous streamlines velocity around the blades turbine.
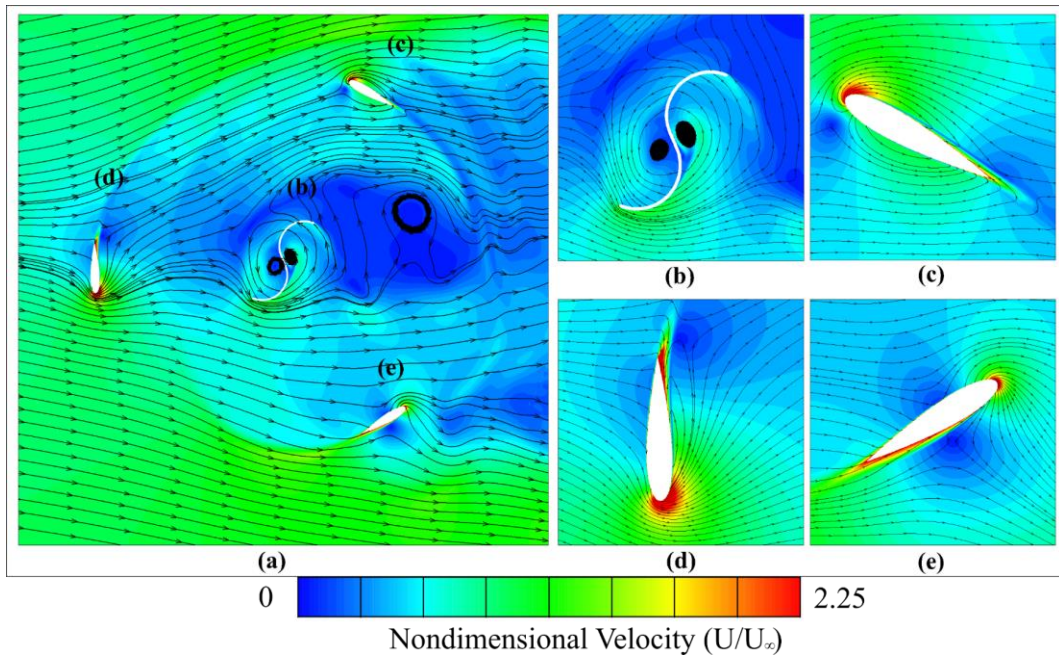

Figure 4.33 The velocity contour at 50 deg of the turbine rotated, (b), (c), (d), and (e) are the magnitude velocity profiles and velocity instantaneous streamlines around the blades turbine.
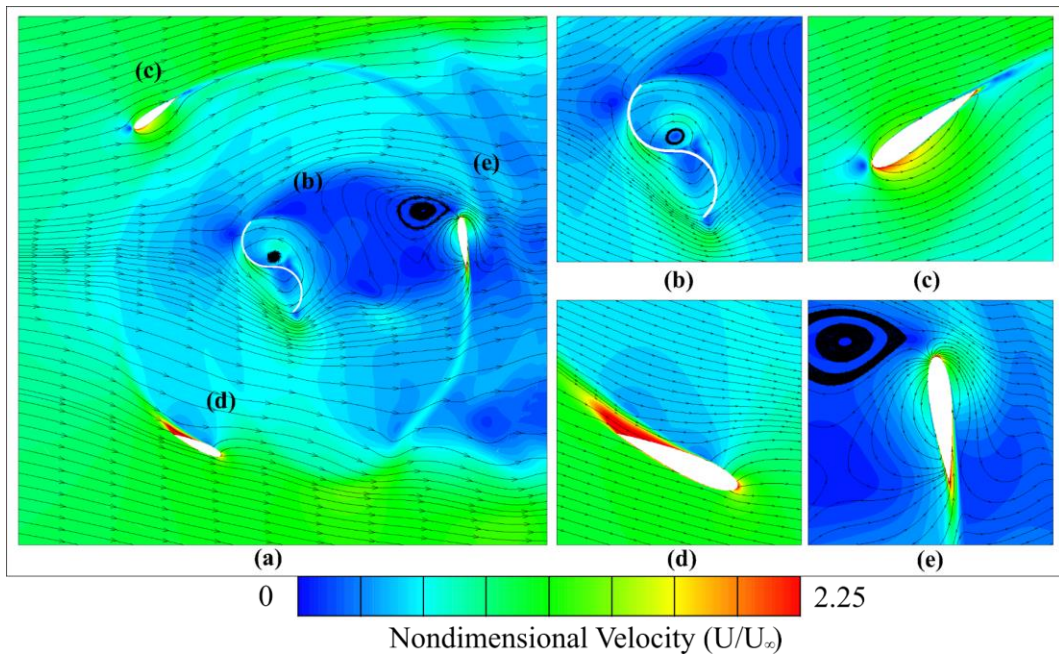
Figure 4.34 The velocity contour at 100 deg of the turbine azimuth angle, (b), (c), (d), and (e) are the magnitude velocity profile and velocity instantaneous streamlines around the blades turbine.
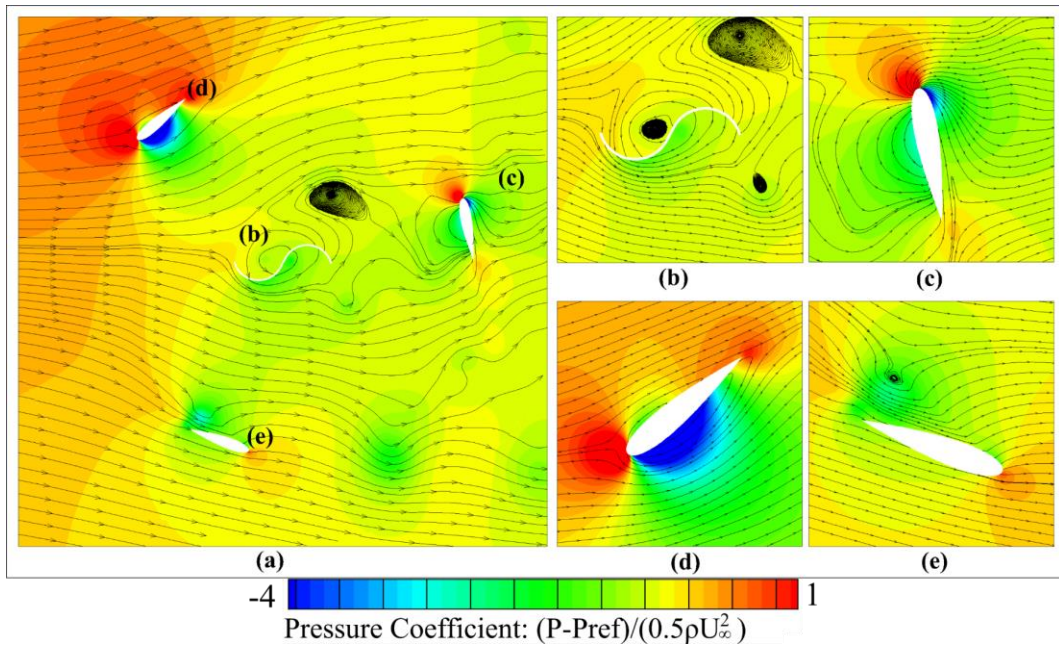
Figure 4.35 The pressure profiles at 0 deg of the turbine rotated, (b), (c), (d), and (e) are the contours of the pressure coefficient and the instantaneous streamlines pressure close to the blades turbine.

Figure 4.36 the pressure profile at 50 deg of the turbine rotated, (b), (c), (d), and (e) are the pressure coefficient contours and pressure instantaneous streamlines close to the blades turbine

Figure 4.37 The pressure profile at 100 deg of the turbine rotated, (b), (c), (d), and (e) are the contours of the pressure coefficient and pressure instantaneous streamlines close to the blades turbine.

4.4.5 Solidity of 0.6

The solidity of 0.6 is defined as the peak coefficient of the moment at the low TSR of 1.75 as illustrated by Figure 4.59. The graphic is demonstrated the lower C_M at 0 deg and 120 deg and the higher C_M at 50 deg. Figure 4.38 and Figure 4.40 are established the velocity magnitude contours and velocity instantaneous streamlines. However, the streamlines characteristic of the contours of those figures (Figure 4.38 and Figure 4.40) are extremely worthless to produce a better performance as a result of shading regions and wake motions. Another case as shown in Figure 4.39 is also the prescribed velocity contours and streamlines which are related to the fluid color behavior with the blades of the turbine. Also, it is indicated the optimum turbine rotated by extracting the peak C_M (50 deg). Figure 4.41, Figure 4.42, and Figure 4.43 are constructed the coefficient of the pressure and the pressure instantaneous streamline along with the surface blades of the wind turbine. It can be concluded of this characteristic is that at any azimuth angle has been producing some negative torque with more shading contours. It is not recommended to use because it has produced lower performance than a solidity of 0.4.

Figure 4.38 The velocity contour at 0 deg of the turbine azimuth angle, (b), (c), (d), and (e) are the magnitude velocity contours and velocity instantaneous streamlines around the blades turbine.
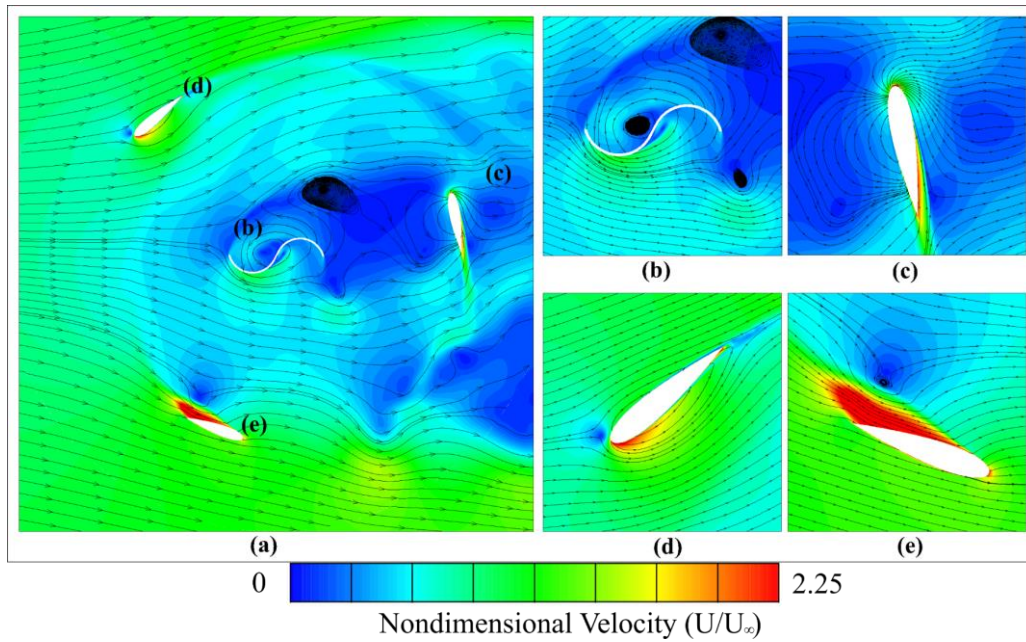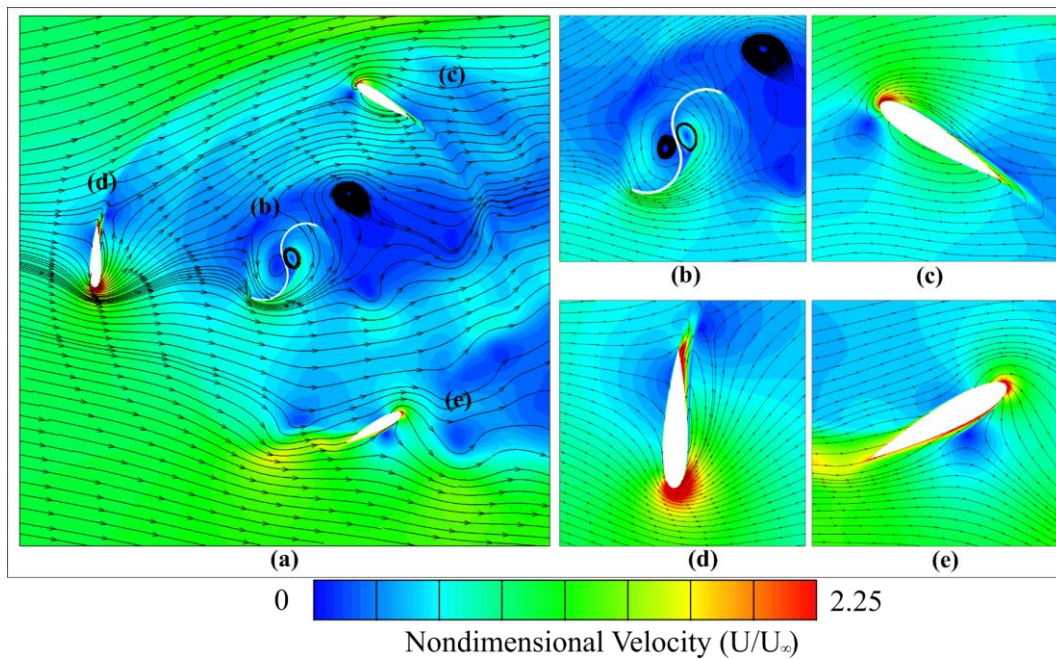
Figure 4.39 The velocity contour at 50 deg of the turbine rotated, (b), (c), (d), and (e) are the magnitude velocity profiles and velocity instantaneous streamlines around the blades turbine.
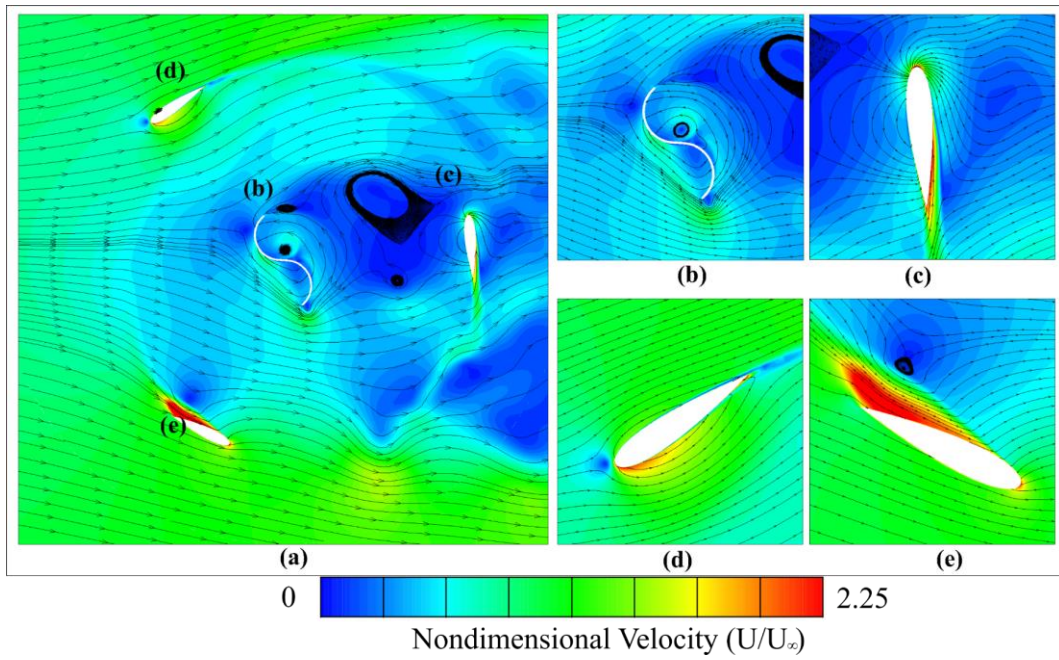

Figure 4.40 The velocity contour at 100 deg of the turbine rotating, (b), (c), (d), and (e) are the velocity magnitude outlines and velocity instantaneous streamlines around the blades turbine

Figure 4.41 The pressure profile at 0 deg of the turbine rotated, (b), (c), (d), and (e) are the pressure coefficient contours and pressure instantaneous streamlines close to the blades turbine.
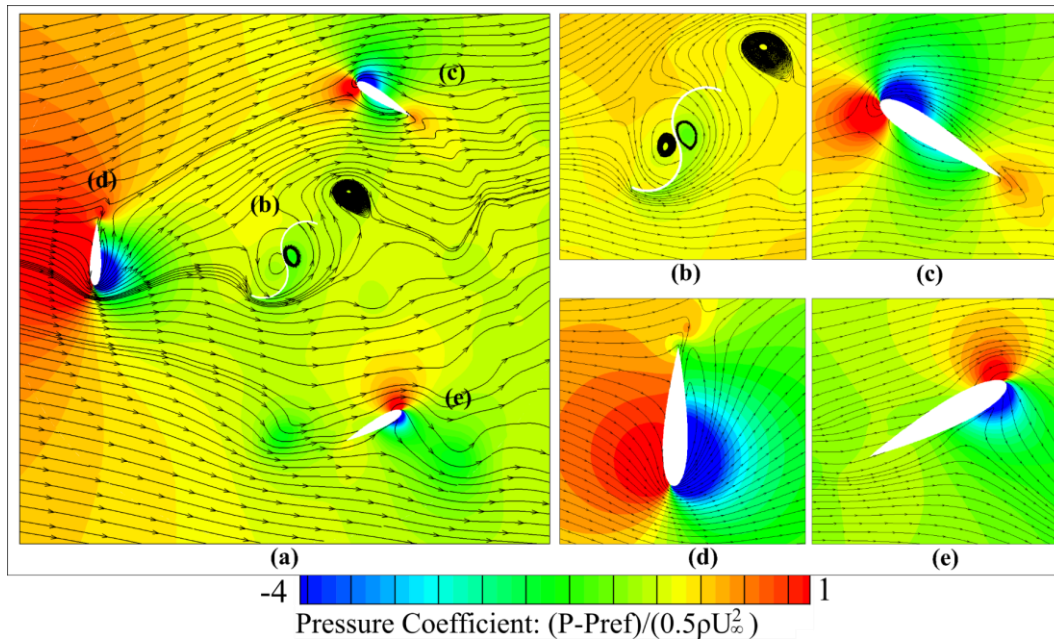

Figure 4.42 The pressure profile at 50 deg of the turbine rotated, (b), (c), (d), and (e) are the pressure coefficient contours and pressure instantaneous streamlines close to the blades turbine.
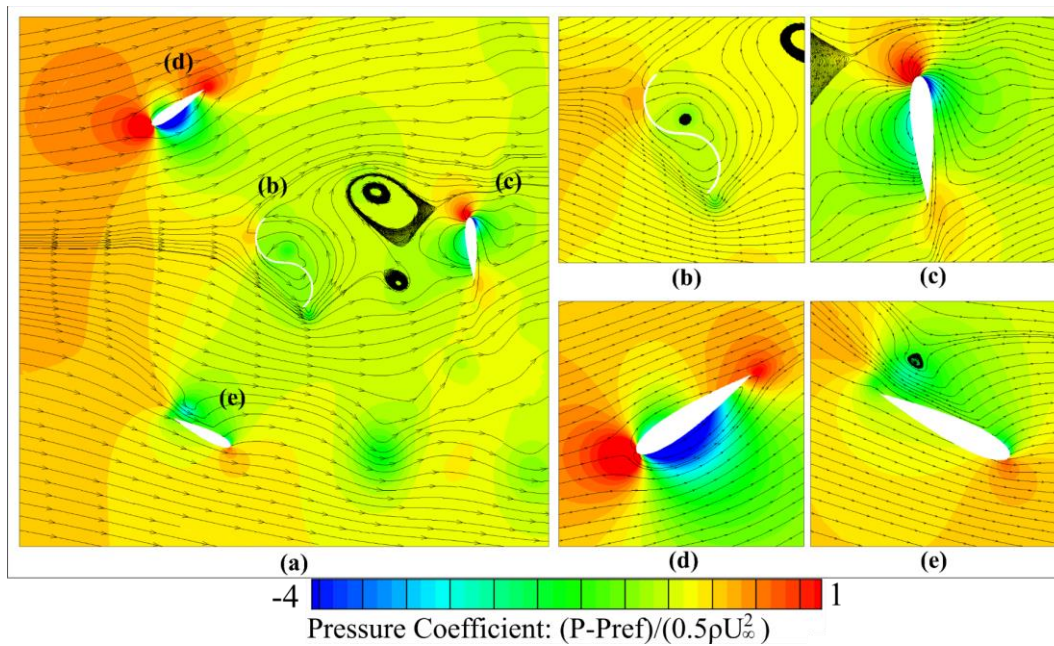
Figure 4.43 The pressure profile at 100 deg of the turbine azimuth angle, (b), (c), (d), and (e) are the pressure coefficient contours and pressure instantaneous streamlines close to the blades turbine

4.4.6 Solidity of 0.7

Another part of this present study is proved the best turbine characteristic and conducted a better aerodynamic performance. However, this case is a high solidity ratio, it conducted an acceptable performance at a low TSR but it is not achievement configuration as long as the low TSR hadn't conducted a higher coefficient of power (C_P) as shown by Figure 4.57. Figure 4.49 is specified the combined rotor rotated character within the low and high C_M to the rotating azimuth angle. Figure 4.44, Figure 4.45, and Figure 4.46 are established the color map of the velocity magnitude and velocity instantaneous streamline over the blades turbine. Base on the color contours, it is exhibited that there are many insignificant for the Savonius turbine as concealing by the airfoil of the Darrieus rotor. Figure 4.47, Figure 4.48, and Figure 4.49 are terms of the pressure coefficient and pressure streamlines over the blades turbine. Also, there are created many effects of the fluid interaction between the H-Darrieus and the Savonius rotor. By the way, it is recommended for using at the low of the TSR because based on the C_M graph this configuration has conducted a high performance at the low range of the TSR value.

Figure 4.44 The velocity contour at 0 deg of the turbine azimuth angle, (b), (c), (d), and (e) are the magnitude velocity profile and instantaneous streamlines velocity around the blades turbine
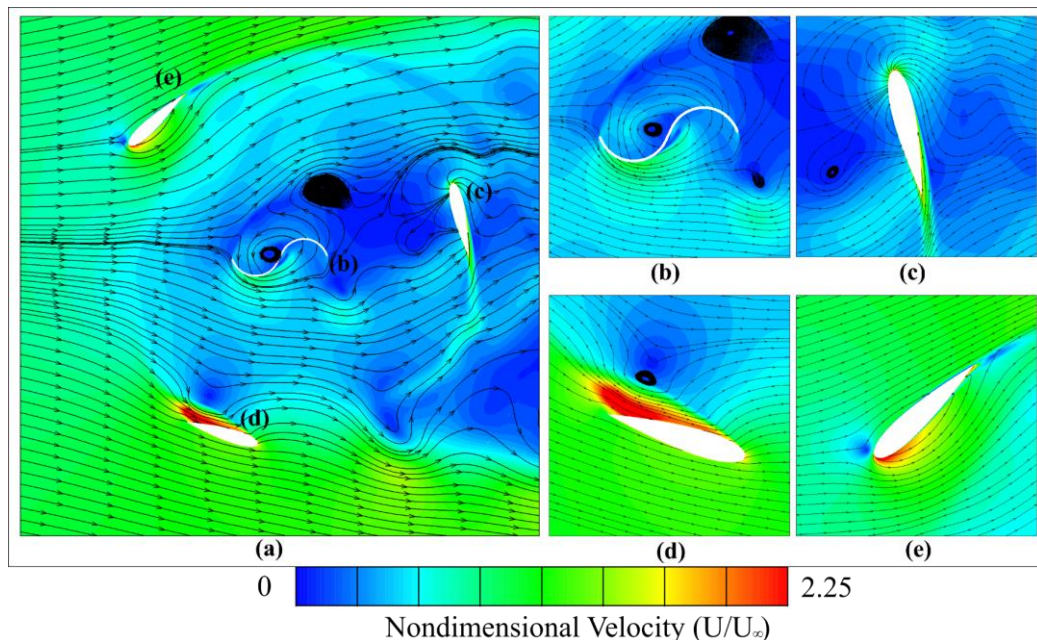

Figure 4.45 The velocity profile at 50 deg of the turbine azimuth angle, (b), (c), (d), and (e) are the magnitude velocity contours and velocity instantaneous streamlines around the blades turbine.
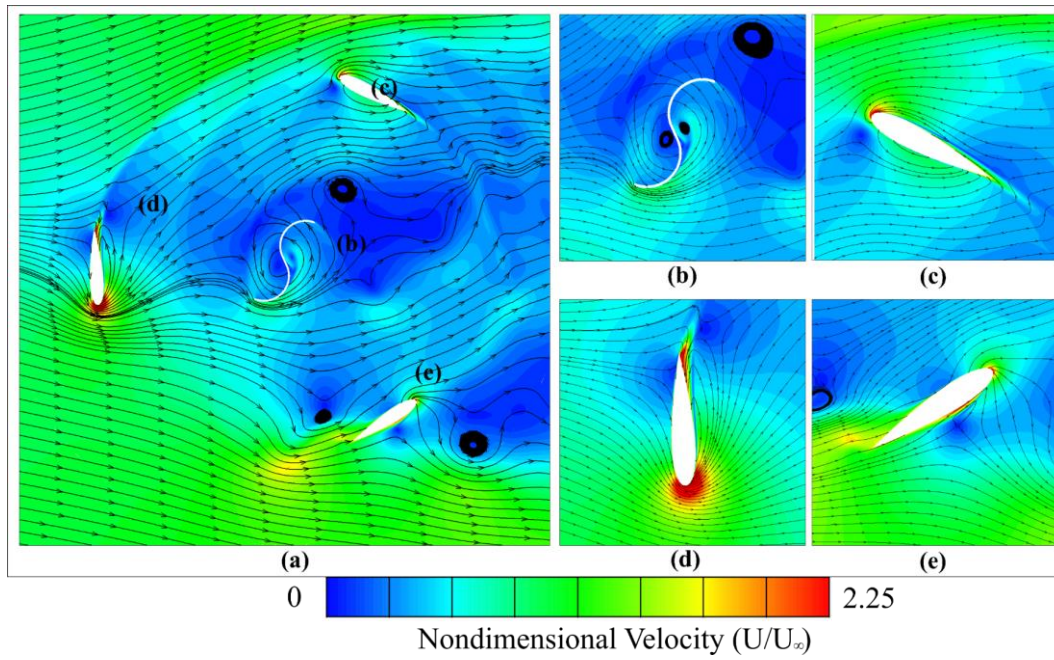
Figure 4.46 The velocity contour at 100 deg of the turbine rotated, (b), (c), (d), and
(e) are the magnitude velocity and the instantaneous streamlines velocity
around the blades turbine.
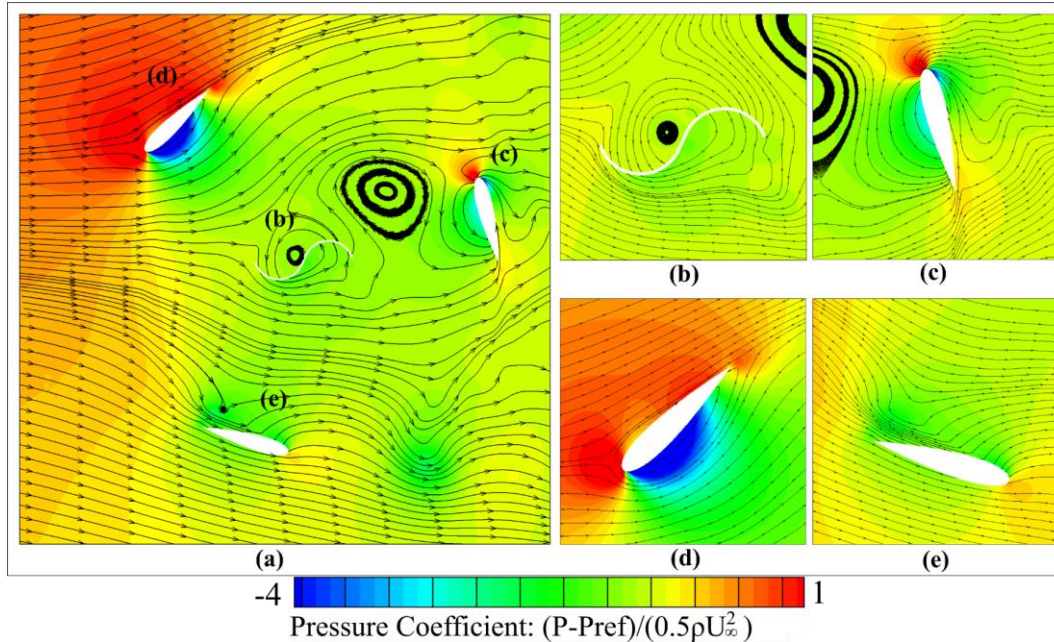
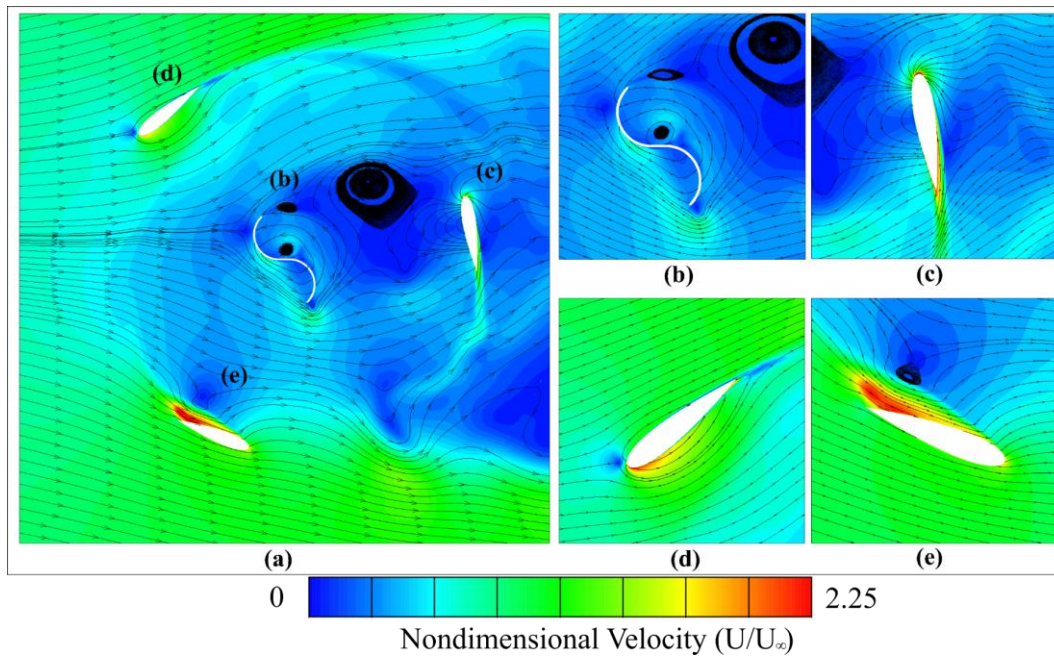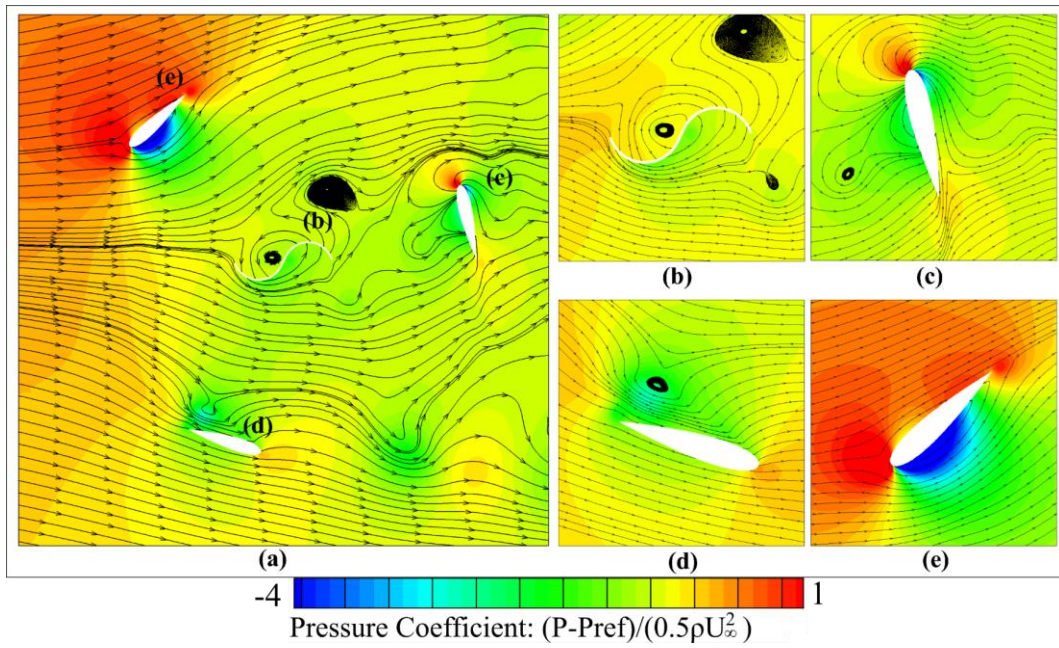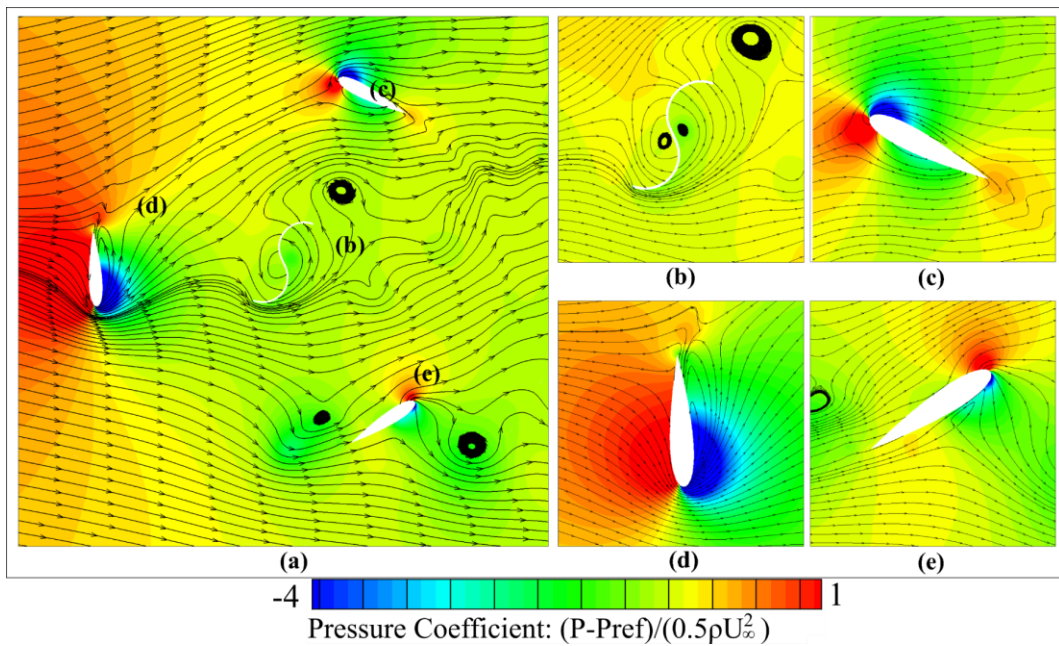Figure 4.47 The pressure profile at 0 deg of the turbine rotated, (b), (c), (d), and (e)
are the pressure coefficient contours and pressure instantaneous
streamlines close to the blades turbine.

Figure 4.48 The pressure contour at 50 deg of the turbine rotated, (b), (c), (d), and (e) are the pressure coefficient outlines and pressure instantaneous streamlines close to the blades turbine.
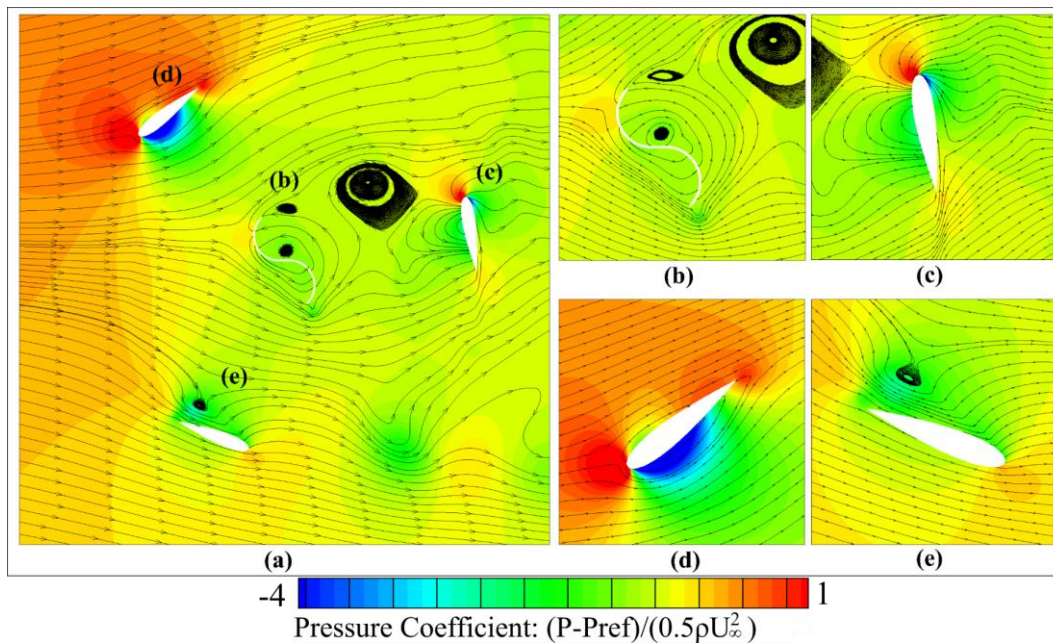

Figure 4.49 The pressure profile at 100 deg of the turbine azimuth angle, (b), (c), (d), and (e) are the pressure coefficient contours and pressure instantaneous streamlines close to the blades turbine

4.4.7 Solidity of 0.8

In the present study, the hybrid turbine through higher solidity is 0.8. This combined rotor has constituted the coefficient of the moment based on the rotating angle as presented by Figure 4.59. Contingent on this Figure 4.59, it has constructed with the higher chord length and much surfaces which is better interacted with the fluid through the entire turbine. Also, it has conducted a higher C_M than conventional analysis at a low TSR of 1.5. Figure 4.50, Figure 4.51, and Figure 4.52 are the contours of the velocity magnitude and velocity streamline along with the blades of the combined rotor. The velocity contours are appeared more effects on the Savonius turbine by the blades obscuring. Figure 4.53, Figure 4.54, and Figure 4.55 are established the pressure coefficient contours and pressure instantaneous streamlines through the blades turbine. There are satisfied to create pressure on the surface blades. However, it is an acceptable configuration, but it is not the achievement for selecting as a better performance because the coefficient of power has been demonstrating in the lowest value compared to the previous analysis. Another evidence, the pressure, and velocity contours have presented much insignificant to generate the force to push the turbine rotating based on shading and high vortex of each turbine blades. However, this configuration (σ=0.8) is highly recommended for designing in the future application at the lower to the TSR because it can be produced a higher performance and better interaction of fluid flow through the turbine. In contrast, it is can't be chosen for the high range of the TSR. According to the C_M graph (Figure 4.56) is determined that at the lower of the TSR the turbine is generated higher of C_M but at a large range of the TSR ($\lambda \geq 3$) this configuration will be produced as the negative torque while it was operating. As the reason why it will be produced negative torque has been explaining in the introduction section of the effect on the solidity ratio. Finally, it is not the best fit configuration for operating along with the large range of the TSR. However, other configuration such (σ=0.4) is more convenient and recommended configuration to use for this present study because it can be operated along with the large range of the TSR and conducted self-starting by the Savonius rotor at the low of TSR.
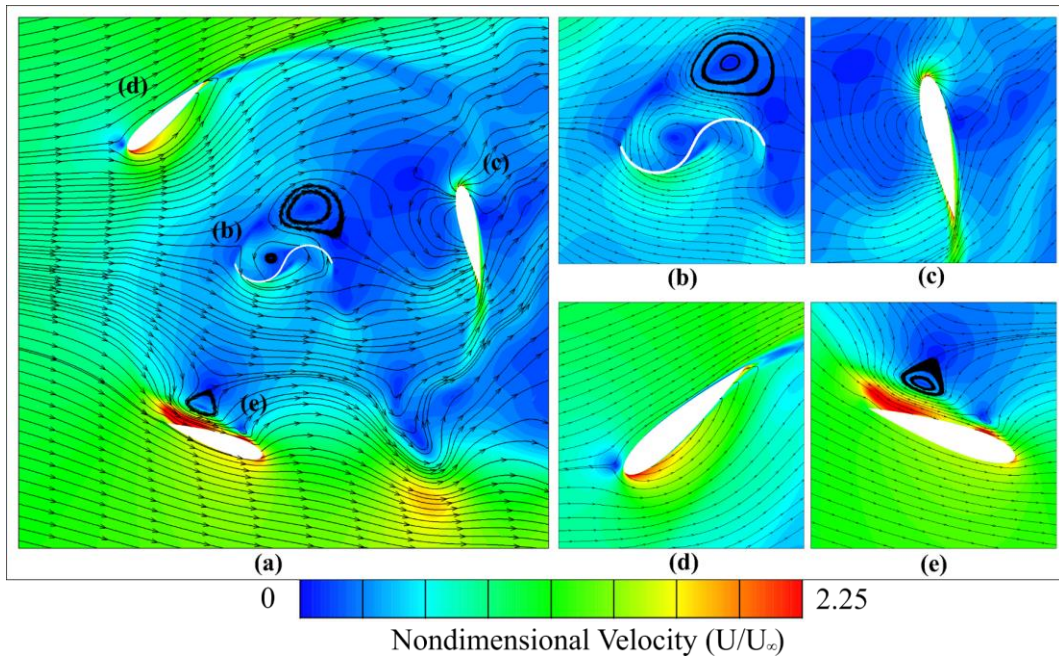
Figure 4.50. The velocity contour at 0 deg of the turbine rotated, (b), (c), (d), and (e) are the magnitude velocity profiles and velocity instantaneous streamlines around the turbine blades.
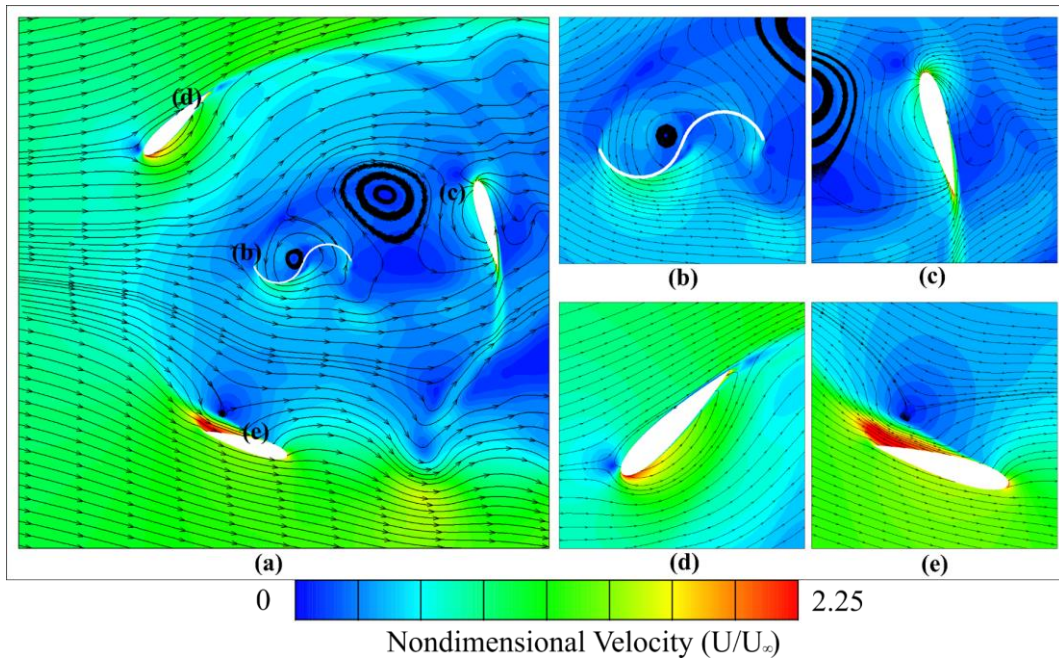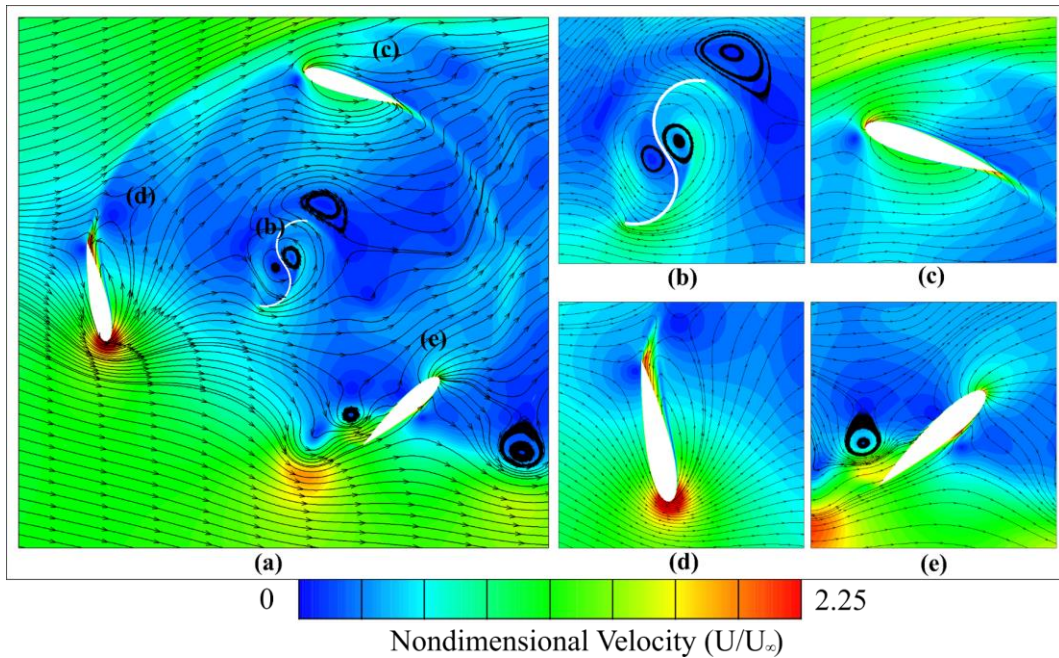

Figure 4.51 The velocity contour at 50 deg of the turbine rotating, (b), (c), (d), and (e) are the magnitude velocity profile and velocity instantaneous streamlines around the blades turbine
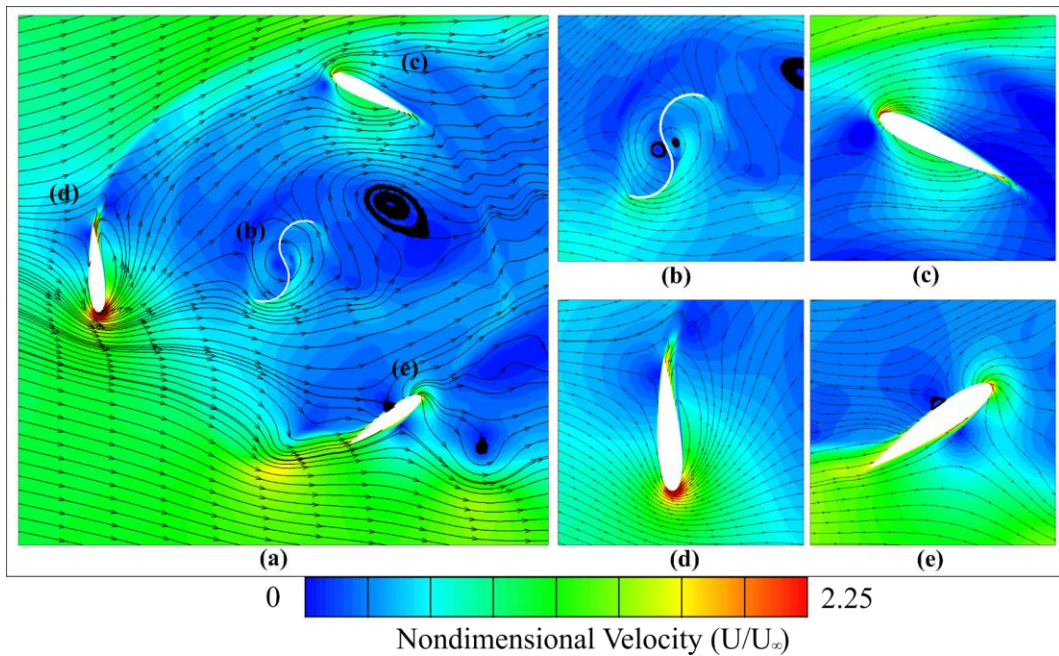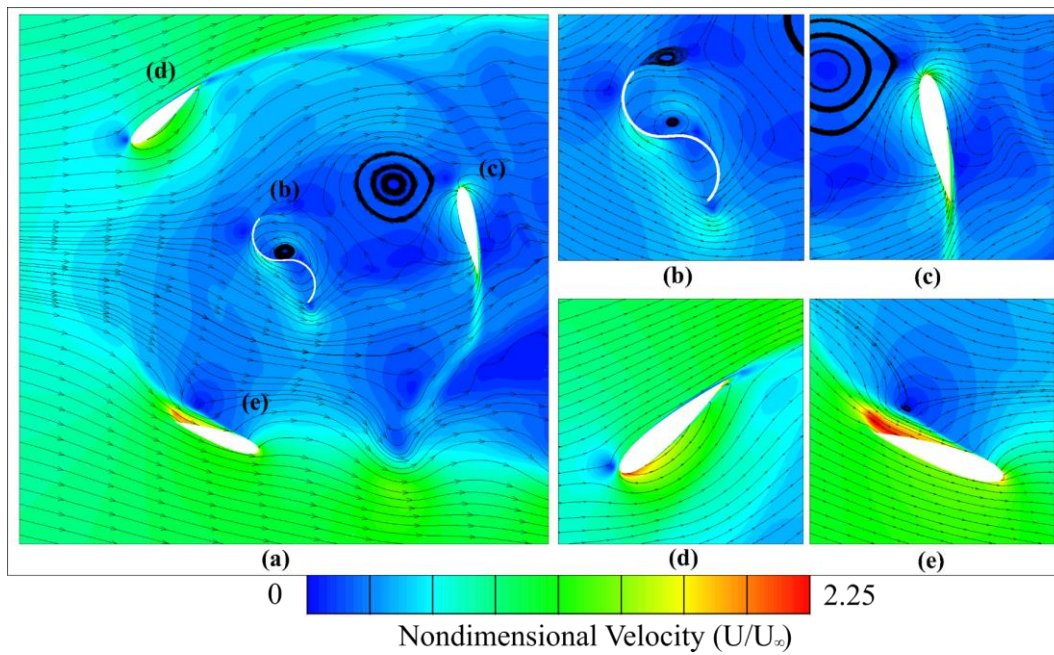
91
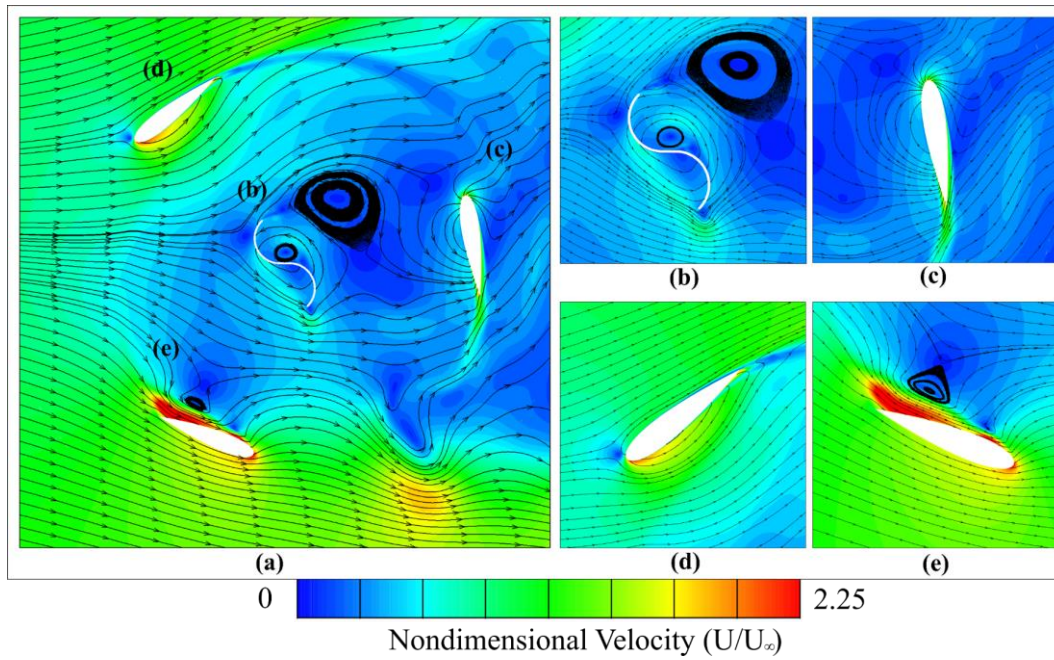
Figure 4.52 The velocity contour at 100 deg of the turbine rotated, (b), (c), (d), and (e) are the magnitude velocity and the instantaneous of the velocity streamlines circumference of the blades turbine
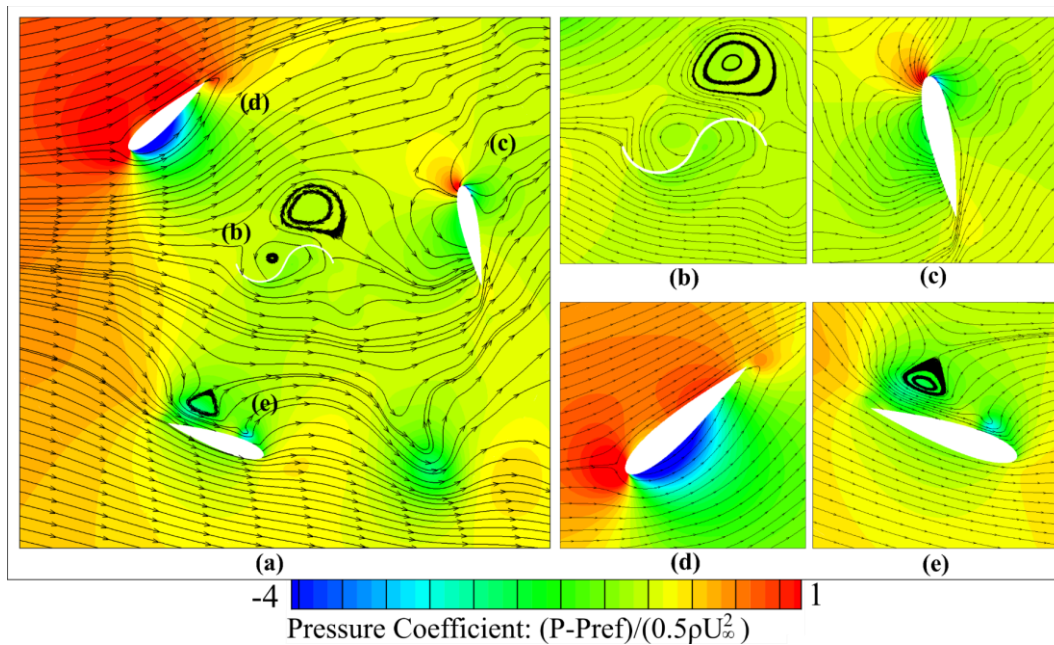
Figure 4.53 The pressure profile at 0 deg of the turbine rotating, (b), (c), (d), and (e) are of the pressure coefficient contours and pressure instantaneous streamlines close to the blades turbine.
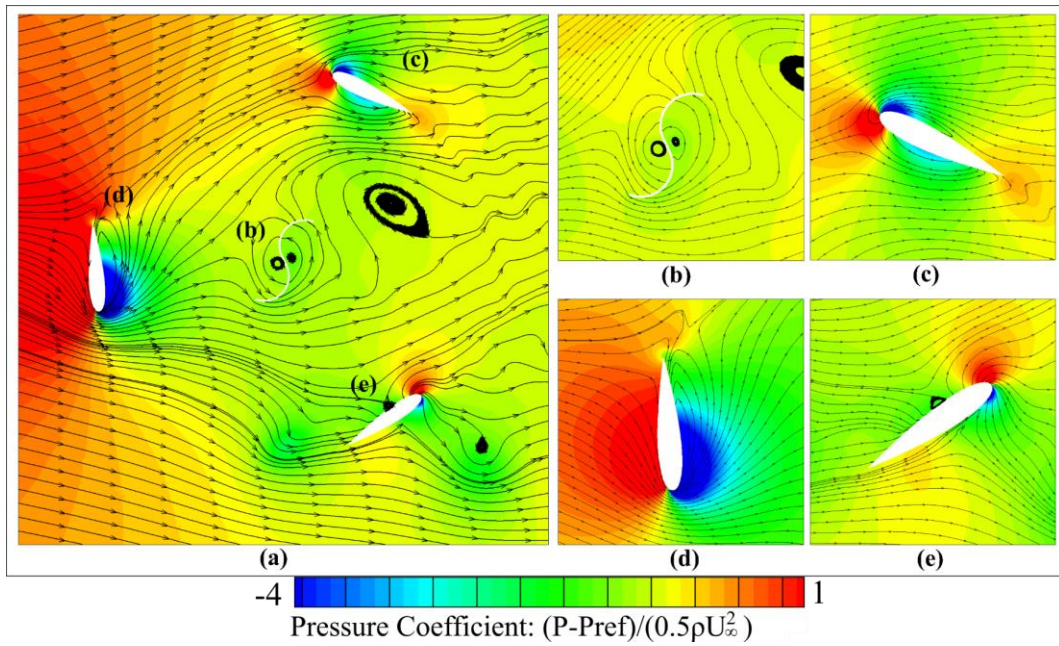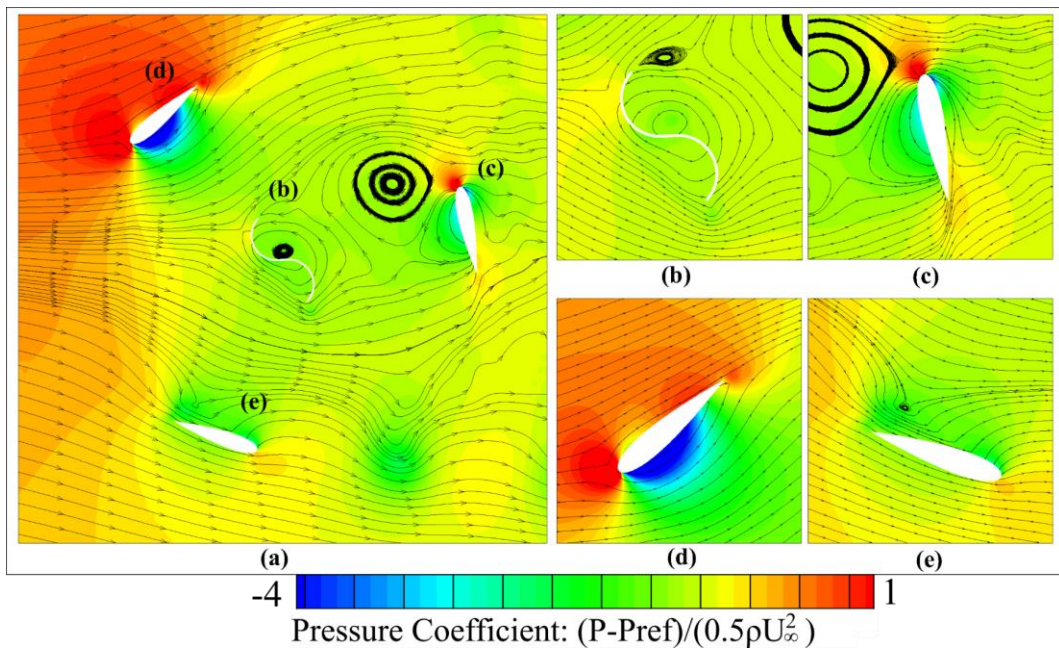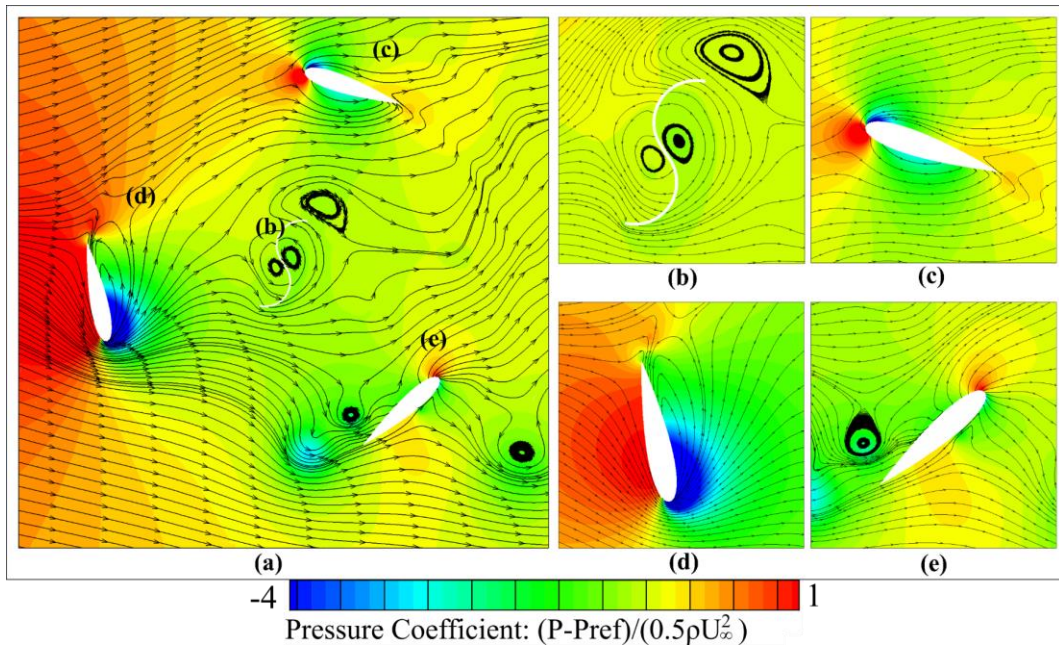
Figure 4.54 The pressure profile at 50 deg of the turbine azimuth angle, (b), (c), (d), and (e) are the pressure coefficient and instantaneous streamlines pressures close to the blades turbine
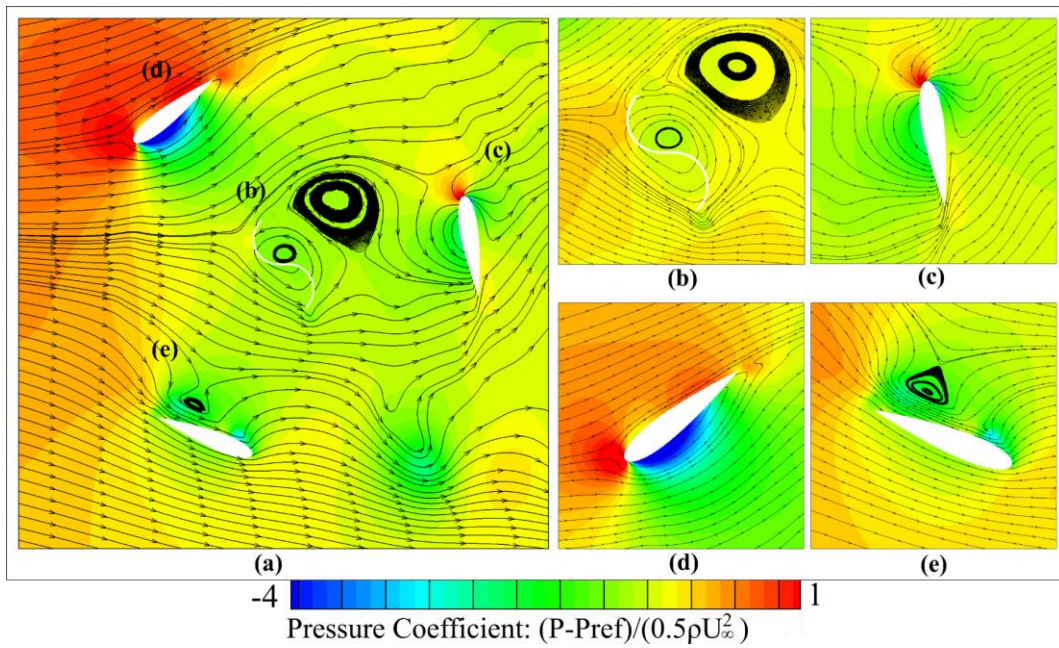
Figure 4.55 The pressure profile at 100 deg of the turbine azimuth angle, (b), (c), (d), and (e) are the pressure coefficient contours and the instantaneous of the pressures streamlines close to the blades turbine.
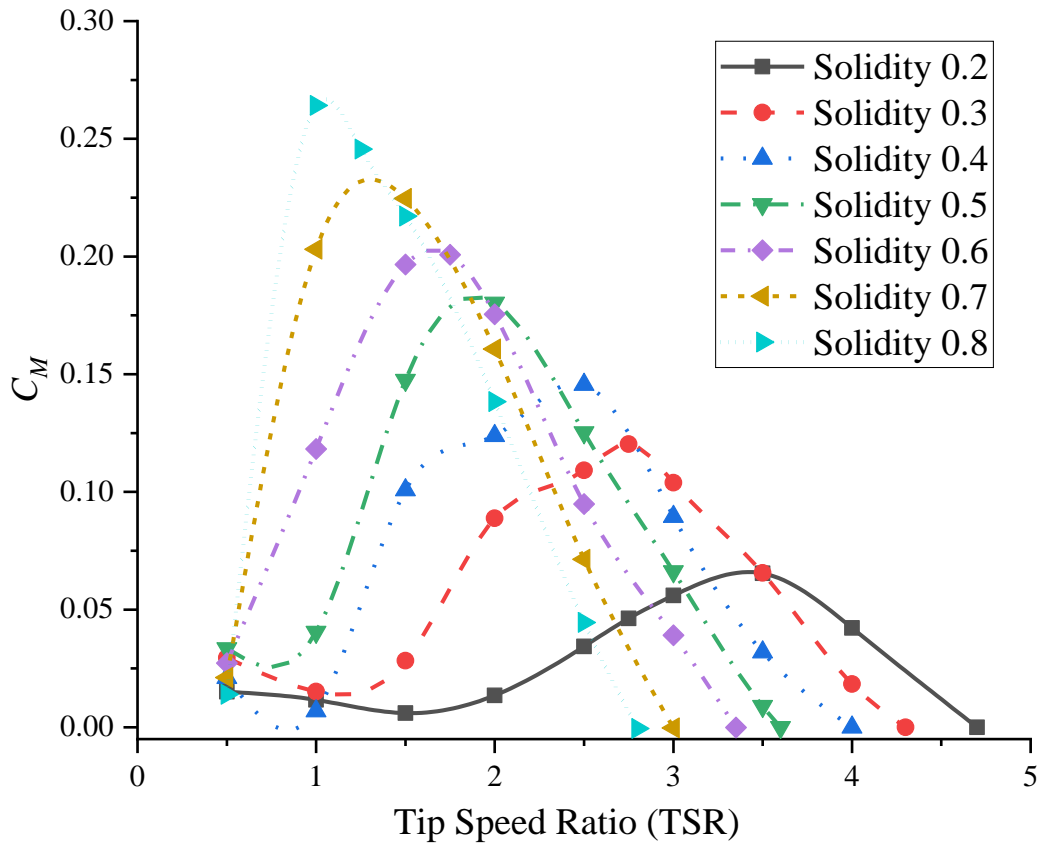
Figure 4.56. The solidities ratios performance in a different range of TSRs.

Following graphs performance (C_P & C_M) as shown above section for the variation of the turbine solidity, however, Figure 4.59 is established the graphs of each solidity ratio at the optimum TSR. Also, each graphics are contained three curves such as Darrieus rotor, Savonius rotor, and combined rotor. Definitely, the combined rotor at the low solidity ratio generated the optimum performance at the large range of the TSR. On the other hand, based on the higher solidity ratio of the combined rotor has defined the optimum performance at the low range of TSR. An extremely, the medium of the solidity ratio produced a higher performance at the TSR of 2.5. Figure 4.60 as illustrated below are velocity contours and velocity instantaneous streamlines along with blades turbine of each solidity. Figure 4.61 is the pressure coefficient contours and pressures instantaneous streamlines. The lower solidity contour has been illustrated better aerodynamic performance within low shading and less vortex profile between the turbine contours.
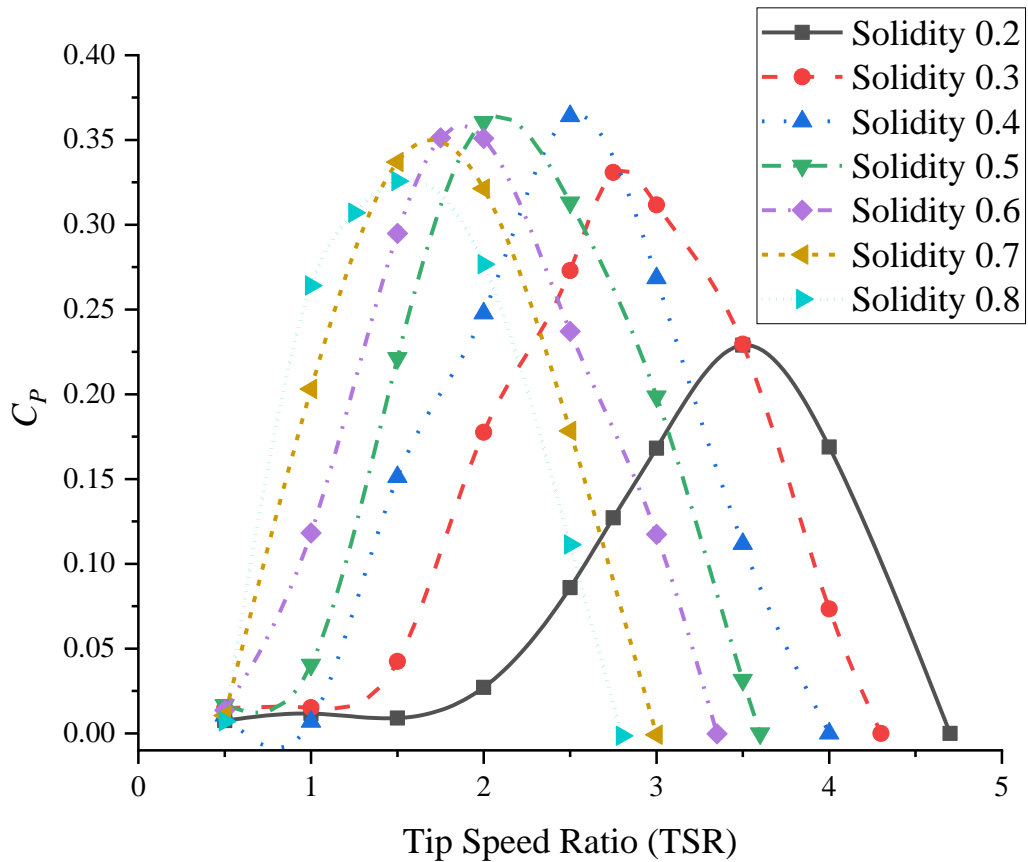
Figure 4.57. The graph of the coefficient of the power in different of solidities ratio with the range or TSRs.

The effect of the solidity ratio has occurred while the chord length of the Darrieus rotor changed or it seems like the aerodynamic interacted changing with the turbine blades. The performance of the combined rotor is extremely found to distinguish at the lower of the TSR as shown in Figure 4.58. This graph's figure has illustrated the better performance of the Savonius rotor at some of the azimuth angles at the lower solidity of the combined rotor. But, the performance of the H-Darrieus rotor in this condition is defined as the negative value. Finally, between the H-Darrieus rotor and the Savonius rotor better-related where can push the combined rotor rotating at the low wind speed and lower solidity. At the higher of the solidity ratio with the lower of the TSR, it can be notified that the Savonius rotor still worthless of work. Also, the combined rotor has extracted the performance approximately the same as the H-Darrieus rotor. For the medium solidity ratio, both Savonius and H-Darrieus rotors have been better in generating aerodynamic and power performance.
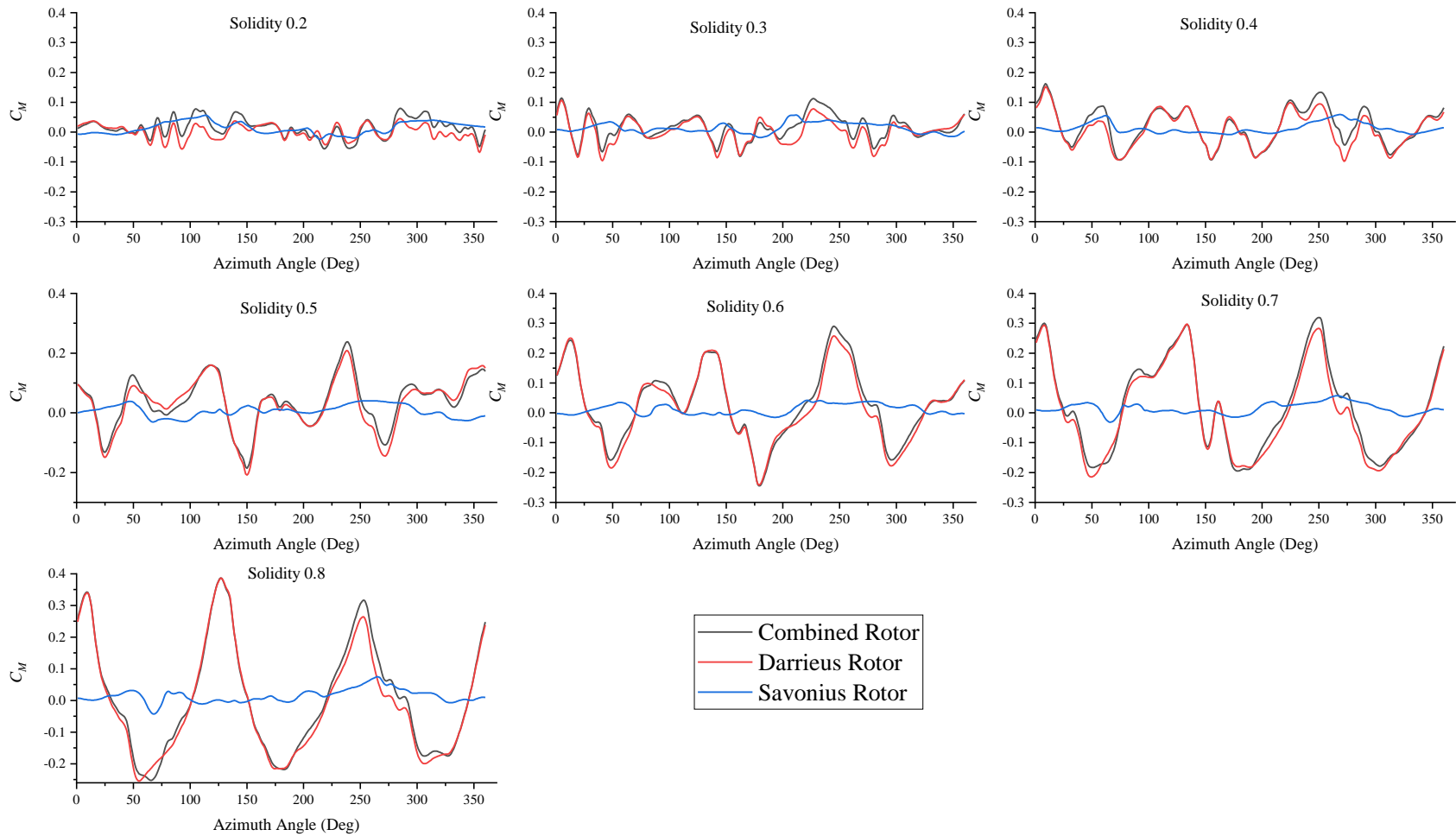
Figure 4.58. The coefficient of the moment of each turbine rotor at the lower TSR of 0.5.
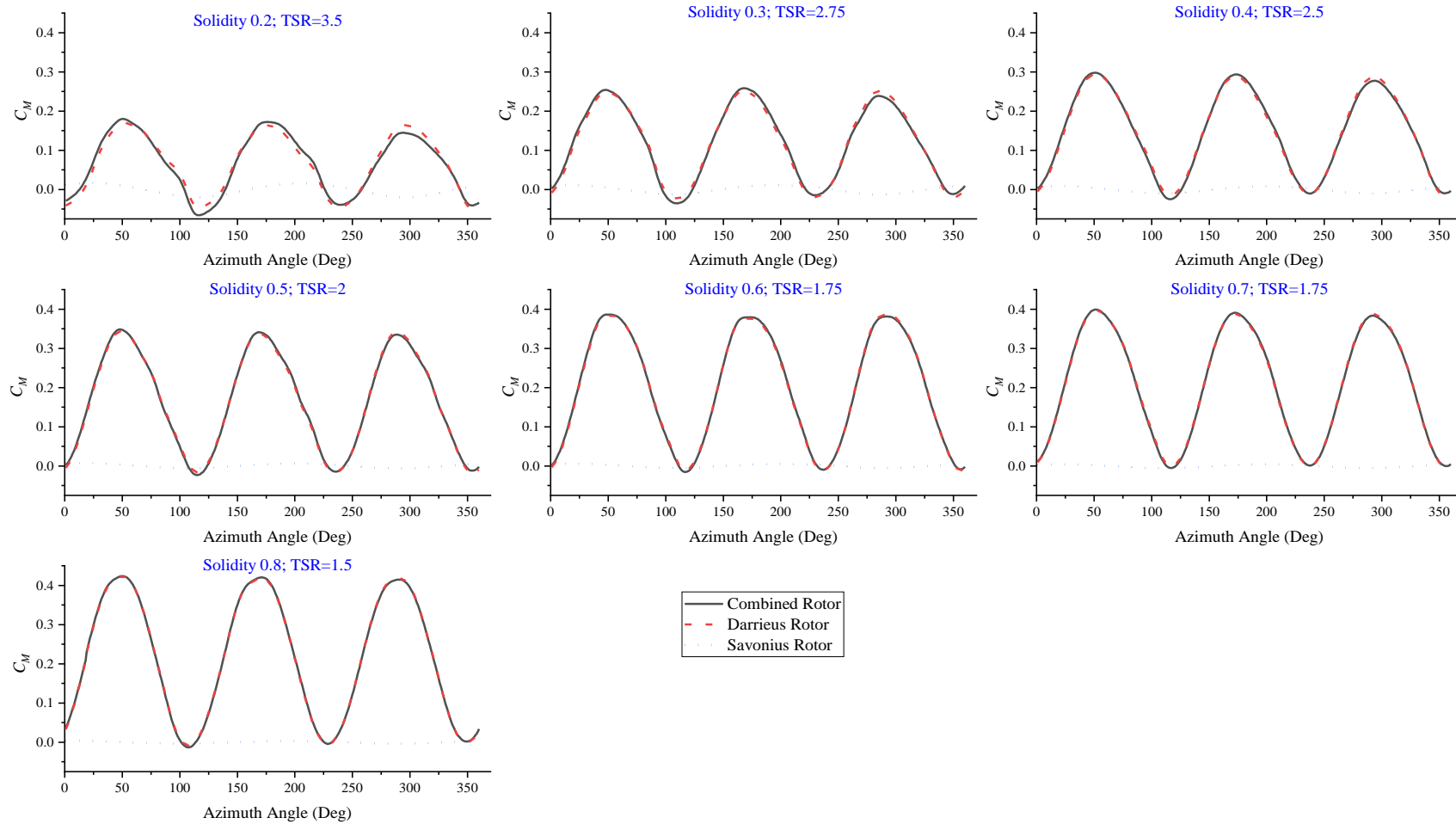
Figure 4.59. The graphs of the optimum TSR of the combined rotor, comparing C_M value at a different range of the solidity ratio (0.2-0.8)

(Solidity 0.2) (Solidity 0.3) (Solidity 0.4) (Solidity 0.5)

(Solidity 0.6) (Solidity 0.7) (Solidity 0.8)

0 2.25

Nondimensional Velocity (U/U_∞)
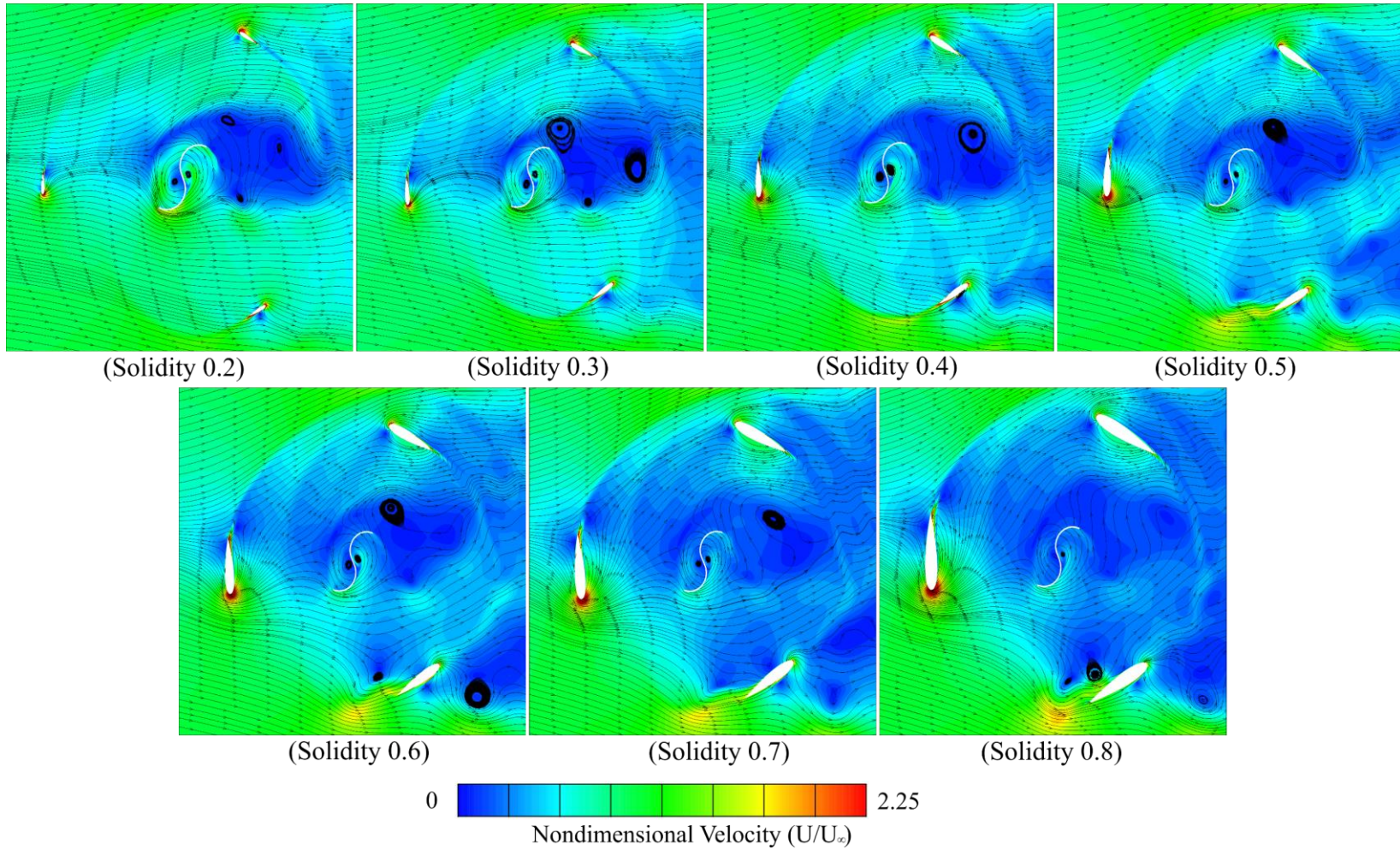
Figure 4.60. The velocity contours of the combined rotor in different solidities ratios at an optimum azimuth angle of 50 deg.

(Solidity 0.2)   (Solidity 0.3)   (Solidity 0.4)   (Solidity 0.5)

(Solidity 0.6)   (Solidity 0.7)   (Solidity 0.8)

Pressure Coefficient: $(P-Pref)/(0.5\rho U_\infty^2)$
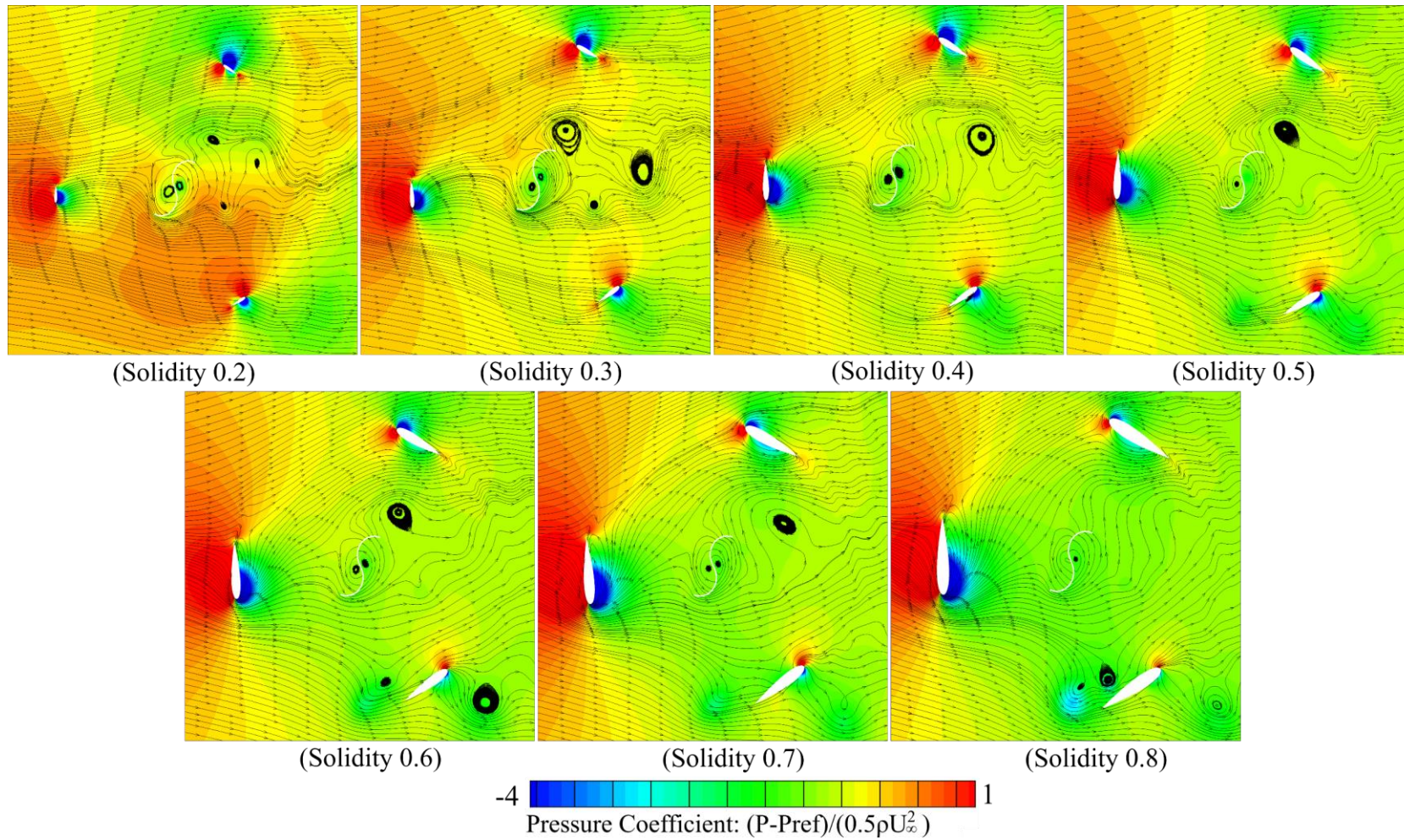
Figure 4.61. The pressure contours and pressure instantaneous streamlines of the combined rotor at an optimum azimuth angle.

CHAPTER 5
CONCLUSION

The entire models of the hybrid turbines have been completed for the present study. The designation and simulation progression based on the two rotors is introduced by H-Darrieus and Bach-type modified Savonius rotor. The research progress included theoretical analysis and commercial CFD program for analyzing the performance of the wind turbine. Also, all the results of each case of this implementation are extracted and explained in the discussion section. The objective of this present study was to perform the efficiency of the combined rotor with self-starting capability, presenting the aerodynamic properties at the range of the rotating angle. Moreover, at the lowest coefficient of the moment at some azimuth angle are approximate to zero. Each case of the model evaluated at various TSRs to optimize the optimum numerical value of C_P and C_M. Furthermore, numerical simulation is presented to vary the important parameters such as the shape of airfoils, and the solidity ratio of the combined rotor. Definitely, the outcome of each turbine specified that:

The first achievement of this present study indicated the shape of the airfoil. Hybrid turbines included two NACA standard symmetric and asymmetric airfoil which was generated different efficient and aerodynamic properties. The symmetric is conducted the numerical coefficient of the moment less than asymmetric 10%. Based on the feature of the asymmetric airfoil is modified for a better producing lift force including with high pressure on the airfoil surface. But, there is a small value of different efficiency of these two types of the airfoil, also the symmetric airfoil is basically for manufacturing. Thus, NACA-0018 is chosen for the further testing model.

After the shape of the airfoil is considered to choose for an achievement efficient and aerodynamic properties. The analysis of the solidity ratio as illustrated in the discussion section. While the high solidity (σ=0.8) of the wind turbine has much higher performance at the smaller and a short range of TSRs due to the blades having better contact with the coming flow in the upstream region. On the other

hand, the lower solidity (σ=0.2) of the wind turbine has conducted a high coefficient of power over a large range of TSRs. Except, the medium of the solidity ratio (σ =0.4) achieved C_P maximum (36.41%) by determining a peak efficiency among of solidities ratios due to lower blockage and less shading during blades rotation. Definitely, it represented the coefficient of the moment about 0.145 at a TSR of 2.5.

The Savonius turbine located in the middle affecting the drag force of the combined rotor at high TSR, reducing the aerodynamic torque on the blade and leading to low performance. But, at the lower of the TSR, the combined rotor could be conducting self-rotating by the Savonius rotor

Although this design is also to propose the self-starting capabilities from the Savonius turbine locating in the middle of the H-Darrieus rotor. Finally, the questions of the affection by airfoils shape and solidity ratio for the combined rotor are answered by describing and analyze in the discussion section.

REFERENCES

[1]   W. E. C. GLOBAL, "GWEC| GLOBAL WIND REPORT 2018," ed: Bruselas. Recuperado el Enero de, 2019.

[2]   F. M. White, *Fluid Mechanics*. McGraw-Hill, 2003.

[3]   S. J. Savonius, *The Wing-rotor in Theory and Practice*. Savonius, 1925.

[4]   M. Lates and R. Velicu, "CFD analysis and theoretical modelling of multiblade small Savonius wind turbines," in *Sustainable Energy in the Built Environment-Steps Towards nZEB*: Springer, 2014, pp. 403-415.

[5]   M. Ragheb and A. M. Ragheb, "Wind turbines theory-the betz equation and optimal rotor tip speed ratio," *Fundamental and advanced topics in wind power,* vol. 1, no. 1, pp. 19-38, 2011.

[6]   B. Greschner, C. Yu, S. Zheng, M. Zhuang, Z. Wang, and F. Thiele, "Knowledge based airfoil aerodynamic and aeroacoustic design," in *11th AIAA/CEAS Aeroacoustics Conference*, 2005, p. 2968.

[7]   N. Alom and U. K. Saha, "Influence of blade profiles on Savonius rotor performance: Numerical simulation and experimental validation," *Energy Conversion and Management,* vol. 186, pp. 267-277, 2019.

[8]   A. Rezaeiha, H. Montazeri, and B. Blocken, "Towards optimal aerodynamic design of vertical axis wind turbines: Impact of solidity and number of blades," *Energy,* vol. 165, pp. 1129-1148, 2018.

[9]   A. Hosseini and N. Goudarzi, "Design and CFD study of a hybrid vertical-axis wind turbine by employing a combined Bach-type and H-Darrieus rotor systems," *Energy conversion and management,* vol. 189, pp. 49-59, 2019.

[10]   H. Beri and Y. Yao, "Effect of camber airfoil on self starting of vertical axis wind turbine," *Journal of environmental Science and Technology,* vol. 4, no. 3, pp. 302-312, 2011.

[11]   V. S. Djanali, Z. Fathurrahman, B. A. Dwiyantoro, and N. Ikhwan, "Numerical study of savonius wind turbines with standard and Bach-profile blade variations," in *AIP Conference Proceedings*, 2019, vol. 2187, no. 1: AIP Publishing LLC, p. 020041.

[12]   M. Islam, D. S.-K. Ting, and A. Fartaj, "Aerodynamic models for Darrieus-type straight-bladed vertical axis wind turbines," *Renewable and sustainable energy reviews,* vol. 12, no. 4, pp. 1087-1109, 2008.

[13]   L. Daróczy, G. Janiga, K. Petrasch, M. Webner, and D. Thévenin, "Comparative analysis of turbulence models for the aerodynamic simulation of H-Darrieus rotors," *Energy,* vol. 90, pp. 680-690, 2015.

[14]   Y. Kyozuka, "An experimental study on the Darrieus-Savonius turbine for the tidal current power generation," *Journal of Fluid Science and Technology,* vol. 3, no. 3, pp. 439-449, 2008.

[15]   C.-C. Chen and C.-H. Kuo, "Effects of pitch angle and blade camber on flow characteristics and performance of small-size Darrieus VAWT," *Journal of Visualization,* vol. 16, no. 1, pp. 65-74, 2013.

[16]   M. F. Ramlee, A. Fazlizan, and S. Mat, "Performance Evaluation of H-Type Darrieus Vertical Axis Wind Turbine with Different Turbine Solidity,"

Journal of Computational and Theoretical Nanoscience, vol. 17, no. 2-3, pp. 833-839, 2020.

[17]   X. Liang, "Darrieus Savonius Combined Rotor Research Study for Vertical Axis Small Wind Turbine Optimization Design " Master of Philosophy, Fok Ying Tung Graduate School Innovative Technologies Leadership, The Hong Kong University of Science and Technology, 2015.

[18]   C. Song, G. Wu, W. Zhu, and X. Zhang, "Study on Aerodynamic Characteristics of Darrieus Vertical Axis Wind Turbines with Different Airfoil Maximum Thicknesses Through Computational Fluid Dynamics," *Arabian Journal for Science and Engineering,* pp. 1-10, 2019.

[19]   Y. Wang, X. Sun, X. Dong, B. Zhu, D. Huang, and Z. Zheng, "Numerical investigation on aerodynamic performance of a novel vertical axis wind turbine with adaptive blades," *Energy Conversion and Management,* vol. 108, pp. 275-286, 2016.

[20]   X. Liang, S. Fu, B. Ou, C. Wu, C. Y. Chao, and K. Pi, "A computational study of the effects of the radius ratio and attachment angle on the performance of a Darrieus-Savonius combined wind turbine," *Renewable energy,* vol. 113, pp. 329-334, 2017.

[21]   G. Aboufares, "Performance Characteristics of a Vertical Axis Wind Turbine Operating in Different Environmental Conditions," Master, University of Huddersfield, 2015. [Online]. Available: http://eprints.hud.ac.uk/id/eprint/28340

[22]   J. Bukala *et al.*, "Small Wind Turbines: Specification, Design, and Economic Evaluation," *Wind Turbines: Design, Control and Applications,* p. 73, 2016.

[23]   T. M. Letcher, *Wind energy engineering: a handbook for onshore and offshore wind turbines*. Academic Press, 2017.

[24]   W. W. E. Association, "Wind Power Capacity Worldwide Reaches 597 GW, 50, 1 GW added in 2018," *Accessed: Sep,* vol. 17, p. 2019, 2018.

[25]   A. Ghosh, A. Biswas, K. Sharma, and R. Gupta, "Computational analysis of flow physics of a combined three bladed Darrieus Savonius wind rotor," *Journal of the Energy Institute,* vol. 88, no. 4, pp. 425-437, 2015.

[26]   A. Roshan, A. Sagharichi, and M. J. Maghrebi, "Nondimensional Parameters' Effects on Hybrid Darrieus–Savonius Wind Turbine Performance," *Journal of Energy Resources Technology,* vol. 142, no. 1, 2020.

[27]   I. Paraschivoiu, *Wind Turbine Design: With Emphasis on Darrieus Concept*. Polytechnic International Press, 2002.

[28]   J. R. ker Lund, "The ERIGEN combined Darrieus-Savonius type of wind generator," *Ericsson Power Systems,* pp. 8-163.

[29]   D. G. J. Marie, "Turbine having its rotating shaft transverse to the flow of the current," ed: Google Patents, 1931.

[30]   J. D. Anderson Jr, *Fundamentals of aerodynamics*. Tata McGraw-Hill Education, 2010.

[31]   I. H. Abbott, A. E. Von Doenhoff, and L. Stivers Jr, "Summary of airfoil data," 1945.

[32] A. Rezaeiha, I. Kalkman, and B. Blocken, "Effect of pitch angle on power performance and aerodynamics of a vertical axis wind turbine," *Applied Energy,* vol. 197, pp. 132-150, 2017, doi: 10.1016/j.apenergy.2017.03.128.

[33] R. Gupta and K. Sharma, "Flow physics of a combined Darrieus-Savonius rotor using computational fluid dynamics (CFD)," *International Research Journal of Engineering Science, Technology and Innovation,* vol. 1, no. 1, pp. 1-13, 2012.

[34] S. Bhuyan and A. Biswas, "Investigations on self-starting and performance characteristics of simple H and hybrid H-Savonius vertical axis wind rotors," *Energy conversion and management,* vol. 87, pp. 859-867, 2014.

[35] A. Tools, "NACA 4 digit airfoil generator," *National Advisory Committee for Aeronautics,* 2015.

[36] A. Inc, "ANSYS FLUENT theory guide," ed: Release, 2013.

[37] H. K. Versteeg and W. Malalasekera, *An Introduction to Computational Fluid Dynamics: The Finite Volume Method*. Pearson Education Limited, 2007.

[38] A. FLUENT, "12.0/12.1 Documentation, ANSYS," ed: Inc, 2009.

[39] P. J. Roache, "QUANTIFICATION OF UNCERTAINTY IN COMPUTATIONAL FLUID DYNAMICS," *Annual Review of Fluid Mechanics,* vol. 29, no. 1, pp. 123-160, 1997, doi: 10.1146/annurev.fluid.29.1.123.

[40] R. Lanzafame, S. Mauro, and M. Messina, "2D CFD modeling of H-Darrieus wind turbines using a transition turbulence model," *Energy Procedia,* vol. 45, pp. 131-140, 2014.

[41] X. Sun, Y. Wang, Q. An, Y. Cao, G. Wu, and D. Huang, "Aerodynamic performance and characteristic of vortex structures for Darrieus wind turbine. I. Numerical method and aerodynamic performance," *Journal of Renewable and Sustainable Energy,* vol. 6, no. 4, p. 043134, 2014.

[42] Y.-b. Liang, L.-x. Zhang, E.-x. Li, X.-h. Liu, and Y. Yang, "Design Considerations of Rotor Configuration for Straight-Bladed Vertical Axis Wind Turbines," *Advances in Mechanical Engineering (Hindawi Publishing Corporation),* 2014.

[43] H. Beri and Y. Yao, "Double multiple streamtube model and numerical analysis of vertical axis wind turbine," *Energy and Power Engineering,* vol. 3, no. 03, p. 262, 2011.

APPENDIX A

Table A. 1 was the column datasheets that are numeric of the shape of airfoils. Also, airfoils symmetric and asymmetric are established by the coordinator of the XY-axis. This present study is token those XY coordinates to a designation program (Solidwork) for conducting the shape of the airfoil.

Table A. 1. Airfoil data for symmetric and asymmetric.

NACA-2415				NACA-0018			
Airfoil surface (mm)		Camber line (mm)		Airfoil surface (mm)		Camber line (mm)	
X	Y	X	Y	X	Y	X	Y
74.3	0.1166	0	0	74.3	0.1404	0	0
74.1068	0.16568	0.11962	0.43131	70.585	0.89903	0.9287	0
73.50499	0.311317	0.652354	0.253171	66.87	1.613796	1.8575	0
72.50937	0.549077	1.593735	0.313936	59.44	2.923705	3.715	0
71.12962	0.870796	2.936336	0.412078	52.01	4.083528	5.5725	0
69.37911	1.266815	4.667526	0.537881	44.58	5.085835	7.43	0
67.27716	1.725989	6.770216	0.682395	37.15	5.900163	11.145	0
64.84533	2.233458	9.221373	0.838331	29.72	6.467815	14.86	0
62.10811	2.777334	11.99351	0.995706	22.29	6.689229	18.575	0
59.09525	3.342014	15.05392	1.145651	18.575	6.621616	22.29	0
55.83942	3.913381	18.36845	1.278137	14.86	6.394258	29.72	0
52.37407	4.476575	21.89547	1.384606	11.145	5.957374	37.15	0
48.73709	5.017479	25.59486	1.456149	7.43	5.218832	44.58	0
44.96933	5.521233	29.42057	1.485763	5.5725	4.6809	52.01	0
41.11093	5.97372	33.29457	1.478461	3.715	3.961676	59.44	0
37.20498	6.361566	37.20498	1.448732	1.8575	2.914046	66.87	0
33.29457	6.670654	41.11093	1.396265	0.92875	2.110863	70.585	0
29.42057	6.889096	44.96933	1.322344	0	0	74.3	0
25.59486	6.990887	48.73709	1.228224	0.92875	-2.11086		

21.89547	6.958938	52.37407	1.116197	1.8575	-2.91405		
18.36845	6.79102	55.83942	0.990956	3.715	-3.96168		
15.05392	6.490848	59.09525	0.855867	5.5725	-4.6809		
11.99351	6.065109	62.10811	0.716242	7.43	-5.21883		
9.221373	5.526434	64.84533	0.576611	11.145	-5.95737		
6.770216	4.88894	67.27716	0.442653	14.86	-6.39426		
4.667526	4.171945	69.37911	0.31897	18.575	-6.62162		
2.936336	3.392538	71.12962	0.210843	22.29	-6.68923		
1.593735	2.57078	72.50937	0.121772	29.72	-6.46782		
0.652354	1.723017	73.50499	0.055275	37.15	-5.90016		
0.119623	0.862623	74.10682	0.014458	44.58	-5.08584		
0	0	74.3	0	52.01	-4.08353		
0.287541	-0.82176			59.44	-2.92371		
0.971844	-1.56253			66.87	-1.6138		
2.04325	-2.21786			70.585	-0.89903		
3.487642	-2.78476			74.3	-0.14043		
5.286445	-3.25954			74.3	0.140427		
7.419598	-3.63996			70.585	0.89903		
9.863325	-3.92453			66.87	1.613796		
12.59014	-4.11548			59.44	2.923705		
15.57328	-4.21727			66.87	4.083528		
18.78155	-4.23733			70.585	5.085835		
22.18375	-4.18532			74.3	5.900163		
25.74569	-4.07387						
29.43172	-3.9171						
33.23959	-3.71723						
37.09502	-3.47204						
40.95565	-3.19341						
44.77838	-2.8925						
48.52236	-2.5797						

52.14671	-2.26466						
55.61058	-1.9526						
58.87681	-1.65095						
61.90825	-1.36415						
64.67072	-1.09741						
67.13302	-0.85519						
69.26618	-0.64047						
71.04715	-0.45769						
72.45439	-0.31132						
73.47156	-0.20433						
74.08602	-0.13894						
74.3	-0.11665						

APPENDIX B

For Savonius turbine was captured by the standard of PVC pipe as dimensional showing by Table B. 1. Definitely, it is the facility for selecting material designation of the configuration of the Savonius blade.

Table B. 1. PVC size for implementing of Savonius rotor

Nominal Pipe Size	O.D.	Average I.D.	Min. Wall	Nominal wt./ft.	Maximum W.P PSI
1/8"	.405	.249	.068	.051	810
1/4"	.540	.344	.088	.086	780
3/8"	.675	.473	.091	.115	620
1/2"	.840	.602	.109	.170	600
3/4"	1.050	.804	.113	.226	480
1"	1.315	1.029	.133	.333	450
1-1/4"	1.660	1.360	1.140	.450	370
1-1/2"	1.900	1.590	.145	.537	330
2"	2.375	2.047	.154	.720	280
2-1/2"	2.875	2.445	.203	1.136	300
3"	3.500	3.042	.216	1.488	260
3-1/2"	4.000	3.521	.226	1.789	240
4"	4.500	3.998	.237	2.188	220
5"	5.563	5.016	.258	2.874	190
6"	6.625	6.031	.280	3.733	180
8"	8.625	7.942	.322	5.619	160
10"	10.750	9.976	.365	7.966	140
12"	12.750	11.889	..406	10.534	130
14"	14.000	13.073	.437	12.462	130
16"	16.000	14.940	.500	16.286	130
18"	18.000	16.809	.562	20.587	130
20"	20.000	18.743	.593	24.183	120
24"	24.000	22.544	.687	33.652	120